Fall 2021

Impact of Acetylcholine on Internal Pathways To Basal Amygdala Pyramidal Neurons

Tyler Daniel Anderson-Sieg

IMPACT OF ACETYLCHOLINE ON INTERNAL PATHWAYS TO BASAL AMYGDALA PYRAMIDAL NEURONS

by

Tyler Daniel Anderson-Sieg

Bachelor of Science
University of Missouri, 2016

Bachelor of Arts
University of Missouri, 2016

Submitted in Partial Fulfillment of the Requirements

For the Degree of Doctor of Philosophy in

Biomedical Science

School of Medicine

University of South Carolina

2021

Accepted by:

David Mott, Major Professor

Alexander McDonald, Major Professor

James Fadel, Committee Member

Robert Price, Committee Member

Jun Zhu, Committee Member

Tracy L. Weldon, Interim Vice Provost and Dean of the Graduate School

DEDICATION

This manuscript is dedicated to my mom, dad, grandparents on both sides, Robert, Tanya, and other family members. I have been very fortunate to have grown up surrounded by your constant love, support, patience, guidance, encouragement, and so many other things I do not have the space to mention here. A special thanks to Tanya. These past five plus years have kept me extremely busy and you have been extraordinarily patient and understanding the entire way. Thanks for embarking on this adventure with me and I look forward to the next steps in our journey. To all mentioned above, words cannot express how thankful I am, but thank you, nevertheless.

ACKNOWLEDGEMENTS

Thank you, Dr. Mott, for bringing me into the lab. I have really enjoyed your enthusiasm for science and working under your mentorship has been a pleasure. Not only are you passionate about science and your job, but you really care about the success of your students, which is evidenced by your approachability and willingness to be available regardless of how busy you are. Finally, thank you for teaching me whole-cell electrophysiology, a technique that is extremely complicated and difficult to perform. I could not have completed my work without your training and expertise.

Thank you, Dr. McDonald, for serving on my committee and your mentorship over the years. Your advice and comments are always detailed and thoughtful and have greatly improved the overall quality of my work.

Thank you, Dr. Price, for serving on my committee and training me on the principles of immunohistochemistry and microscopy. Your knowledge of the subjects is supreme, and you communicate it very well. Thank you also for managing the IRF and making the anatomical techniques used in this work possible.

And thank you Dr. Fadel and Dr. Zhu for serving on my committee and taking the time to provide helpful feedback and educate me through coursework.

ABSTRACT

The basolateral nuclear complex of the amygdala (BNC) – consisting of the lateral (LA), basolateral (BL), and basomedial nuclei (BM) – detects salient environmental stimuli (cue-detection) and motivates appropriate behavioral responses to their implied meaning (cue-guided behavior) via a precise pattern of internal circuitry. Glutamatergic signals representing environmental stimuli enter the LA and split into parallel streams that activate pyramidal neurons (PNs) in the anterior and posterior BL (BLa and BLp), which putatively mediate negative and positive emotions, respectively. The BL is the most densely innervated target of the cholinergic basal forebrain (CBF) and ACh transients (phasic ACh) in cortex are critical for cue-detection and cue-guided behavior. Despite the overlapping functions of the BNC and cortical phasic ACh, it is not known whether phasic ACh differentially impacts BLa and BLp PNs or their responses to LA inputs. The BNC is also a crucial storage site of associative emotional memories and ACh can facilitate learning and memory. NMDA receptors in the BNC are essential gatekeepers for the acquisition of associative emotional memories and ACh can facilitate long-term potentiation, the neuronal substrate of learning, by potentiating NMDA receptor currents in hippocampal PNs. Interestingly, despite similar cell types between the hippocampus and BNC, no studies have determined whether ACh also potentiates NMDA receptor currents in BL PNs. We addressed these critical knowledge gaps by employing confocal

immunohistochemistry and brain slice electrophysiology combined with optogenetics and pharmacology. Three core findings emerged from these studies. First, phasic ACh temporally and associatively enhances the signal-to-noise ratio at the LA-BLa pathway. Phasic ACh depolarizes BL PNs via presynaptic α7 and α4β2 nAChRs on non-LA inputs before hyperpolarizing them via postsynaptic M1 muscarinic ACh receptors (M1Rs) coupled to GIRK channels, creating a biphasic response that bidirectionally modulates the ability of LA inputs to fire them by bringing their membrane potential closer to or farther from action potential threshold when they arrive. Second, M1Rs can reduce or potentiate NMDA receptor currents depending on whether they are stimulated by phasic ACh or bath-applied muscarine, respectively. The reduction and potentiation are mediated by GIRK and SK channels, respectively. Finally, the CBF preferentially impacts BLa over BLp PNs and their responses to LA inputs. M1R expression is substantially higher in the BLa; BLa PNs are more sensitive and have larger response components to phasic ACh; and BLa PNs have larger depolarizing responses to bath-applied muscarine. The effect of phasic ACh on LA-driven output was also more muted in BLp PNs, with no nicotinic facilitation and a smaller muscarinic reduction. Together, our results provide novel insight into the circuit- and molecular- mechanisms by which ACh signaling could modulate attention, learning and memory, and valence processing mediated by the BNC.

TABLE OF CONTENTS

LIST OF TABLES

LIST OF FIGURES

LIST OF SYMBOLS

±	Plus/minus
α	Alpha
β	Beta
γ	Gamma
Ω	Ohm
μ	Micro
Hz	Hertz
A	Ampere
V	Volt
M	Molar

LIST OF ABBREVIATIONS

Acetyl-CoA ..... Acetyl-Coenzyme A

ACh ..... Acetylcholine

AChE ..... Acetylcholinesterase

AChR(s) ..... Acetylcholine Receptor(s)

AMPA ..... α-Amino-3-Hydroxy-5-Methyl-4-Isoxazole Propionic Acid

BL ..... Basal Nucleus

BLa ..... Anterior Division of the Basal Nucleus

BLp ..... Posterior Division of the Basal Nucleus

BM ..... Basomedial Nucleus

BMP ..... Posterior Division of the Basomedial Nucleus

BNC ..... Basolateral Nuclear Complex

CBF ..... Cholinergic Basal Forebrain

CeA ..... Central Nucleus

CeC ..... Capsular Division of the Central Nucleus

CeI ..... Intermediate Division of the Central Nucleus

CeL ..... Lateral Division of the Central Nucleus

CeM ..... Medial Division of the Central Nucleus

ChAT ..... Choline Acetyltransferase

ChT ..... Choline Transporter

CNS ..... Central Nervous System

CS(s) ..... Conditioned Stimuli

EPSC ..... Excitatory Postsynaptic Current

EPSP ..... Excitatory Postsynaptic Potential

GABA ..... Gamma Aminobutyric Acid

GDP ..... Guanosine Diphosphate

GIRK ..... G Protein-Gated Inwardly Rectifying Potassium

GPCR(s) ..... G Protein-Coupled Receptor(s)

GTP ..... Guanosine Triphosphate

HDB ..... Horizontal Limb of the Diagonal Band of Broca

IPSC ..... Inhibitory Postsynaptic Current

IPSP ..... Inhibitory Postsynaptic Potential

LA ..... Lateral Nucleus

LTP ..... Long-Term Potentiation

M1R(s) ..... M1 Muscarinic Acetylcholine Receptor(s)

mAChR(s) ..... Muscarinic Acetylcholine Receptor(s)

mPFC ..... Medial Prefrontal Cortex

NAc ..... Nucleus Accumbens

nAChR(s) ..... Nicotinic Acetylcholine Receptor(s)

NMDA ..... N-Methyl-D-Aspartate

PN(s) ..... Pyramidal Neuron(s)

PNS ..... Peripheral Nervous System

SK ..... Small Conductance Calcium-Activated Potassium

SNR ..... Signal to Noise Ratio

vAChT ..... Vesicular Acetylcholine Transporter

vHPC ..... Ventral Hippocampus

US(s) ..... Unconditioned Stimuli

CHAPTER 1

GENERAL INTRODUCTION

1.1. SIGNIFICANCE

According to the National Institute of Mental Health, nearly one in ten U.S. adults experienced a mood disorder in the past year and roughly one in five will experience one at some point in their lifetime. Despite the prevalence of mood disorders, there is still a need for improved therapies, the development of which will be facilitated by acquiring a deeper understanding of the brain's emotional circuitry. The amygdala is of particular interest in this regard, as it is commonly described as the brain's emotional hub (LeDoux 2000). Abnormal development and/or dysfunction of the amygdala is not only associated with mood disorders like anxiety, social phobia, bipolar disorder, and depression, but also addiction and neuropsychiatric disorders like autism and schizophrenia (Drevets, 2003; Nestler et al., 2002; Schumann et al., 2011). These observations highlight the importance of normal amygdala function in maintaining mental health.

The basolateral nuclear complex of the amygdala (BNC) – consisting of the lateral (LA), basolateral (BL), and basomedial nuclei (BM) – draws attention to emotionally salient stimuli, determines their valence (negative or positive), and motivates appropriate behaviors (e.g., avoidance/freezing or approach) (Adolphs et al., 1994; Blanchard and Blanchard 1972; Brown and Schafer 1888; Klüver and Bucy 1937; LeDoux et al., 1990; McDonald 2020; Pitkänen et al., 1997;

Weiskrantz 1956). The BNC also stores associative memories of emotionally salient experiences through Pavlovian conditioning, whereby neutral stimuli (CSs) acquire salience and the same valence as the stimuli that initiate the emotional experiences (USs). This process promotes survival by enabling CSs to predict outcomes and motivate behaviors related to the USs when these CSs are reencountered (Fernando et al., 2013).

These functions are accomplished via a precise pattern of internal circuitry under the control of diverse extra-amygdala inputs (Pitkänen et al., 1997). The BL receives the densest cholinergic innervation from the basal forebrain, suggesting acetylcholine (ACh) is a crucial regulator of BNC circuitry and normal BNC function. Supporting this, patients with Alzheimer's – a disease associated with the loss of cholinergic cells – commonly display emotional disturbances (Lyketsos et al., 2011; Mori et al., 1999) and are more likely to have post-traumatic stress disorder (PTSD) than their healthy counterparts (Desmarais et al., 2020), implicating the loss of cholinergic signaling in the amygdala in this deficit. Further, aberrant cholinergic signaling in cortical regions is associated with many of the same disorders mentioned above, including depression and schizophrenia (Higley and Picciotto 2014; Lustig and Sarter 2016).

Despite the importance of the amygdala in mental health and evidence that ACh signaling is a crucial regulator of BNC circuitry and normal function, surprisingly few studies have examined the molecular- and circuit-level mechanisms by which ACh impacts computations performed by BNC circuitry. We sought to fill this knowledge gap via the combined application of anatomy

(confocal immunohistochemistry), brain slice electrophysiology (whole-cell and single unit recordings combined with pharmacology and electrical stimulation of LA), and optogenetics. The experiments performed herein will probe the circuit- and molecular-level mechanisms by which ACh signaling could facilitate the attentional, motivational, and learning aspects of amygdala function described above. By doing so, we hope to shed new light on the mechanisms by which ACh modulates emotional circuitry and facilitate future efforts to improve therapies for conditions associated with disrupted amygdala and cholinergic function, like mood disorders, addiction, and schizophrenia, among others.

1.2. AMYGDALA FUNCTION

The amygdala has been implicated in a variety of functions. For example, it has been reported to be involved in the perception of body movements (Bonda et al., 1996) and pain (Neugebauer, 2015), as well as generating the emotional aspects of dreams (Maquet et al., 1996; Scarpelli et al., 2019). However**,** the most extensively studied and best understood function of the amygdala is to draw attention to emotionally salient stimuli, determine their valence, and motivate appropriate behaviors by predicting biologically relevant outcomes (Adolphs et al., 1994; Blanchard and Blanchard 1972; Brown and Schafer 1888; Klüver and Bucy 1937; LeDoux et al., 1990; McDonald 2020; Pitkänen et al., 1997; Weiskrantz 1956). It was initially thought that the amygdala only responded to stimuli with negative valence, but it is now well-appreciated that the amygdala also processes positive stimuli (Baxter and Murray 2002; Pignatelli and Beyeler 2019).

Key aspects of this function were first revealed long ago in pioneering studies that performed bitemporal lobectomies in non-human primates that impacted the amygdala among other structures (Brown and Schafer, 1888; Klüver and Bucy, 1937). These studies reported drastic changes in the monkeys' temperament (tameness was a key feature), as well as a phenomenon they termed "psychic blindness", whereby the monkeys no longer recognized the emotional or behavioral significance of sensory stimuli. These findings were so impactful that Klüver-Bucy syndrome became the term to describe symptoms of patients suffering from damage to both temporal lobes. Subsequent studies selectively lesioning the amygdala in monkeys (Aggleton and Passingham, 1981; Weiskrantz, 1956), rats (Blanchard and Blanchard 1972; LeDoux et al., 1990), and humans (Adolphs et al., 1994; Anderson and Phelps, 2001) have replicated key aspects of these findings, not only driving home to point that the amygdala is essential for connecting stimuli with their emotional meaning, but also demonstrating that amygdala function is conserved across animal species (discussed further in Janak and Tye 2015).

Another key function of the amygdala is its ability to form and store associative emotional memories of negative and positive valence (Beyeler et al., 2016, 2018; Fernando et al., 2013; Namburi et al., 2015). The term used to describe this form of learning is Pavlovian conditioning. Through this process, neutral stimuli (conditioned stimuli or CSs) acquire salience and the same valence as the stimuli that initiate the original emotional experience (unconditioned stimuli or USs). Normally, Pavlovian conditioning is an adaptive

process because it enables CSs (e.g., neutral odor) to predict biologically relevant outcomes (e.g., foot shock or food consumption) and motivate appropriate behaviors (e.g., avoidance or approach) that can promote survival (Domjan 2005; Fernando et al., 2013). However, it is speculated that abnormalities in the circuitry underlying this process can also lead to maladaptive behaviors and conditions like persistent and generalized anxiety, panic disorders, phobias, PTSD, and drug addiction (Adinoff 2004; Careaga et al., 2016; Otto et al., 2014; Pape and Pare 2010; Sun et al., 2020).

Taken together, the amygdala is involved in numerous functions, but it is best understood to assign attention to negative and positive salient stimuli; layer new meaning onto initially neutral stimuli through experience-dependent and associative learning; and motivate appropriate behaviors to salient stimuli (whether innate or learned and negative or positive).

1.3. FUNCTIONAL NEUROANATOMY OF THE AMYGDALA

1.3.1. GENERAL ANATOMY

The amygdala is a structure located in the medial temporal lobe of each hemisphere. It comprised of more than a dozen interconnected nuclei, which themselves are comprised of several subdivisions (McDonald 2020; Pessoa 2010; Sah et al., 2003). Data on the contributions that many of these nuclei make to behavior is surprisingly sparse. However, two subgroupings of these nuclei have been well-studied, especially with respect to the functions described above. One is the basolateral nuclear complex of the amygdala (BNC) – consisting of

the lateral (LA), basolateral (BL), and basomedial nuclei (BM) – and the other is the central nucleus (CeA) (Zhang et al., 2021).

The BNC and CeA are comprised of different cell types. Each nucleus of the BNC is considered cortex-like because, although they are subcortical in location, they share the same cell types that are found in the cortex (also the hippocampus) (McDonald 2020; Muller et al., 2006; Zhang et al., 2021). These are local inhibitory interneurons (INs) that release GABA and long-range excitatory pyramidal neurons (PNs) that release glutamate (Janak and Tye 2015; McDonald 2020; Sah et al., 2003). PNs far outnumber INs in the BNC, constituting roughly 85 percent of the total neurons (Muller et al., 2006). Meanwhile, the CeA is more similar to the striatum in its cell type composition, being comprised primarily of long-range inhibitory medial spiny neurons that release GABA (McCullough et al., 2018; McDonald 1982; Zhang et al., 2021).

As mentioned above, the nuclei comprising the BNC and CeA can be further divided into smaller divisions that are distinguishable based on cytoarchitectonics, chemoarchitectonics, and fiber connections (Pitkänen et al., 1997). The LA can be subdivided into the dorsolateral (LA_{DL}), ventrolateral (LA_{VL}), and the medial (LA_{M}) divisions; the BL can be subdivided into the anterior (BLa), intermediate (BL_{I}), and posterior (BLp) divisions; and the CeA can be subdivided into the capsular (CeC), lateral (CeL), the intermediate (CeI), and the medial (CeM) divisions (McDonald 2020; Pitkänen et al., 1997; Sah et al., 2003). Each of these nuclei and their subdivisions are highly interconnected with one another. It has been proposed that each nucleus and subdivision represent

discrete computational units and that the processing of information within the amygdala involves highly organized patterns of communication within and between them (Pitkänen et al., 1997).

Each nucleus of the BNC and CeA also receives inputs from multiple brain regions and forms reciprocal and unidirectional connections with the same and other brain regions (Sah et al., 2003). A full discussion of all the extrinsic connections of the BNC and CeA is beyond the scope of this review, but some highlights are as follows. The BNC communicates with higher order cortical areas in the prefrontal, temporal, insular, and hippocampal cortices and striatum, whereas the CeA does not (Pape and Pare 2010). In contrast, the CeA heavily projects to the brainstem, while the BNC sparsely does, if at all (Pape and Pare 2010). The thalamus projects to BNC and CeA and both regions project to the lateral hypothalamus, cholinergic basal forebrain, and BNST (McDonald 2020; Pape and Pare 2010; Penzo et al., 2015). This extremely diverse connectivity positions the amygdala as a central integrator of sensory information from diverse sources, as well as a primary influencer of various physiological processes including autonomic and motor control, memory formation, and neuromodulation (Pape and Pare 2010; Zhang et al., 2021).

1.3.2. INFORMATION FLOW THROUGH THE BNC AND CEA

A simplified view of how sensory information flows through the amygdala to mediate its function is as follows. First, glutamatergic signals from thalamus, associative cortex, and brainstem representing multimodal sensory information enter the LA (Zhang et al., 2021), which has been called the “sensory interface”

or “gatekeeper” of the amygdala (LeDoux 2007; LeDoux et al., 1990; Maren, 2001). Upon arrival in LA, sensory signals split into parallel streams that move through the divisions of LA and into BL (Pitkänen et al., 1997). These streams can also travel to the basomedial nucleus (BM) and CeA, but the function of the BM is less known and LA connections to CeA are relatively sparse (LeDoux 2007; Pitkänen et al., 1997). Thus, BL is a primary liaison between LA and CeA (LeDoux 2007).

As the parallel sensory information streams travel into BLa and BLp from LA, they can be independently modified by numerous external inputs (Pitkänen et al., 1997), including those from the medial prefrontal cortex (mPFC; top-down information), ventral hippocampus (vHPC; contextual information), and neuromodulatory regions like the ventral tegmental area (dopamine), dorsal raphe nucleus (serotonin), locus coeruleus (noradrenaline), and the basal forebrain (ACh) (LeDoux 2007; Zhang et al., 2021). According to the serial model of information flow, these independent sensory streams ultimately converge in the CeA, the main output nucleus of the amygdala, which elicit changes in heart rate and breathing by way of its connections with the hypothalamus and brainstem (Pitkänen et al., 1997). However, the BL itself is also an important output region of the amygdala, as it is connected to numerous behaviorally relevant regions besides the CeA, such as the NAc, mPFC, and vHPC (Janak and Tye 2015; LeDoux 2007; Zhang et al., 2021) in addition to receiving such diversified inputs. Thus, the BL is an intriguing region of interest because its net output and thus contribution to behavior is highly malleable dependent upon

dynamic interactions between BLa and BLp PNs and internal LA and various external inputs.

1.3.3. THE ROLE OF BL PYRAMIDAL NEURONS IN VALENCE

Importantly, BLa and BLp PNs have been shown to preferentially processes negative and positive emotions, respectively (Kim et al., 2016, 2017; Pi et al., 2020; Yang et al., 2016; Zhang et al., 2020), introducing the possibility that LA-BLa and LA-BLp pathways are negative and positive circuits, as well. Notably, other studies have reported that negative and positive emotions are preferentially processed by intermingled populations of PNs defined by differential projection targets (Ambroggi et al., 2008; Beyeler et al., 2016, 2018; Namburi et al., 2015; Paton et al., 2006; Stuber et al., 2011; Tye et al., 2008). There are ways to explain these seemingly contradicting findings. First, that negative and positive cells are intermingled, not spatially segregated, may have been concluded from recordings taken from intermediate regions of BL, where BLa and BLp are adjacent. Second, rather than being monolithically negative or positive, projector populations could be negatively or positively biased depending on whether a larger proportion resides in the BLa or BLp, respectively. This latter hypothesis has seen experimental support (Kim et al., 2016, 2017). For example, *in vivo* optical activation of nucleus accumbens (NAc) projectors residing in the BLa generates negative behaviors despite NAc projectors being reported as positive cells (Kim et al., 2016, Supplementary Figure 9). They also reported that approximately 70 percent of their NAc projectors resided in the positive BLp. In a

follow-up study, the same group reported a similar trend upon investigation of the putatively negative CeA projectors (Kim et al., 2017).

1.3.4. BNC ANATOMY, LEARNING, AND MEMORY

BNC circuitry is also essential for the acquisition of fear and reward associations (Baxter and Murray 2002; Beyeler et al., 2016, 2018; Cardinal et al., 2002; Fernando et al., 2013; Maren 1999; Namburi et al., 2015; Pape and Pare 2010; Sah et al., 2003). For example, pre-training lesions of the BNC severely attenuate the acquisition of fear conditioning to both contextual and discrete conditioned stimuli (Maren, 2001) and lesions of the BL impair performance on tasks that require linking an object with the positive value of a rewarding stimulus (Baxter and Murray 2002). These associative memories form in the BNC through long-term potentiation (LTP) (Bocchio et al., 2017; Carrere and Alexandre 2015; Maren 1999; Namburi et al., 2015; Pape and Pare 2010; Tye et al., 2008), the cellular and molecular correlate of learning (Luscher and Malenka 2012; Lynch, 2004). LTP is a process whereby the communication strength between neurons co-activated during an experience become enhanced for a prolonged period (Luscher and Malenka 2012; Yang and Calakos 2013).

Although there are numerous forms of LTP (Citri and Malenka 2008), substantial evidence suggests that fear (Campeau et al., 1992; Fanselow and Kim 1994; Gewirtz and Davis 1997; Johansen et al., 2011; Maren 1999; Miserendino et al., 1990; Pape and Pare 2010; Rodrigues et al., 2001) and at least some forms of reward-related memories (Baldwin et al., 2000; Burns et al., 1994; Feltenstein and See 2007; Namburi et al., 2015; Tye et al., 2008) require

the activation of NMDA receptors in the BNC. It is well-acknowledged – especially in fear learning – that these NMDA receptors are located on postsynaptic LA PNs (Johansen et al., 2011; Tye et al., 2008) where sensory inputs converge, although important roles for NMDA receptors on BL PNs cannot be ruled out because most studies that infused NMDA receptor antagonists into the BNC also impacted BL PNs (Campeau et al., 1992; Fanselow and Kim 1994; Gewirtz and Davis 1997; Johansen et al., 2011; Maren 1999; Miserendino et al., 1990; Pape and Pare 2010; Rodrigues et al., 2001). There is also evidence that LTP at synapses between LA and BL PNs depends on the NMDA receptor (Rammes et al., 2000). Since BL PNs are a primary target LA PNs (Bazelot et al., 2015; Jolkkonen and Pitkänen 1998; Pu et al., 2009; Rammes et al., 2000; Wang et al., 2002) and the BL is a primary liaison between LA inputs and numerous behaviorally relevant regions, LA-BL synapses are likely to store associative memories via NMDA receptor-dependent LTP.

The NMDA receptor is essential for this form of LTP because it gates the influx of calcium entry into the postsynaptic PN, which initiates intracellular mechanisms underlying LTP expression (Luscher and Malenka 2012). During Pavlovian conditioning, LTP occurs when initially weak sensory inputs representing neutral stimuli (conditioned stimuli or CSs) signal to the same cells that are also being fired by different sensory inputs representing salient stimuli (foot shock or food reward). The strong depolarization resulting from co-activation of postsynaptic PNs removes Mg^{2+} ions blocking NMDA receptors at CS synapses and enables calcium influx that initiates postsynaptic molecular

changes that strengthen the CS-PN synapses. This process enables CS inputs to access the same BNC circuitry (and the behaviors they mediate) when detected alone in the future. This learning process is adaptive (Domjan 2005; Fernando et al., 2013) because it enables learned cues to predict biologically relevant outcomes in the future and guide appropriate behaviors that promote organism survival (e.g., approach or avoid an area were food or a predator was last encountered when a certain smell is detected). Calcium entry through NMDA receptors is also under the control of numerous molecular mechanisms (Bazzari and Parri 2019; Kantamneni 2015; Luján et al., 2009; MacDonald et al., 2007), introducing numerous means by which LTP magnitude can be modulated by outside influences such as neuromodulatory inputs.

1.4. ACETYLCHOLINE

1.4.1. A BRIEF HISTORICAL INTRODUCTION

Acetylcholine (ACh) was the first neurotransmitter discovered over 100 years ago at the neuromuscular junction (Haam and Yakel 2017; Mineur and Picciotto 2021). At the time, most efforts were focused on its effects in the peripheral nervous system (PNS). Otto Leowi famously called it “vagusstoff” when noting its bradycardic effects on the frog heart. His work, in conjunction with Henry Dale and the observations reported in other studies, were so impactful that both scientists shared the 1936 Nobel Prize in Physiology or Medicine for revealing that neurotransmission has a chemical, in addition to an electrical, component. Since its discovery, ACh has been well-studied in numerous organisms, leading to the conclusion that it is evolutionarily conserved.

It is also now appreciated that ACh has crucial roles at other mammalian end organs in addition to the neuromuscular junction and heart (Mineur and Picciotto 2021).

1.4.2. ACETYLCHOLINE IN THE CNS

ACh has essential roles in the central nervous system (CNS) in addition to the PNS. In the CNS, ACh exerts highly diverse effects on cellular and synaptic physiology, depending on numerous variables including, but not limited to, the brain region, receptor type and subtype, cell type, and the location of ACh receptors with respect to different cell types and cellular components (Picciotto et al., 2012). ACh signaling, by exerting these dynamic circuit and molecular effects, has been shown to contribute to switching network dynamics that lead to behavioral transitions such as from sleep to wakefulness, distraction to attention, and learning to recall (Colangelo et al., 2019; Hasselmo and Sarter 2011).

ACh is synthesized in cholinergic terminals by the enzyme choline acetyltransferase (ChAT) (Oda 2002), which does so by combining the two precursor molecules acetyl-coenzyme A (acetyl-CoA) and choline (Taylor and Brown 1999). For ChAT to use choline for ACh synthesis, choline must be taken into the cholinergic terminals from the extracellular space via the choline transporter (ChT), a protein residing in the terminal membrane. Importantly, choline uptake by ChT is the rate-limiting step of ACh synthesis (Taylor and Brown 1999). Once ACh is synthesized by ChAT, it is then loaded into vesicles by the vesicular acetylcholine transporter (VAChT) that resides on vesicles within the cholinergic terminals (Fisher and Wonnacott 2012). When a depolarizing

wave propagates into the terminal during an action potential, it activates voltage-sensitive calcium channels also in the terminal that enable calcium influx. The consequent elevation in calcium concentration in cholinergic terminals facilitates interactions between ACh vesicles and vesicular release machinery, resulting in ACh release (Sam and Bordoni 2021). Once ACh is released from cholinergic terminals, it is rapidly degraded back into acetyl-CoA and choline via the highly efficient catalytic enzyme acetylcholinesterase (AChE) (Trang and Khandhar 2021), whereupon ChT reuptakes choline again and the cycle repeats.

After ACh is released from cholinergic terminals, it diffuses outward and binds to two broad categories of ACh receptors: nicotinic ACh receptors (nAChRs) and muscarinic ACh receptors (mAChRs). These receptors were named after the agonists that preferentially bind them: nicotine and muscarine (Karczmar 2007). nAChRs are ionotropic and, most commonly, generate depolarizing currents characterized by a fast onset and short duration. These receptors are generally permeable to Na^+, K^+, and Ca^{2+} and can rapidly desensitize (Hahn 2015). They are also pentamers that contain different combinations of subunits, although heteromeric α4β2 and homomeric α7 nAChRs are most common and can reside on presynaptic and postsynaptic components of cells (Hahn 2015). CNS nAChRs have important roles in healthy cognition and their dysregulation is associated with conditions like Alzheimer's disease (AD), addiction, schizophrenia, and others (Schaaf, 2014).

In contrast to nAChRs, mAChRs are metabotropic and can generate a wide variety of effects in addition to alterations of the membrane potential by

initiating complex intracellular signaling cascades (Picciotto et al., 2012). Their membrane potential effects can be hyperpolarizing and/or depolarizing (Radnikow and Feldmeyer 2018) and are generally slower-onset and longer in duration (Jones et al., 2012). They are proteins comprised of seven transmembrane segments and couple to G-proteins comprised of α, β, and γ subunits (Haga 2013). When mAChRs are inactive, the G-proteins are typically unassociated with the mAChRs and form αβγ trimers with guanosine diphosphate (GDP) bound to the α subunit (de Oliveira et al., 2019). When mAChRs activate via ACh binding, they undergo conformational changes that signals the αβγ trimers to interact with them (de Oliveira et al., 2019). Upon mAChR-αβγ trimer interaction, GDP in the α subunit is replaced with guanosine triphosphate (GTP) and the trimer splits into an α monomer and βγ dimer that go on to perform different downstream functions (de Oliveira et al., 2019). When ACh is no longer bound to the mAChRs, the α subunit eventually inactivates by hydrolyzing its GTP back into GDP (de Oliveira et al., 2019), leading subsequent re-trimerization of the α, β, and γ subunits (Offermanns 2003; Hollmann et al., 2005; Baltoumas et al., 2013).

There are five subtypes of mAChRs in the CNS: M1, M2, M3, M4, and M5 (Haga 2013). The odd subtypes (M1, M3, and M5) are $G_{\alpha q/11}$-coupled and the even subtypes (M2 and M4) are $G_{\alpha i/O}$-coupled (Santiago and Abrol 2019), which are functionally distinguishable based on key differences in their downstream effects and effectors. In general, $G_{\alpha q/11}$-coupled mAChRs (M1, M3, and M5) increase activity of phospholipase C (PLC), reduce the M-current, and elevate

intracellular calcium concentration (Wess et al., 2007). In contrast, $G_{\alpha I/O}$-coupled mAChRs (M2 and M4) reduce activity of adenylyl cyclase and voltage-gated calcium channels and activate G-protein coupled inwardly rectifying potassium (GIRK) channels (Wess et al., 2007). Both types can activate mitogen-activated protein (MAP) kinases (Wess et al., 2007). Just like nAChRs, mAChRs can be found pre- and postsynaptically. CNS mAChRs modulate cognitive, behavioral, sensory, motor, and autonomic processes and their dysregulation is associated with pathologies AD, schizophrenia, depression, among other conditions.

1.4.3. SPATIOTEMPORAL DYNAMICS OF ACETYLCHOLINE SIGNALING

There is much ongoing debate over how ACh signals in the brain and the spatiotemporal nature of its release in target brain regions (Disney and Higley 2020; Sarter et al., 2009; Sarter and Lustig 2020). It was initially thought that ACh signaling in the CNS led to slow changes in the extracellular concentration of ACh (volume neurotransmission) that primarily mediated transitions between brain states (Giocomo and Hasselmo 2007; Hasselmo and Sarter 2011; Sarter et al., 2009). However, it is now appreciated that ACh also signals as a classical, rapid, point-to-point neurotransmitter (wired neurotransmission) with causal roles in behavior (Mineur and Picciotto 2021; Sarter et al., 2009; Sarter and Lustig 2020). It has been proposed that ACh likely signals both ways, with transient (or phasic) modes of release under certain behavioral circumstances and sustained modes under others (Disney and Higley 2020; Sarter and Lustig 2020). It has also been suggested that the spread of ACh may span a continuum of multiple

spatiotemporal zones that depend on the mode of ACh signaling (Disney and Higley 2020; Mineur and Picciotto 2021; Sarter and Lustig 2019, 2020). Thus, phasic ACh release may be more restricted and its actions more synaptic, whereas sustained ACh release may be more diffuse and its actions more extrasynaptic. If this is true, it introduces the interesting possibility that ACh can exert different effects on target circuits by recruiting different sets of functionally distinct ACh receptors, at different distances from ACh release sites, and potentially located on distinct cellular compartments and cell types. Indeed, there is experimental evidence supporting this in the amygdala (Aitta-aho et al., 2018; Unal et al., 2015), where phasic and sustained endogenous ACh signaling generate different effects on membrane potential and excitability, which the authors attributed to functionally distinct subtypes of synaptic and extrasynaptic M1 mAChRs on BLa PNs.

1.4.4. ACETYLCHOLINE AND VALENCE

Until recently, studies involving the CBF did not compare its roles in negative and positive emotional processing, which may have been due to the traditional view that it mediates general functions like arousal or consciousness via slow and diffuse signaling across distributed networks (Hasselmo and Sarter 2011). Recently, however, numerous studies have begun to do so (Aitta-aho et al., 2018; Chubykin et al., 2013; Crouse et al., 2020; Gritton et al., 2016; Guo et al., 2019; Hangya et al., 2015; Harrison et al., 2016; Howe et al., 2017; Jiang et al., 2016; Kuchibhotla et al., 2017; Laszlovszky et al., 2020; Letzkus et al., 2011; Lin and Nicolelis, 2008; Liu et al., 2015; Lu et al., 2020a; Paolone et al., 2013;

Parikh et al., 2007; Sturgill et al., 2020; Teles-Grilo Ruivo et al., 2017), and their results have contributed to the modern view that the CBF also mediates specific cognitive operations via precisely orchestrated and spatially restricted ACh release (Hasselmo and Sarter 2011; Sarter and Lustig 2019).

Despite some discrepancies between individual studies, general trends emerge when they are considered together. First, both negative and positive stimuli can activate CBF neurons, generally strongly and rapidly (phasic ACh release). Second, phasic ACh release can drive behaviors and facilitate learning. Third, many of these studies note that the transient activation patterns of CBF neurons may track salience, suggesting phasic ACh release conveys importance more than value, per se. Supporting this, phasic ACh release into cortex is essential for cue-detection and cue-guided behavior, highlighting its important role in attention. Finally, one study concludes transient activation of the CBF encodes valence-free reinforcement prediction error (Sturgill et al., 2020). Taken together, CBF neurons transiently activate in response to negative and positive stimuli while obeying the principles of prediction error (i.e., signaling during reinforcement, prediction, and surprise) (Sturgill et al., 2020), but this activity pattern seems to track the salience of stimuli irrespective of valence. Further, the phasic ACh release it generates can drive behavior and facilitate attentional performance and learning via its impact on downstream circuits.

1.4.5. ACETYLCHOLINE AND ATTENTION

It has been appreciated for decades that ACh has a vital role in attention (Picciotto et al., 2012; Sarter and Lustig 2019). Numerous lesion studies

performed in the 90's and early 2000's established that the CBF generally, as well as CBF projections to cortex more specifically, reported significant disruption of various attentional functions (Hasselmo and Sarter 2011). Intriguingly, there is strong evidence that the impairments stemming from cholinergic deafferentation of cortex are both robust and selective to attention, as non-attentional behaviors were not disrupted by the procedure (Baxter et al., 1999; Chiba et al., 1995; Dalley et al., 2004; McGaughy et al., 1996, 2000; McGaughy and Sarter, 1998; Newman and McGaughy, 2008; Turchi and Sarter, 1997). These findings have also been verified by numerous microdialysis studies, which found that elevations in cortical ACh were specifically associated with attentional performance (Arnold et al., 2002; Dalley et al., 2001; Himmelheber et al., 2000; Kozak et al., 2006; Parikh et al., 2007; Passetti et al., 2000; Sarter et al., 2006). Interestingly, these studies also reported that greater ACh levels were associated with greater attentional effort, but not attentional performance, on various tasks.

The evidence above clearly supports a critical role of ACh in mediating attention. However, "attention" is a catch all phrase encompassing numerous and specific forms. Intriguingly – thanks to improved technologies enabling sub-second monitoring of ACh release and rapid manipulation of cholinergic terminals *in vivo* – it is now understood that ACh contributes to different aspects of attention, depending on the mode of CBF signaling (Hasselmo and Sarter 2011; Sarter and Lustig 2019). Specifically, rapid cholinergic transients (sub-seconds to seconds long) in the cortex are essential for cue-detection and cue-guided behaviors (Gritton et al., 2016; Howe et al., 2017; Lu et al., 2020; Parikh et al.,

2007), whereas longer-term ACh signaling (tens to hundreds of seconds) is more important for sustaining attention (Sarter and Lustig 2019).

Given the complexity of attention, it comes as no surprise that the cellular and molecular mechanisms underlying the cholinergic enhancement of attentional are also complex. Although there are likely additional mechanisms involved, a popular theory is that ACh enhances attention by maximizing the signal-to-noise ratio (SNR) of afferent pathways to cortical regions (Colangelo et al., 2019; Picciotto et al., 2012). In cellular terms, ACh accomplishes this by making target circuitry more receptive to specific sensory inputs representing behaviorally relevant stimuli, while simultaneously reducing the impact of other inputs representing distracting or irrelevant stimuli (Lustig and Sarter 2016; Mineur and Picciotto 2021).

It is believed that elevated ACh concentrations enhance SNR by boosting glutamate release from external inputs (generally thalamic) via presynaptic nAChRs, while suppressing glutamate release from recurrent inputs via mAChRs (Hasselmo 2006). This has been observed in various areas of cortex and hippocampus (Hasselmo 2006). There is evidence that the nAChRs that enhance glutamate release are the α4β2 subtype (Lustig and Sarter 2016), although α7 and α5 containing nAChRs could be involved since they can also improve attention (Mineur and Picciotto 2021). In addition, ACh suppresses GABA release from soma-targeting PV+ interneurons (INs), which increases PN responsiveness to the same thalamic inputs that ACh is boosting presynaptically and makes them more likely to fire (Lustig and Sarter 2016). Finally, ACh directly

enhances the excitability of dendrite-targeting INs via nAChRs and postsynaptic PNs via mAChRs (Lustig and Sarter 2016). All these mechanisms happen in concert to facilitate attention by increasing the receptiveness of target circuitry to behaviorally relevant inputs.

1.4.6. ACETYLCHOLINE, LEARNING, AND MEMORY

Attention, learning, and memory are closely related cognitive functions, as memory encoding follows attentional processes (Mineur and Picciotto 2021). Thus, it not surprising that, in addition to facilitating attention, ACh is also important for learning and memory. For example, abnormally regulated cholinergic neurotransmission has been hypothesized to contribute to the cognitive symptoms of neuropsychiatric disorders including schizophrenia, and the loss of cholinergic neurons is associated with severe forms of dementia and Alzheimer's disease (Haam and Yakel 2017; Hasselmo and Sarter 2011; Lustig and Sarter 2016). These deficits are likely to stem from abnormal interactions between ACh and nAChRs and mAChRs. Both α7 and α4β2 nAChRs are involved in new memory formation in the amygdala and hippocampus (Mineur and Picciotto 2021) and nAChR deficits are closely associated with cognitive impairments in Alzheimer's disease (Levin, 2002). Likewise, mAChR antagonists disrupt memory function in humans, non-human primates, and rodents (Hasselmo and Bower 1993) and AChE inhibitors can reverse these effects (Hasselmo and Sarter 2011). In fact, AChE inhibitors alone enhance cognitive performance (Hasselmo and Sarter 2011) and are currently the only class of cholinergic compounds approved by the FDA to treat Alzheimer's disease

(Hampel et al., 2018). Together these data clearly indicate an essential role of ACh in maintaining, if not facilitating, learning and memory.

Mechanistically, ACh is thought to facilitate learning by enhancing LTP, the cellular and molecular substrate of learning and memory (Luscher and Malenka 2012). ACh enhances LTP in numerous areas, including hippocampus, entorhinal cortex, and piriform cortex (Hasselmo 2006). Although there are numerous forms of LTP, most of ACh's enhancing effects appear to be associated with ACh receptor-mediated enhancement of NMDA receptor activation (Palacios-Filardo and Mellor 2019). There is some evidence that ACh can enhance NMDA receptor currents via nAChRs. For example, nAChRs on astrocytes can do so by evoking D-serine release (Papouin et al., 2017), and nAChRs on PNs can do so by depolarizing cells (Gu and Yakel 2011) or interacting with NMDA receptors directly (Li et al., 2013). However, there has been more focus on mAChRs in this regard. mAChRs have also been reported to enhance NMDA receptors via diverse mechanisms. mAChRs can enhance NMDA receptors via direct interactions (Fernández de Sevilla and Buño, 2010), by inhibiting the activity of voltage-dependent potassium channels (Losonczy et al., 2008; Palacios-Filardo and Mellor 2019; Petrovic et al., 2012), and by inhibiting the activity of voltage-independent, calcium-activated SK channels, which negatively regulate NMDA receptor currents (Buchanan et al., 2010; Calabresi et al., 1998; Dennis et al., 2016; Giessel and Sabatini 2010; Marino et al., 1998; Sur et al., 2003; Tigaret et al., 2018). Finally, both nAChRs and mAChRs on various types of INs can reconfigure network excitability to favor

NMDA-dependent LTP at specific synapses while inhibiting others (Palacios-Filardo and Mellor 2019).

1.5. SIGNIFICANCE REVISITED

Throughout the brain, there is abundant support for a facilitative role of ACh signaling in cognitive functions like attention and learning (Colangelo et al., 2019; Hasselmo and Sarter 2011; Palacios-Filardo and Mellor 2019; Picciotto et al., 2012). Two primary functions of the amygdala, mediated in large part by the circuitry of the BNC, involve cue-detection – which is closely tied to attention – and emotional memory – which is closely tied to LTP and learning. There is strong evidence from studies in the cortex that phasic activation of the CBF is essential for cue-detection and cue-driven behavior (Gritton et al., 2016; Howe et al., 2017; Lu et al., 2020b; Parikh et al., 2007), strongly overlapping with functions of the amygdala (Janak and Tye 2015). Interestingly, despite the very dense CBF innervation to the BL – a bridge between internal LA sensory inputs, outside modulatory glutamatergic inputs, outside neuromodulatory inputs, and numerous behaviorally relevant downstream brain regions (McDonald 2020; Sah et al., 2003) – no studies have probed the circuit- and molecular- level mechanisms by which endogenous ACh signaling might facilitate attention and LTP/learning at the LA-BL pathway. Further, the BNC contains distinct circuits that mediate the processing of negative and positive stimuli (Janak and Tye 2015; Kim et al., 2016, 2017; Pi et al., 2020; Yang et al., 2016; Zhang et al., 2020). Although evidence from a large body of recent literature seems to suggest that transient activity of CBF neurons

obeys prediction error principles and is most concerned with tracking the salience of stimuli irrespective of valence (Aitta-aho et al., 2018; Chubykin et al., 2013; Crouse et al., 2020; Guo et al., 2019; Hangya et al., 2015; Harrison et al., 2016; Jiang et al., 2016; Kuchibhotla et al., 2017; Laszlovszky et al., 2020; Letzkus et al., 2011; Liu et al., 2015; Sturgill et al., 2020; Teles-Grilo Ruivo et al., 2017), the possibility remains that the CBF differentially contributes to amygdalar valence processing by differentially impacting putative negative and positive circuits in the BL. Aberrant cholinergic signaling and dysfunction of the amygdala are both closely associated with various mood disorders, Alzheimer's disease, schizophrenia, among other conditions that currently lack effective treatments.

The experiments performed herein were designed to probe the circuit- and molecular-level mechanisms by which endogenous ACh might facilitate the attentional and learning-related functions of the amygdala by employing optogenetics, *in vitro* electrophysiology, and various anatomical techniques. Results generated from these studies offer new insight into the impact of ACh signaling on emotional circuitry that is required for maintaining mental health and could inform ongoing efforts to understand circuit dysfunction underlying and pharmacological treatments for such conditions.

CHAPTER 2

GENERAL METHODS

2.1. ANIMALS

2.1.1. ANIMAL CARE AND USE PROCEDURES

All animal care, use, and surgical procedures were performed in compliance with the National Institutes of Health guidelines for care and use of laboratory animals and approved by The Institutional Animal Care and Use Committee (IACUC) of the University of South Carolina. All mice were housed in temperature-controlled cages (with maximum of 5 mice per cage) and maintained on a 12-hour light/dark cycle with ad libitum food and water.

2.1.2. SURGICAL PROCEDURES FOR INJECTIONS OF RETROGRADE TRACERS

Stereotaxic injections were conducted on male and female ChAT-Cre mice (8-12 weeks, Jackson Laboratory, Bar Harbor, ME). All surgical procedures were performed under aseptic conditions using a stereotaxic instrument (Stoelting, IL) equipped with a 2µL, 30 gauge Hamilton Neuros Syringe. Mice were first anesthetized in an enclosed container with gaseous isoflurane (5%) and kept under anesthesia (2% isoflurane) using the stereotaxic frame for the

entire surgery. Mice were then unilaterally dual-injected into the NAc (AP: +2.5mm, ML: -1.0mm, DV: -4.7mm) and CeA (AP: -0.1mm, ML: -2.4mm, DV: -5.3mm) with Cholera Toxin Subunit B conjugated to Alexa Fluor 647 and 555 (CTB 647 and CTB 555), respectively.

2.1.3. ANIMALS USED FOR ELECTROPHYSIOLOGY

In most experiments, six- to 24-week-old ChAT-Cre/Ai32(ChR2-EYFP) transgenic mice of either sex were used, which express ChR2(H134R)-EYFP in cholinergic neurons. These were generated by crossing ChAT-Cre animas (#006410, The Jackson Laboratory) with Cre-dependent reporter Ai-ChR2-eYFP animals (#012569, Jackson Labs). In Chapter 4 experiments where muscarine was applied (Fig. 4.6.G-I.), male and female ChAT-Cre mice of a similar age were used instead.

2.2. SLICE PREPARATION FOR ELECTROPHYSIOLOGY RECORDINGS

Animals were deeply anesthetized with isoflurane and the brain was quickly extracted and submerged in ice-cold artificial cerebrospinal fluid (ACSF) saturated with 95% O2 and 5% CO2 and containing the following (in mM): 110 choline chloride, 2.5 KCL, 25 NaHCO3, 1.0 NaH2PO4, 20 glucose, 5 MgCl2, 0.5 CaCl2. Coronal brain slices (300μM thick) containing amygdala were sectioned using a vibratome (VT1000S; Leica, Nussloch, Germany) and immediately transferred to ACSF (saturated with 95% O2 and 5% CO2) containing (in mM) 125 NaCl, 2.7 KCl, 25 NaHCO3, 1.25 NaH2 PO4, 10 glucose, 5 MgCl2, 0.5

CaCl2. All slices were incubated at 34-36°C for a minimum of 20 minutes before the solution was allowed to equilibrate to room temperature.

2.3. ELECTROPHYSIOLOGY RECORDINGS

Individual slices were transferred from an incubating chamber to a recording chamber maintained at 32-34°C and continuously perfused with ACSF (saturated with 95% O2 and 5% CO2) containing 2 mM calcium and 1 mM magnesium. Pyramidal neurons were visualized using infrared-differential interference contrast optics through a 40x objective (Olympus BX51WI). Recordings were made using a Multiclamp 700B amplifier and filtered at 1 kHz. Recordings were digitized by a Digidata 1440A analog-todigital (A-D) board (Molecular Devices, Sunnyvale, CA) in a Windows-based computer using pClamp 10 software.

2.3.1. WHOLE-CELL RECORDINGS

Borosilicate glass electrodes of 4-6 MΩ resistance were used and filled with potassium gluconate internal solution consisting of (in mM) 130 K-gluconate, 5 KCl, 10 HEPES, 2 MgCl2, 2 MgATP, 0.3 NaGTP, 0.5 EGTA (pH 7.3). To patch a cell, positive pressure was first applied through the recording electrode and the electrode was lowered until a dimple surrounding the tip could be seen in the cell membrane. At this point, positive pressure was released, and, after a brief pause to allow membrane relaxation, negative pressure was subsequently and slowly applied until a cell membrane-electrode seal of giga-ohm resistance was formed. After another brief pause to allow things to settle, negative pressure was

delicately applied once more until the giga-ohm seal was broken and access to the inside of the cell was achieved.

2.3.2. SINGLE-UNIT RECORDINGS

As before, borosilicate glass electrodes of 4-6 MΩ resistance were used, but this time filled with recording ACSF instead of internal solution. The same steps described above were used to patch the cell with two exceptions: a loose seal of much lower resistance (200-500 MΩ) was acceptable, and the cell membrane was left intact. Compared to whole-cell recordings, this technique is 1) generally easier to perform, 2) preserves (or does not alter) the intracellular contents of the recorded cell, and 3) (related to #2) provides a more stable recording environment enabling longer recording sessions. A major disadvantage is that it only allows you to detect cell firing (i.e., you cannot monitor membrane potential changes).

2.4. OPTOGENETICS

Phasic and endogenous ACh release was evoked by delivering brief, single flashes of blue light (473nM; Thor Labs) directly over the recorded cells through a 40x lens, which activate ChR2 within cholinergic terminals in the slice. Light flashes were always applied at 60 sec intervals to avoid potential buildup of residual ACh in brain slices over the course of experiments.

2.5. BATH APPLICATION OF DRUGS

For some experiments, drugs were applied to the entire brain slice. Whenever applied this way, drugs were added to the recording ACSF and perfused through the recording chamber. Rarely, drugs were applied using a peristaltic pump. More commonly, they were applied via gravity-fed syringes. The latter approach is more convenient because it enables drugs to be applied much quicker due to a shorter distance to recording chamber, and multiple syringes containing different drugs can be successively applied in the same experiments. The flow rate of solutions applied via syringes was adjusted via clamps applied to the tubing leading to the recording chamber. For both methods, the flow rate was adjusted to be the same (roughly 2mL/min).

2.6. PUFF APPLICATION OF NMDA

For some experiments, NMDA was applied onto recorded cells via pressure-ejection. NMDA was dissolved in the same recording ACSF used for electrophysiology recordings and transferred into the same borosilicate glass electrodes described above. The same electrode puller was used to create tips with the same 4-6 MΩ resistance as recording electrodes, as well. These electrodes were then mounted onto a pipette holder that was connected via tubing to a picopump unit and an air tank. On the picopump unit itself, various pressure settings could be adjusted, such as the pressure strength and duration. Puff electrodes were always positioned approximately 50-100μM away from the cell body.

2.7. CONFOCAL IMMUNOFLUORESCENCE MICROSCOPY

2.7.1. GENERATION OF SLICES FOR SUBSEQUENT IMMUNOHISTOCHEMISTRY

Mice were anesthetized with isoflurane and intracardially perfused with ice-cold 0.1M phosphate buffered saline (PBS, pH 7.4) containing 0.5% sodium nitrite followed by ice-cold 4% paraformaldehyde (PFA) in 0.4M phosphate buffer (PB, pH 7.4). Brains were immediately extracted and postfixed overnight in 4% PFA in PB (0.4M, pH7.4) at 4°C. A Vibratome (Leica Microsystems) was used to collect sections at a thickness of 50 µm, which were then stored in 0.1M PBS (pH 7.4) at 4°C until further processing. All sections from each animal were later used for immunohistochemical processing.

2.7.2. GENERAL IMMUNOHISTOCHEMICAL PROCESSING OF SECTIONS

Sections were washed 3 times, 30 min total, in 0.05M tris-buffered saline solution (TBS pH 7.6). Sections were blocked with TBS containing 10% normal goat serum (NGS) and permeabilized with 0.5% Triton-X100 for 30 min. Sections were then washed with TBS (0.05M pH7.6) for 5 min 3 times. Sections were incubated overnight at room temperature with the primary antibody in 0.5% Triton and 2% NGS. The following day, sections were thoroughly washed with 0.05M TBS 3 times, 10 min per wash. Sections were then incubated for 3 hours, covered from light, with the secondary antibody in 0.5% Triton and 2% NGS.

Sections were washed for 5 min 3 times in 0.05M TBS and then 5 min 2 times in 0.05M tris-buffered solution (TB pH7.4), mounted on 0.5% gelatinized slides, and coverslipped with Prolong Diamond Antifade Mountant (Invitrogen, Thermo Fisher). In some cases, ProLongTM Antifade Mountant with DAPI (Invitrogen, Thermo Fisher) was used instead. All slides were kept in 4°C until imaging.

2.7.3. POST HOC VISUALIZATION OF RECORDED CELLS FILLED WITH BIOCYTIN

In some cases, biocytin (Sigma, St. Louis, MO) 0.2–0.4% was added to the internal recording solution used for electrophysiology experiments to enable later visualization of the neuron morphology. This tissue was processed as follows. After recordings were performed, slices were transferred from the recording chamber to 4% paraformaldehyde in 0.1 M phosphate buffer, where they remained for a minimum of 24-hours at 4 degrees C for fixation. Later, slices were resectioned at 50-75 µm on a vibratome. Sections were then rinsed in 3 changes of TBS (10 min each) and permeabilized with 0.5% Triton-X100 for 30 min, before incubation in Alexa-488-conjugated streptavidin (1:1,000; Invitrogen, Thermo Fisher) for 2-3 hours. Sections were then rinsed in 3 changes of TBS (10 min each), mounted on glass slides using Vectashield mounting medium (Vector Laboratories, Burlingame, CA) and examined with an Invitrogen EVOS FL Auto 2.0 Imaging system (Thermo Fisher Scientific Inc., USA) or a Leica SP8 Multiphoton Confocal System (Leica Microsystem Inc., IL, USA).

* See individual chapters for more detailed information pertaining to each study *

2.8. STATISTICAL ANALYSES

2.8.1. ELECTROPHYSIOLOGY

Data from electrophysiological recordings was analyzed using Clampfit 10.7 (Molecular Devices) and figures were made using Origin Lab Pro software. Statistical comparisons were performed using the appropriate t test or ANOVA with post hoc test. Values are given as mean ± SEM. A minimum of three animals were used for data presented in each figure.

2.8.2. CONFOCAL MICROSCOPY

All cell counting and M1R fluorescent intensity measurements were done using Fiji ImageJ 1.52i (National Institutes of Health, USA). For all ImageJ analysis performed, images were first converted to 8-bit greyscale. The Polygon Selection Tool was used to outline the borders between the various nuclei comprising the basolateral nuclear complex (BNC), which were determined by referencing a DAPI or Nissl counterstain in the same or a similar section and The Mouse Brain in Stereotaxic Coordinates (Paxinos and Franklin 2013). The borders of each nucleus were then added and saved to ROI manager. NAc and CeA projectors within the amygdala of each section were also outlined, added, and saved to the ROI manager, only instead by using the Oval Selection Tool. Ovals placed over each cell were identical in shape and size and did not overlap. Total projectors within the amygdala of each section were simply equal to the number of projector ROIs saved to the ROI manager for that population. The count of each type of projector within a given nucleus was determined using the

following steps. First, “Edit → Clear Outside” was performed with all ROIs of a given projector population selected, leaving behind the outline of only those projectors within the amygdala. Second, “Edit → Clear Outside” was repeated, only this time with the ROI of a nucleus of interest. This left behind only the projectors of a given population within that nucleus. Finally, these projectors were counted by ImageJ by first performing “Image → Adjust → Threshold” and then “Analyze → Analyze Particles”. These steps repeated for each projector population within each nucleus of each section of each animal. The CTB channel corresponding to the projector population being analyzed was used, although which channel is chosen should not matter because pixel intensity is not being measured. Average M1R intensity per nucleus was measured using the Measure function within the ROI manager while having a given nucleus selected in the M1 channel. Likewise, average M1R intensity per projector population was measured by repeating these steps while having the projector ROIs selected, instead. All final M1R intensities utilized during statistical tests were background subtracted values. Based on its consistently low M1R labeling, the average M1R intensity of the region approximating the stria terminalis – which was determined by comparing the Nissl or DAPI counterstain channel with The Mouse Brain in Stereotaxic Coordinates (Paxinos and Franklin 2013) – was used for background subtractions. Prior to T-tests, F-tests were performed to determine whether the variances between each group were equal or unequal. Afterwards, a student’s T-test was performed and interpreted based on the outcome of the preceding F-test.

CHAPTER 3

DIFFERENCES IN M1 MUSCARINIC RECEPTOR EXPRESSION BETWEEN PYRAMIDAL NEURONS OF THE BASOLATERAL NUCLEAR COMPLEX OF THE AMYGDALA

3.1. INTRODUCTION

The basolateral nuclear complex of the amygdala (BNC) – consisting of the lateral (LA), basolateral (BL), and basomedial nuclei (BM) – detects biologically important environmental stimuli and orchestrates appropriate behavioral responses to their implied meaning (Adolphs et al., 1994; Blanchard and Blanchard 1972; Brown and Schafer 1888; Klüver and Bucy 1937; LeDoux et al., 1990; McDonald 2020; Pitkänen et al., 1997; Weiskrantz 1956). The BNC processes representations of negative and positive stimuli, but there is ongoing debate over how its circuitry is organized to support these distinct computations (Ambroggi et al., 2008; Baxter and Murray 2002; Beyeler et al., 2016, 2018; Goosens and maren 2001; Gore et al., 2015; Janak and Tye 2015; Killcross et al., 1997; Kim et al., 2016, 2017; Namburi et al., 2015; Paton et al., 2006; Pignatelli and Beyeler 2019; Stuber et al., 2011; Tye 2018; Tye et al., 2008; Zhang et al., 2020).

Two bodies of literature have emerged describing the organization of negative and positive circuits within the BNC, with each emphasizing an

important role for pyramidal neurons (PNs) residing in the BL. Some studies suggest that PNs in the anterior BL (BLa) and posterior BL (BLp) correspond to negative and positive circuits, respectively (Kim et al., 2016, 2017; Pi et al., 2020; Yang et al., 2016; Zhang et al., 2020), while others suggest that intermingled populations of BL PNs projecting to different regions correspond to negative and positive circuits, with central amygdala (CeA) and nucleus accumbens (NAc) projectors representing two primary pathways that mediate the former and latter, respectively (Ambroggi et al., 2008; Beyeler et al., 2016, 2018; Namburi et al., 2015; Stuber et al., 2011; Tye et al., 2008).

The BL is heavily innervated by the cholinergic basal forebrain (Carlsen and Heimer 1986; Muller et al., 2011) and recent studies have shown that endogenous ACh signaling in this region is important for negative and positive emotional processing (Aitta-aho et al., 2018; Crouse et al., 2020; Guo et al., 2019; Hangya et al., 2015; Jiang et al., 2016). However, no studies published in peer-reviewed journals have directly compared whether ACh differentially modulates negative and positive emotional circuits within the BNC or BL using the projection- and location-based definitions described above.

A couple of anatomical studies from one group did examine the distribution and neuronal localization of the M1 muscarinic ACh receptor (M1R) in the rat BNC and observed that, in addition to being almost exclusively expressed on PNs, making them an ideal marker for this study, M1R labeling appeared most robust in the BLa compared to its other regions (McDonald and Mascagni 2010; Muller et al., 2013). However, because these studies were conducted

before the location-based definition of negative and positive circuits emerged, this finding was not reported in the context of valence processing. In addition, these studies did not quantify their reported differences in M1R expression between BCN regions. Finally, no studies published in peer-reviewed journals have attempted to compare M1R expression between projection-defined populations of neurons residing in the BNC or BL.

We had two hypotheses in this study. First, we thought M1R expression would be greatest in the BLa compared to the other regions of the BNC. Second, we believed M1R expression would be higher on whichever projector population (NAc or CeA projectors) had a larger proportion that resided in the BLa. We addressed these hypotheses with two aims. First, we quantified the average M1R immunofluorescence intensity of the BLa and compared it against the average intensity of the other regions of the BNC. Second, we compared M1R expression levels between CeA and NAc projectors. In the latter case, we first compared M1R expression of all CeA projectors in the BNC against all NAc projectors of the BNC. Subsequently, we repeated this comparison focusing on only the NAc and CeA projectors that resided in the BL (BLa and BLp), excluding the projectors of each population residing in the other BNC regions from analysis. Findings from this study will offer a fresh take on whether there is an anatomical basis for differential cholinergic modulation of putative negative and positive emotional circuits in the BNC and contribute to an understanding of ACh's role in valence processing in the amygdala by indicating whether putative negative and positive emotional circuits are differentially modulated by ACh signaling.

3.2. MATERIALS AND METHODS

3.2.1. ANIMALS

All animal care, use, and surgical procedures were performed in compliance with the National Institutes of Health guidelines for care and use of laboratory animals and approved by The Institutional Animal Care and Use Committee (IACUC) of the University of South Carolina. All mice were housed in temperature-controlled cages (with maximum of 5 mice per cage) and maintained on a 12-hour light/dark cycle with ad libitum food and water.

3.2.2. TISSUE PREPARATION, IMMUNOHISTOCHEMISTRY, AND RETROGRADE TRACING

3.2.2.A. M1R immunolabeling study design

Male ChAT-Cre mice (8-12 weeks, Jackson Laboratory, Bar Harbor, ME) were anesthetized with isoflurane and intracardially perfused with ice-cold 0.1M phosphate buffered saline (PBS, pH 7.4) containing 0.5% sodium nitrite followed by ice-cold 4% paraformaldehyde (PFA) in 0.4M phosphate buffer (PB, pH 7.4). Brains were immediately extracted and postfixed overnight in 4% PFA in PB (0.4M, pH7.4) at 4°C. A Vibratome (Leica Microsystems) was used to collect horizontal sections along the entire dorsal-ventral axis of the amygdala at a thickness of 50 μm, which were then stored in 0.1M PBS (pH 7.4) at 4°C until further processing. All sections from each animal were later used for M1R labeling. During M1R labeling, all sections from the same animal were processed in the same well and sections from different animals were processed in different wells simultaneously. Sections were washed 3 times, 30 min total, in 0.05M tris-

buffered saline solution (TBS pH 7.6). Sections were blocked with TBS containing 10% normal goat serum (NGS) and permeabilized with 0.5% Triton-X100 for 30 min. Sections were then washed with TBS (0.05M pH7.6) for 5 min 3 times. Sections were incubated overnight at room temperature with the primary antibody (see Table 1 below for product details) in 0.5% Triton and 2% NGS. The following day, sections were thoroughly washed with 0.05M TBS 3 times, 10 min per wash. Sections were then incubated for 3 hours, covered from light, with the secondary antibody (see Table 1 below for product details) in 0.5% Triton and 2% NGS. Sections were washed for 5 min 3 times in 0.05M TBS and then 5 min 2 times in 0.05M tris-buffered solution (TB pH7.4), mounted on 0.5% gelatinized slides, and coverslipped with Prolong Diamond Antifade Mountant (Invitrogen, Thermo Fisher). All slides were kept in 4°C until imaging.

3.2.2.B. Combined retrograde tracing and M1R immunolabeling study

Stereotaxic injections were conducted on male and female ChAT-Cre mice (8-12 weeks, Jackson Laboratory, Bar Harbor, ME). All surgical procedures were performed under aseptic conditions using a stereotaxic instrument (Stoelting, IL) equipped with a 2µL, 30 gauge Hamilton Neuros Syringe. Mice were first anesthetized in an enclosed container with gaseous isoflurane (5%) and kept under anesthesia (2% isoflurane) using the stereotaxic frame for the entire surgery. Mice were then unilaterally dual-injected into the NAc (AP: +2.5mm, ML: -1.0mm, DV: -4.7mm) and CeA (AP: -0.1mm, ML: -2.4mm, DV: -5.3mm) with Cholera Toxin Subunit B conjugated to Alexa Fluor 647 and 555 (CTB 647 and CTB 555), respectively (see Table 1 for product and injection

details). Ten days after injections, animals were perfused as indicated above. Coronal sections 50 μm thick were collected using a Vibratome (Leica Microsystems) and stored in 0.1M PBS (pH 7.4) at 4°C for later immunohistochemical processing. Consecutive sections were taken along the entire anteroposterior axis of the nucleus accumbens (NAc) and amygdala to verify the accuracy of both injection sites and capture the full extent of NAc and CeA projector and M1R distribution throughout the amygdala. Only mice with centers of injections confined to both the NAc and CeA in the same animal were selected for further processing and analysis (N =4, 1 male and 3 female). Three sections containing amygdala at predetermined anterior (-1.07mm AP), intermediate (-1.91mm AP), and posterior (-2.15mm AP) planes relative to Bregma according to The Mouse Brain in Stereotaxic Coordinates (Paxinos and Franklin 2013) were imaged to assess projector distribution and chosen to undergo subsequent M1R labeling, which involved the same procedure as above and the additional use of ProLongTM Antifade Mountant with DAPI.

3.2.3. IMAGE ACQUISITION AND DATA ANALYSIS

All images of NAc and CeA injection sites were collected using the Invitrogen EVOS FL Auto 2.0 Imaging system (Thermo Fisher Scientific Inc., USA). All sections collected from each animal containing NAc and CeA were imaged to verify the accuracy and spread of the injections. Tiled images were acquired with the 4x objective to view all sections on each slide. All images were captured using the brightfield setting. The NAc and CeA injections were visualized using the GFP and Cy5 filter cubes, respectively. The center, spread,

and localization of each injection were determined referencing The Mouse Brain in Stereotaxic Coordinates (Paxinos and Franklin 2013). Only mice with centers of injections confined to both the NAc and CeA in the same animal were selected for further processing and analysis (N =4, 1 male and 3 female). All sections containing amygdala that were processed and used for analysis were imaged using a Leica SP8 Multiphoton Confocal System (Leica Microsystem Inc., IL, USA). The same scope imaging settings were used for all confocal images collected (see Table 2 below for details). All cell counting and M1R fluorescent intensity measurements were done using Fiji ImageJ 1.52i (National Institutes of Health, USA). For all ImageJ analysis performed, images were first converted to 8-bit greyscale. The Polygon Selection Tool was used to outline the borders between the various nuclei comprising the basolateral nuclear complex of the amygdala (BNC), which were determined by referencing a DAPI or Nissl counterstain in the same or a similar section and The Mouse Brain in Stereotaxic Coordinates (Paxinos and Franklin 2013). The borders of each nucleus were then added and saved to ROI manager. NAc and CeA projectors within the amygdala of each section were also outlined, added, and saved to the ROI manager, only instead by using the Oval Selection Tool. Ovals placed over each cell were identical in shape and size and did not overlap. Total projectors within the amygdala of each section were simply equal to the number of projector ROIs saved to the ROI manager for that population. The count of each type of projector within a given nucleus was determined using the following steps. First, “Edit → Clear Outside” was performed with all ROIs of a given projector

population selected, leaving behind the outline of only those projectors within the amygdala. Second, “Edit → Clear Outside” was repeated, only this time with the ROI of a nucleus of interest. This left behind only the projectors of a given population within that nucleus. Finally, these projectors were counted by ImageJ by first performing “Image → Adjust → Threshold” and then “Analyze → Analyze Particles”. These steps repeated for each projector population within each nucleus of each section of each animal. The CTB channel corresponding to the projector population being analyzed was used, although which channel is chosen should not matter because pixel intensity is not being measured. Average M1R intensity per nucleus was measured using the Measure function within the ROI manager while having a given nucleus selected in the M1 channel. Likewise, average M1R intensity per projector population was measured by repeating these steps while having the projector ROIs selected, instead. All final M1R intensities utilized during statistical tests were background subtracted values. Based on its consistently low M1R labeling, the average M1R intensity of the region approximating the stria terminalis – which was determined by comparing the Nissl or DAPI counterstain channel with The Mouse Brain in Stereotaxic Coordinates (Paxinos and Franklin 2013) – was used for background subtractions. Prior to T-tests, F-tests were performed to determine whether the variances between each group were equal or unequal. Afterwards, a student’s T-test was performed and interpreted based on the outcome of the preceding F-test.

3.3. RESULTS

3.3.1. DIFFERENTIAL EXPRESSION OF THE M1R IN THE BNC

First, we sought to quantify differences in M1R expression between regions of the BNC by applying an antibody targeting the M1R to sections containing the amygdala and comparing M1R immunofluorescence intensity between regions of interest within the BNC. Horizontal sections were used because they contain the full anteroposterior axis of the amygdala. We applied the antibody to multiple sections taken from various points along the dorsoventral axis of the amygdala to assess the distribution of M1R expression throughout the entire BNC. We observed strong perikaryal staining confined to the cytoplasm and avoiding the nucleus (Fig. 3.1.A.). We also observed significant but slightly lighter labeling of the surrounding neuropil, which was punctate in nature (Fig. 3.1.A.). Both observations are consistent with previous reports (McDonald and Mascagni 2010; McDonald and Mott 2021; Muller et al., 2013).

We also observed significant variation in M1R immunolabeling along the anteroposterior axis of the amygdala, especially in intermediate sections containing BLa and BLp. The anterior half of the BL had a relatively uniform labeling pattern that was distinct from the posterior half (Fig. 3.1.B., right). Within the posterior half of the BL, immunofluorescence intensity was noticeably lighter. The labeling pattern in this region was also slightly different, with markedly fewer M1R+ perikarya and a sparser labeling of the neuropil (Fig. 3.1.B., top left vs. bottom left). These results suggest that the neuronal localization of M1R expression differs between neurons residing in the anterior and posterior BL.

Interestingly, there also appeared to be an M1R gradient along the anteroposterior axis, with the highest and lowest levels of M1R expression corresponding to the anterior and posterior regions, respectively. We also generated heat maps that assign warmer and cooler colors to brighter and darker pixels, which enable better visualization of this M1R expression gradient. An example of one of these heat maps can be seen on the right side of Figure 1C, which depicts and intermediate section containing BLa and BLp. We further quantified this gradient by measuring the average M1R fluorescence intensity of equally sized and spaced regions of interest (ROIs) running along the midline and anteroposterior axis (Fig. 3.1.C.; N=6 male mice). Together, these results suggest the existence of an anteroposterior M1R expression gradient, with the highest and lowest levels corresponding to the anterior and posterior regions, respectively.

We also determined whether M1R expression varies between different regions of the BNC. To do so, we measured the average M1R fluorescence intensity of ROIs outlining the BLa, BLp, LA, and posterior division of the BM (BMP) (Fig. 3.2.A.). Our analysis revealed that the BLa had the greatest M1R fluorescence intensity of all the regions analyzed. Interestingly, we also observed that the BLp had a significantly greater M1R fluorescence intensity than the LA (Fig. 3.2.B.). Although previous studies have already noted that M1R expression appears highest in the BLa (McDonald and Mascagni 2010; McDonald and Mott 2021; Muller et al., 2013), we are the first to quantitatively verify this observation.

3.3.2. DIFFERENTIAL DISTRIBUTION PATTERNS OF CEA AND NAC PROJECTORS AND THEIR CORRELATION WITH THE DISTRIBUTION OF M1R EXPRESSION IN THE BNC

We were ultimately interested in comparing M1R expression between each projector population. However, before we could do so, we first needed to establish the distribution pattern of CeA and NAc projectors throughout the BNC before we could correlate these patterns with the distribution of M1R expression in the same sections. To accomplish this task, we injected the retrograde tracers Cholera Toxin B (CTB) conjugated to Alexa Fluor 555 (CTB 555) into the NAc and CTB 647 into the CeA of the same animals to independently visualize each cell type in the same sections (Fig. 3.3.A.). In all animals, strong CTB 555 fluorescence can be seen in the NAc core and bordering the ventrally adjacent NAc shell, indicating the NAc projectors in the present study are likely a mix of NAc core and shell projectors. The strongest CTB 647 fluorescence of these animals can be seen in the CeL and CeC region, with possibly lighter fluorescence in the CeM, suggesting the CeA projectors in our study could represent a mix of CeL, CeC, and CeM projectors. After waiting for complete retrograde transport, we imaged the anterior, intermediate, and posterior coronal planes of the amygdala to assess and compare CeA and NAc projector distribution patterns throughout the BNC. This strategy successfully labeled three distinct populations of projector types that were differentially distributed throughout the BNC: CeA projectors, NAc projectors, and dual projectors, the latter of which innervate the CeA and NAc simultaneously (Fig. 3.3.B. and

3.3.C.). We counted a total of 2,410 cells, with 663 cells (27%) projecting to CeA, 1,468 cells (61%) projecting to NAc, and 279 cells (12%) projecting to both the CeA and NAc (N =4, 1 male and 3 female). The distribution pattern of each projector type from all animals can be seen in Figure 3.4. We noticed that CeA (red dots) and dual projectors (blue dots) appeared to preferentially localize to the more posterior and lateral aspects of the BNC (Fig. 3.4.B. and 3.4.C.), whereas NAc projectors (green dots) were more evenly distributed along the mediolateral and anteroposterior axes (Fig. 3.4.B.). Interestingly, very few NAc projectors localized to the posterior region of the LA (Fig. 3.4.B.).

Next, we repeated our M1R immunolabeling protocol from above in these same sections to see whether we could correlate the distribution of M1R expression in the BNC with the distribution of CeA and NAc projectors, two prominent examples of projectors associated with negative and positive emotions, respectively. We did not include dual projectors in this analysis because of how few there were and because their relevance to behavior is less known. On average, the intermediate sections of amygdala contained the greatest number of NAc projectors, followed by the anterior and posterior sections in descending order (Fig. 3.5.A., left). The average number of CeA projectors, on the other hand, gradually increased along the anteroposterior axis, with the lowest and highest numbers in the anterior and posterior sections, respectively (Fig. 3.5.A., left). NAc projectors outnumbered CeA projectors in every slice, with significant differences between the average number of NAc and CeA projectors in anterior and intermediate sections, but not posterior sections

(Fig. 3.5.A., left). Interestingly, the ratio by which NAc projectors outnumbered CeA projectors formed a steep and decreasing anteroposterior gradient, with the highest and lowest NAc/CeA ratios corresponding to the anterior and posterior sections, respectively (Fig. 3.5.A., middle). We measured the average M1R fluorescence intensity of the entire amygdala in these same sections and, interestingly, observed a decreasing gradient of M1R expression along anteroposterior axis that paralleled the decreasing anteroposterior NAc/CeA ratio gradient (Fig. 3.5.A., right). Although M1R fluorescence intensity was not significantly different between coronal sections, the decreasing anteroposterior trend we observe in these sections nicely supports our earlier finding that there is a decreasing gradient of M1R expression along anteroposterior axis of BL in horizontal sections (Fig. 3.2.B.). Together, these results establish that M1R expression is highest in sections of the amygdala where NAc projectors most significantly outnumber CeA projectors.

Next, we repeated this analysis focusing on subnuclei of the BNC. NAc projectors outnumbered CeA projectors in all four regions, with significant differences in the BLa and BMP (Fig. 3.5.B., left). Interestingly, the NAc/CeA ratio in the BLa was far greater than it was in the other regions (Fig. 3.5.B., middle). Specifically, the ratio by which NAc projectors outnumbered CeA projectors in the BLa (8.1±1.9) was approximately three time higher than it was in the BLp (2.7±1.1), approximately four times higher than it was in the BMP (2.1±1.1), and approximately five times higher than it was in the LA (1.5±0.5) (Fig. 3.5.B., middle). There were no significant differences between the NAc/CeA ratios of the

other regions. We measured the average M1R fluorescence intensity of the same nuclei in these same sections and, interestingly, found that M1R intensity was highest in the BLa (Fig. 3.5.B., right). Statistically, M1R expression in the BLa was also significantly greater than it was in the BLp, but not the other regions (Fig. 3.5.B., right). Together, these results establish that M1R expression is highest in the BLa, where the ratio by which NAc projectors outnumber CeA projectors is also substantially higher than it is in the other regions of the BNC.

3.3.3. DIFFERENTIAL EXPRESSION OF M1R ON CEA AND NAC PROJECTORS IN THE BNC

Our findings that NAc projectors substantially outnumbered CeA projectors in the same regions of the BNC where M1R expression was the highest led us to hypothesize that all NAc projectors would express more M1R compared to all CeA projectors. To test this hypothesis, we compared the average M1R fluorescence intensity of every NAc projector in the BNC with the average M1R fluorescence intensity of every CeA projector in the BNC. In support of our hypothesis, the average M1R fluorescence intensity of all NAc projectors in the BNC was significantly higher than the average M1R fluorescence intensity of all CeA projectors in the BNC (Fig. 3.6.A. and 3.B., left). Interestingly, 29 percent of all NAc projectors in the BNC resided in the BLa – where M1R intensity is the highest – compared to only 9 percent of all CeA projectors in the BNC (Fig. 3.6.B., middle and right), suggesting NAc projectors in the BNC could express more M1R than CeA projectors in the BNC because a larger portion of them reside in the BLa, where M1R expression is highest.

Reports suggest that CeA projectors and the BLa mediate negative emotions and NAc projectors and the BLp mediate positive emotions (Ambroggi et al., 2008; Baxter and Murray 2002; Beyeler et al., 2016, 2018; Goosens and maren 2001; Gore et al., 2015; Janak and Tye 2015; Killcross et al., 1997; Kim et al., 2016, 2017; Namburi et al., 2015; Paton et al., 2006; Pignatelli and Beyeler 2019; Stuber et al., 2011; Tye 2018; Tye et al., 2008; Zhang et al., 2020). Therefore, we also compared M1R expression levels between only the CeA and NAc projectors that resided in the BL (BLa and BLp combined). Since NAc projectors outnumber CeA projectors in the BLa substantially more than they do in the BLp (Fig. 3.5.B., middle) and M1R expression in the BLa is significantly higher than it is in the BLp (Fig. 3.2.B. and Fig. 3.5.B., right), we hypothesized that NAc projectors in the BL would express more M1R compared to CeA projectors in the BL. In support of our hypothesis, the average M1R fluorescence intensity of all NAc projectors in the BL was significantly higher than the average M1R fluorescence intensity of all CeA projectors in the BL (Fig. 3.7.A.). Interestingly, 43 percent of all NAc projectors in the BL resided in the BLa compared to 17 percent of all CeA projectors in the BL (Fig. 3.7.B.), suggesting NAc projectors in the BL express more M1R than CeA projectors in the BL because a much larger portion of BL NAc projectors reside in the BLa, where M1R expression is highest.

So far, our findings indicate that the location rather than projection target of BNC PNs determines their overall level of M1R expression. This led us to hypothesize that M1R expression of projection-defined PNs residing in the BLa

will have higher M1R expression compared to projection-defined PNs residing in the BLp, regardless of their projection target. Supporting this hypothesis, M1R expression on PNs of a given projector population that resided in the BLa was always significantly higher than M1R expression on PNs of the same projector population that resided in the BLp (Fig. 3.8.A.).

Our data so far has shown that NAc projectors express more M1R than CeA projectors, but whether this is because of where they project or are located within the BL is less clear. To address this, we compared M1R expression between CeA and NAc projectors residing in the same division of BL (BLa or BLp), as well as CeA projectors of the BLa and NAc projectors of the BLp. If projection target is the determining factor, we would expect NAc projectors to have more M1R regardless of location within BL. We found that there were no significant differences between NAc and CeA projectors residing in the same division (BLa or BLp) (Fig. 3.8.B.). Further, NAc projectors in the BLp did not have a higher M1R expression than CeA projectors in the BLa (Fig. 3.8.C.). Together, these results suggest that that the location of BL PNs with respect to the BLa, where M1R expression is highest, is a more important factor in determining whether PNs will express more M1R than their projection target.

3.4. DISCUSSION

Consistent with earlier reports (McDonald and Mascagni 2010; McDonald and Mott 2021; Muller et al., 2013), we found that M1R expression was highest in the BLa compared to the BLp and other regions of the BNC. Our study is the first to quantify these differences, as no studies published in peer-reviewed journals

had done so. We also compared M1R expression between the BLa and BLp because of recent reports suggesting that PNs in the BLa and BLp preferentially process negative and positive emotions, respectively (Kim et al., 2016, 2017; Pi et al., 2020; Yang et al., 2016; Zhang et al., 2020). Our finding of greater M1R expression in BLa compared to BLp may suggest that ACh preferentially modulates negative over positive emotional circuits.

A separate body of literature suggests that negative and positive emotional circuits are determined by downstream region they innervate, with intermingled populations of CeA and NAc projectors representing negative and positive circuits, respectively (Ambroggi et al., 2008; Beyeler et al., 2016, 2018; Namburi et al., 2015; Stuber et al., 2011; Tye et al., 2008). Therefore, we also compared M1R expression between these two cell types to see whether significant differences emerge. Interestingly, we found that NAc projectors distributed throughout the entire BNC and only the BL expressed significantly more M1R than CeA projectors distributed throughout the same regions. In contrast to above, this finding alone suggests ACh would preferentially influence positive over negative emotional circuits.

One hypothesis to explain this seeming contradiction is that NAc projectors in the BLa and BLp mediate negative and positive emotions, respectively, but that the consequence of their combined output (negative or positive valence) is biased towards which BL division most of them reside in. For example, if 75 percent of Population X resides in the positive BLp and 25 percent resides in the negative BLa, activation of 100 percent of them would lead to

positive emotion, since most of the output is positively biased. However, selective activation of the 25 percent of Population X projectors in the BLa would lead to negative emotion. This would be true of any projector population within the BL.

Supporting this, most of the NAc projectors in our study resided in the positive BLp, which is consistent findings from a previous study (Kim et al., 2016). Further, they supported this hypothesis by showing that selective photoactivation of BLa NAc projectors elicits negative, not positive, behaviors (see Kim et al., 2016, Supplemental Figure 9). This is interesting when considering that positive behaviors were produced by photoactivation of BL NAc projectors in earlier studies that didn't consider their distribution between BLa and BLp (Ambroggi et al., 2008; Stuber et al., 2011). It would be interesting to know if more of the BL NAc projectors they stimulated resided in the BLp compared to BLa. Taken together, these observations suggest it is possible that both the location and projection target definitions of negative and positive circuits are true, with projector populations biased toward negative or positive emotions depending on whether a larger fraction of their whole resides in the negative BLa or positive BLp. Within this framework, our findings would suggest that ACh preferentially influences negative over positive emotional circuits via greater M1R expression on negative BLa PNs, including a smaller subset of negative NAc projectors in the BLa.

We also found that more of our CeA projectors resided in the BLp, which is opposite of what we would expect since CeA projectors are reported to process negative emotions. The same group from above probed the CeA

projector population extensively in a follow up study and established that CeA projectors are comprised of negative and positive subsets that project to different nuclei within the CeA (Kim et al., 2016, 2017). Importantly, they found that negative CeA projectors project to the CeC subnucleus and reside in the BLa, while the positive CeA projectors project to the CeL and CeM and reside in the BLp. Therefore, since we observed most of our CeA projectors residing in the BLp, it is possible we preferentially targeted the positive CeA projectors that project to the CeL and CeM with our CTB injections. However, our injection sites indicated sparser CeM labeling, suggesting they might more heavily target the CeL. In a future study, it would be interesting to compare M1R expression between NAc projectors and CeA projectors projecting to each of the different subnuclei of the CeA.

It is also possible that a fraction of our CeA projectors (indicated by CTB 647) are NAc projectors unintentionally labeled by during our CeA injections. A significant portion of the axons from NAc projectors in the BNC pass through the CeA region we injected and a previous study has shown that CTB can enter fibers of passage near injection sites (Chen and Aston-Jones 1995). Iontophoretic injections are smaller than injections using the 30 gauge Hamilton Neuro Syringe and have been shown to avoid labeling fibers of passage. A previous study that used a needle to inject NAc with CTB (as we did here) obtained a similar distribution of NAc projectors to us (Beyeler et al., 2018), whereas the distribution of NAc projectors labeled by iontophoretic injections into NAc of other studies (McDonald 1991a, 1991b) appeared to produce slightly

different patterns, with perhaps sparser labeling of the posterior BLp. Therefore, it is possible some of the most posterior CeA projectors in our study are NAc projects labeled by uptake of CTB 647 into fibers of passage through the CeA region.

Regardless of valence, our results ultimately suggest that differences in M1R expression between PNs is determined by their location in the BNC rather than their projection target. Supporting this, our earlier observation that NAc projectors express more M1Rs than CeA projectors is likely due to a much larger percentage of these cells residing in the BLa, where M1R expression is highest, compared to CeA projectors. Further, PNs located in the BLa always had a higher M1R expression than PNs in the BLp, regardless of where they projected, including BLa CeA projectors compared to BLp NAc projectors.

Interestingly, we also noticed a nonsignificant trend of higher M1R expression on NAc compared to CeA projectors within each division. These observations could suggest an intricate scenario. Broadly, by way of a higher M1R expression in the BLa compared to BLp, ACh could preferentially modulate negative over positive emotional circuits. Simultaneously, however, ACh could also preferentially modulate negative and positive NAc projectors over negative and positive CeA projectors. If true, the precise translation of this observation to behavior is hard to predict. Future studies employing projection-specific in vivo optogenetic techniques should explore this possibility further to determine whether it could be true.

Our results provide an anatomical basis for future physiological and behavioral studies to expand on, as the consequence of a greater M1R expression in the BLa compared to other BNC regions can only be speculated here. M1R are known to increase PN excitability and have been shown to be important for emotional learning and memory consolidation (Power et al., 2003a, 2003b; Power and Sah 2008; Washburn and Moises 1992). Therefore, if the BLa represents an area of the BNC where negative emotions are preferentially processed, ACh may act through these M1R expression differences to preferentially enhance BLa excitability at various points of behavior (encoding, consolidation, etc.), promoting negative emotional bias. If true, perhaps there is an evolutionary advantage of prioritizing negative over positive valence. For example, it may be more beneficial for survival to react to unexpected stimuli with defensive rather than appetitive behavior.

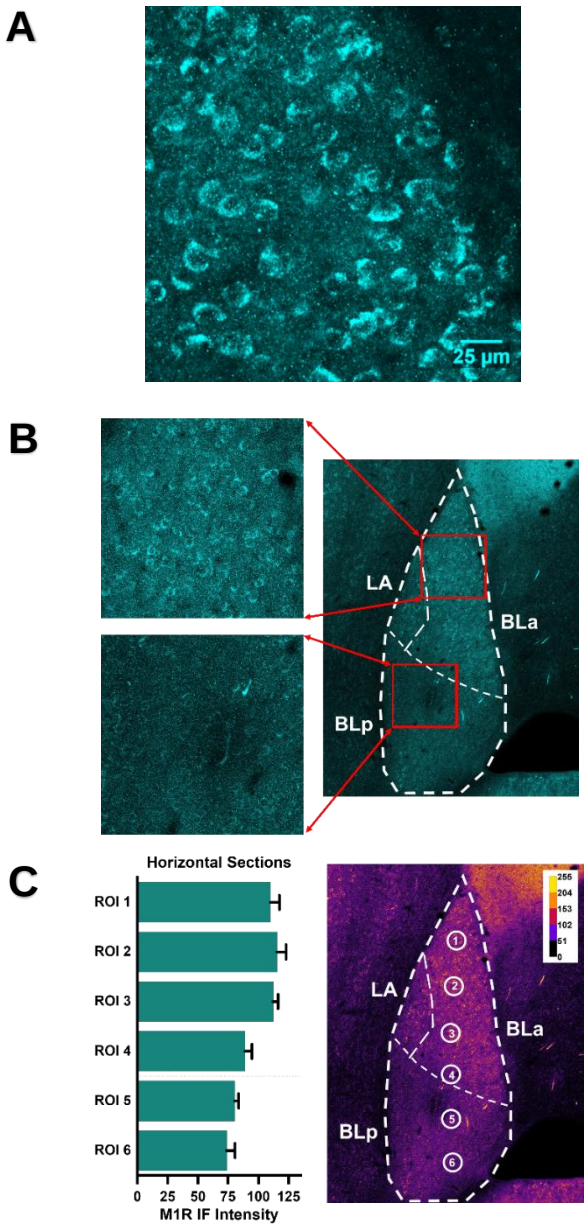

Figure 3.1. M1R expression varies along the anteroposterior axis of the BL. A. Representative image (maximum projected 40x water Z-stack) of M1R immunolabeling in BLa. **B. (Right)** Representative image (maximum projected 20x tiled Z-stack) of M1R immunolabeling in a horizontal section from the intermediate plane of the dorsoventral axis of the amygdala and **(Left)** cropped and zoomed images corresponding to the red squares in right image depicting M1R immunolabeling differences between the BLa and BLp. **C. (Right)** Pixel intensity heat map of the same image from the right side of B. to facilitate visualization of M1R expression differences along the anteroposterior axis of BL and (Left) the average M1R immunofluorescence intensity of

equally sized and spaced ROIs running along the midline and anteroposterior axis of the BL (N = 6 mice). An example of each ROI is illustrated on the heat map on the right side of C.

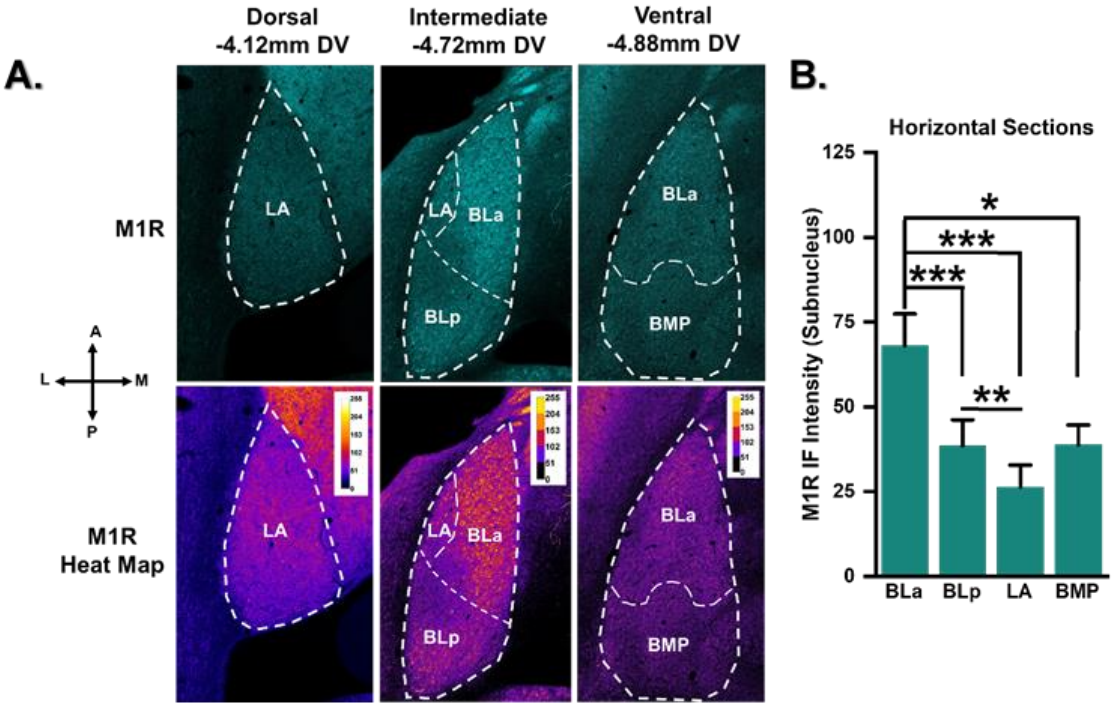

Figure 3.2. M1R expression varies between the different regions of the BNC. A. Representative images (all maximum projected 20x tiled Z-stack) of M1R immunolabeling in horizontal sections from the dorsal **(Left),** intermediate **(Middle)**, and ventral **(Right)** planes of the dorsoventral axis of the amygdala. The images in the bottom row are pixel intensity heat maps of the same images above them to facilitate visualization of M1R expression differences throughout the BNC. **B.** Average M1R immunofluorescence intensity of BLa, BLp, LA, and BMP (N = 6 mice). * = $p < 0.01$, ** = $p < 0.01$, *** $p < 0.001$.

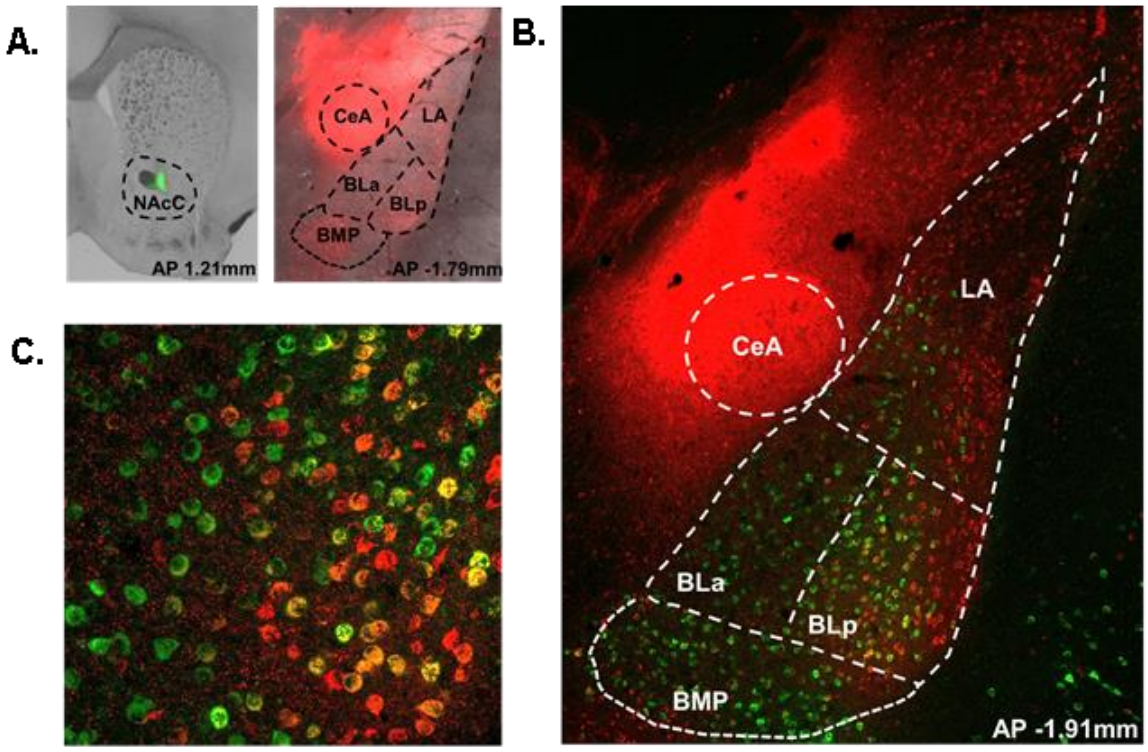

Figure 3.3. Injecting CTB into the NAc and CeA of the same animals labels distinct populations of projection neurons in the BNC. A. Representative EVOS images (4x) of CTB 555 **(Left)** and CTB 647 **(Right)** injections in the NAc and CeA, respectively, of the same mouse. **B.** Representative SP8 image (maximum projected 20x tiled Z-stack) of a coronal section of BNC from the intermediate plane of the anteroposterior axis depicting NAc, CeA, and Dual projectors in the same slice and mouse as A. **C.** Representative image (maximum projected 40x water Z-stack) of NAc, CeA, and Dual projectors in the BLa of the same mouse as B. and C. Green = CTB 555 (NAc projectors), Red = CTB 647 (CeA projectors), Orange = CTB 555 and CTB 647 in came cells (Dual projectors).

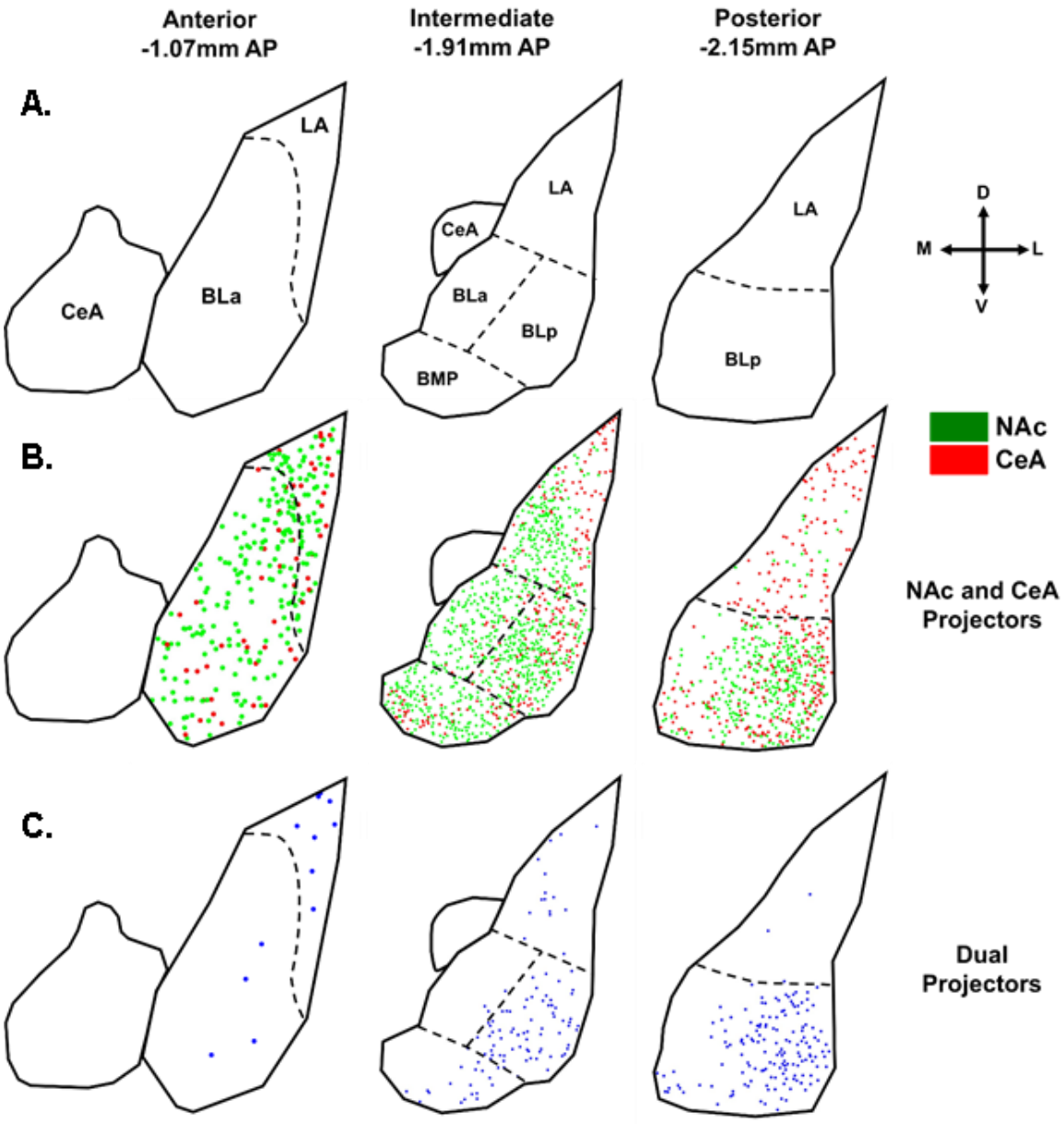

Figure 3.4. NAc and CeA projectors have different distribution patterns throughout the BNC. A. Templates of the anterior **(Left)**, intermediate **(Middle)**, and posterior **(Right)** coronal sections of BNC that were used for mapping projector distributions. **B.** Dot plots depicting the distribution of all NAc and CeA projectors counted (N = 4 mice) on the templates depicted in A. **C.** Same as B. but depicting the Dual projectors instead (same 4 mice).

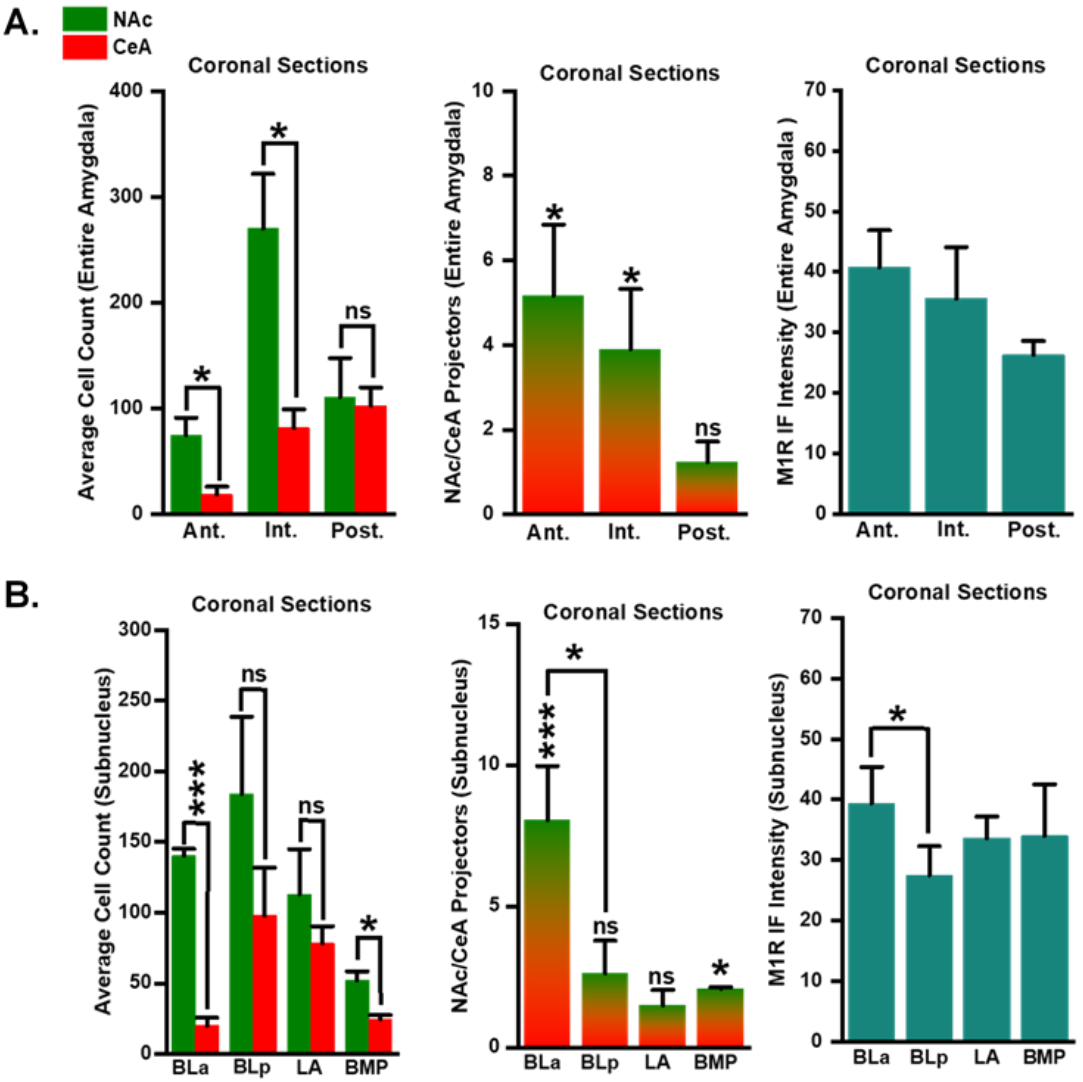

Figure 3.5. M1R expression is highest in regions where NAc projectors outnumber CeA projectors. A. Left. Side-by side comparisons of the average number of NAc and CeA projectors in each coronal plane of the BNC. **Middle.** The average number of NAc projectors in each coronal plane of BNC divided by the average number of CeA projectors in the same coronal planes of the BNC. **Right.** Average M1R immunofluorescence intensities in each coronal plane of the BNC. **B. Left.** Side-by side comparisons of the average number of NAc and CeA projectors in the BLa, BLp, LA, and BMP. **Middle.** The average number of NAc projectors in the BLa, BLp, LA, and BMP divided by the average number of CeA projectors in the same subregions of the BNC. **Right.** Average M1R immunofluorescence intensities in the BLa, BLp, LA, and BMP. All analysis in this figure is of the same 12 sections and 4 mice (an anterior, intermediate, posterior section per animal). * = $p < 0.01$, ** = $p < 0.01$, *** $p < 0.001$.

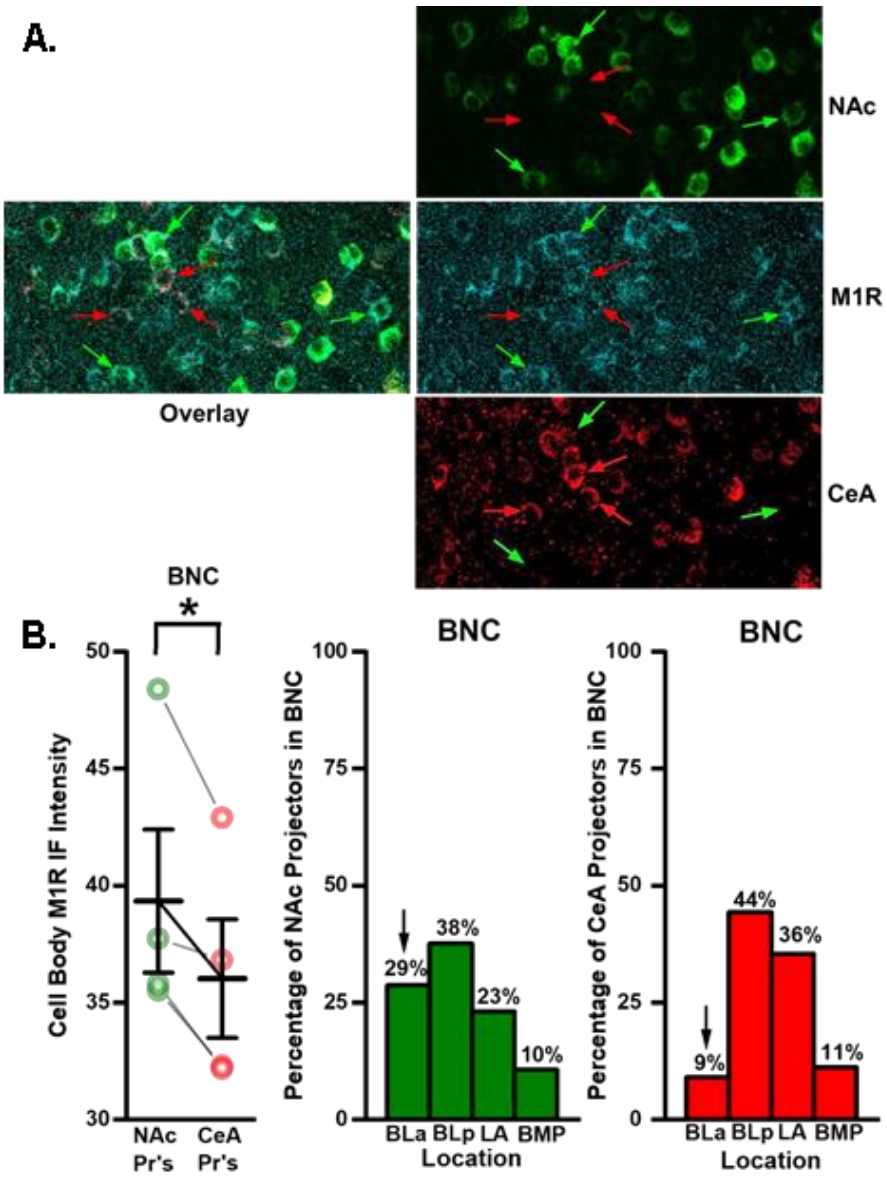

Figure 3.6. NAc projectors in the BNC express more M1R than CeA projectors in the BNC. A. A representative image (maximum projected 40x water Z-stack, zoomed and cropped) of differential M1R immunolabeling of CeA and NAc projectors in the BLa of the same slice. Red arrows point to CeA projectors selectively labeled with M1R. Green arrows point to NAc projectors selectively labeled with M1R. **B. Left.** Average M1R immunofluorescence intensity of all CeA projectors (red dots) and all BLp projectors (green dots) in the entire BNC (N = 4 mice). **Middle and right.** The percentage of all BNC NAc projectors (middle) and all BNC CeA projectors (right), analyzed in B., that distribute into the BLa, BLp, LA, and BMP. Arrows emphasize differences in the BLa, where M1R expression is highest. * = $p < 0.01$, ** = $p < 0.01$, *** $p < 0.001$.

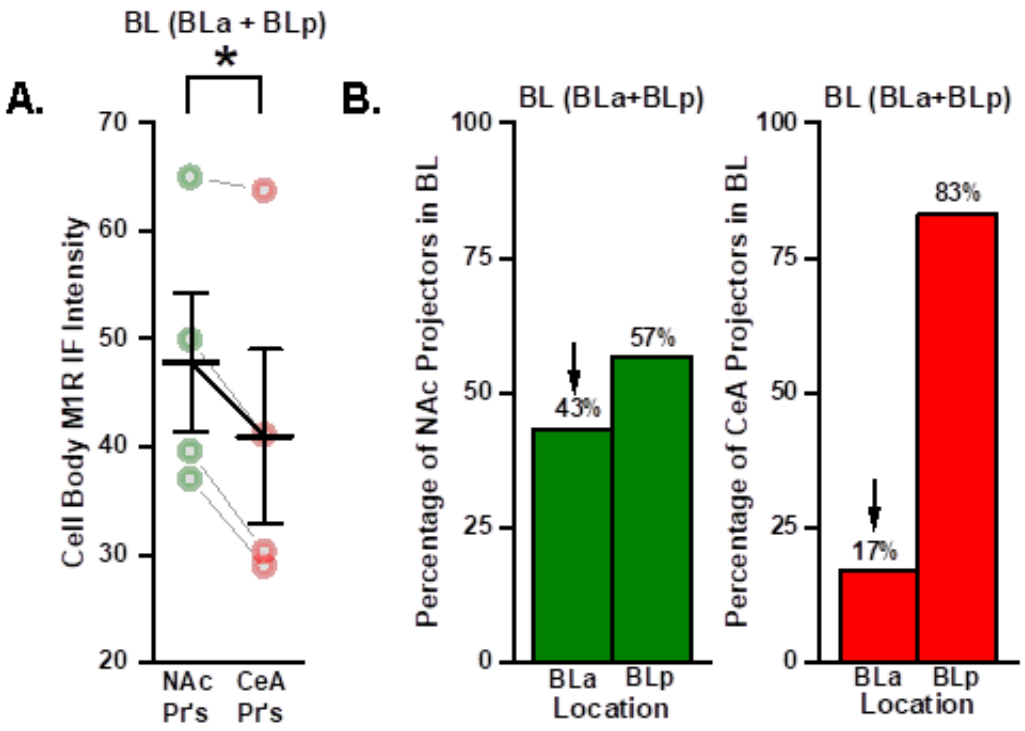

Figure 3.7. NAc projectors in the BL express more M1R than CeA projectors in the BL. A. Average M1R immunofluorescence intensity of only the CeA projectors (red dots) and BLp projectors (green dots) residing in the BL (BLa + BLp) (N = 4 mice). **B.** The percentage of BL NAc projectors (left) and BL CeA projectors (right), which were analyzed in A., that distribute into the BLa or BLp. Arrows emphasize even larger differences in the BLa, where M1R expression is highest. * = $p < 0.01$, ** = $p < 0.01$, *** $p < 0.001$.

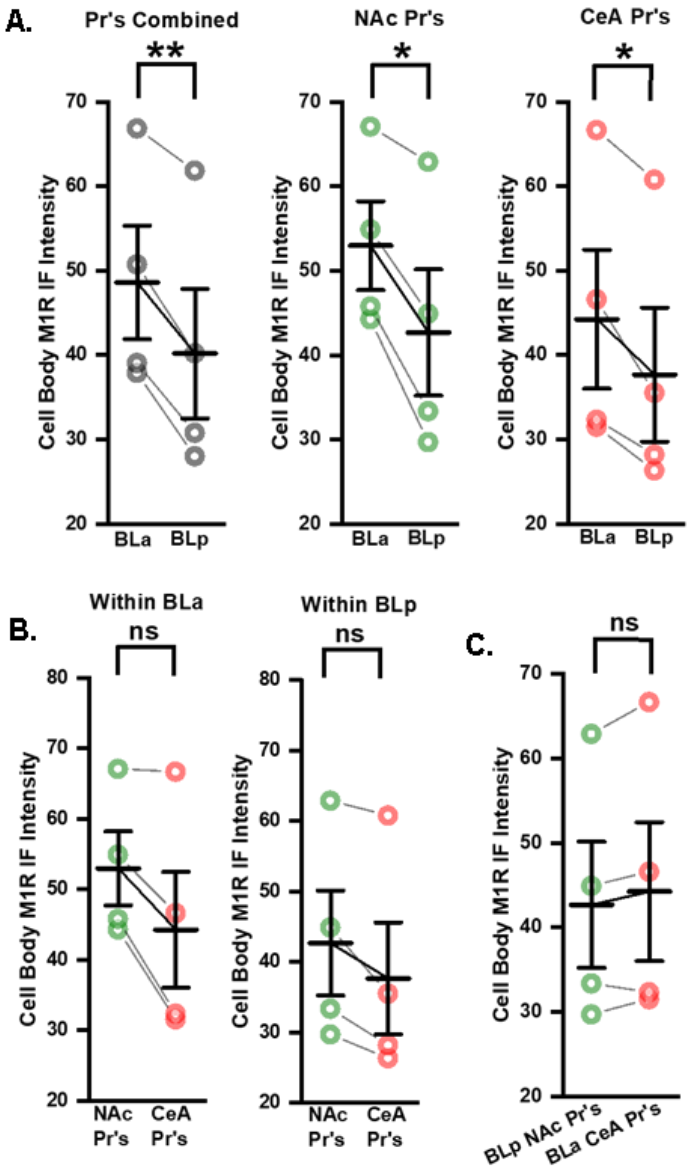

Figure 3.8. M1R expression differences between BL CeA and NAc projectors are determined by distribution with respect to BLa, not projection target. A. Left. Average M1R immunofluorescence intensity of CeA and NAc projectors combined residing in the BLa (left side) and BLp (right side). **Middle.** Average M1R immunofluorescence intensity of NAc projectors residing in the BLa (left side) and BLp (right side). **Right.** Average M1R immunofluorescence intensity of CeA projectors residing in the BLa (left side) and BLp (right side). **B. Left.** Average M1R immunofluorescence intensity of NAc projectors (left side) and CeA projectors (right side) residing within the BLa. **Right.** Average M1R immunofluorescence intensity of NAc projectors (left side) and CeA projectors (right side) residing within the BLp. **C.** Average M1R immunofluorescence intensity of NAc projectors residing in the BLp (left side) and CeA projectors residing in the BLa (right side).

All analysis in this figure is of the same sections from the same 4 mice. * = $p < 0.01$, ** = $p < 0.01$, *** $p < 0.001$.

Table 3.1. Product information.

Antibodies				
Type, Target	**Product Name**	**Company**	**Concentration**	**Product Number**
1° Ab, M1R	Rabbit anti-mAChR-M1-Rb-Af340	Frontier Institute Co., Ltd	1:400	AB_2571791
2° Ab, Rabbit Ab	Goat anti-rabbit-Alexa Fluor 488	Thermo Fisher	1:400	A21447
Counterstain				
Product Name		**Company**	**Concentration**	**Product Number**
NeuroTrace™ 530/615 Red Fluorescent Nissl Stain		Invitrogen	1:100	N21482
ProLong™ Diamond Antifade Mountant with DAPI		Thermo Fisher	N/A	P36971
Retrograde Tracer				
Product Name		**Company**	**Volume Injected**	**Product Number**
Cholera Toxin B, Alexa Fluor™ 555 Conjugate (CTB 555)		Invitrogen	150nL	C34776
Cholera Toxin B, Alexa Fluor™ 647 Conjugate (CTB 647)		Invitrogen	70nL	C34778

Table 3.2. Leica SP8 microscope settings. All images analyzed were collected using these settings. PH 3 was chosen for the 488nm laser because it produced optimal visualization of M1R signal. The same PH 3 was chosen for the other lasers to minimize variations in imaging settings between channels. Fluorescence intensity produced from the 555nm and 638nm lasers were not compared with fluorescence intensity produced from the 488nm laser.

Objective	Pinhole (AU)	Laser Line - Intensity	Gain	Offset	Scan Speed	Z (µm)
10x	3	488nm - 5%	850	-8	600	6.37
20x	3	488nm - 5%	900	-65	400	10.88
		555nm - 5%	740	-13		
		638nM - 3.5%	790	-45		
40x Water	3	488nm - 5%	960	-45	400	15.69
		555nm - 5%	680	-16		
		638nM - 3.5%	720	-47		

CHAPTER 4

PHASIC ACETYLCHOLINE ASSOCIATIVELY AND TEMPORALLY IMPROVES THE SIGNAL-TO-NOISE RATIO OF INTERNAL INPUTS TO PYRAMIDAL NEURONS IN BASAL NUCLEUS OF THE AMYGDALA

4.1. INTRODUCTION

The basolateral nuclear complex of the amygdala (BNC) – consisting of the lateral (LA), basolateral (BL), and basomedial nuclei (BM) – detects salient environmental stimuli (cue-detection) and orchestrates appropriate behavioral responses to their implied meaning (cue-guided behavior) (Adolphs et al., 1994; Blanchard and Blanchard 1972; Brown and Schafer 1888; Klüver and Bucy 1937; LeDoux et al., 1990; McDonald 2020; Pitkänen et al., 1997; Weiskrantz 1956). Whether a selected behavior is appropriate depends partly on the value of the perceived stimulus. Some stimuli have negative value and motivate aversive behaviors (like avoidance), while others have positive value and motivate appetitive behaviors (like approach) (Pignatelli and Beyeler 2019; Tye 2018). The BNC responds to both types of stimuli and mediates both types of behaviors (Belova et al., 2008; Bermudez and Schultz, 2010; Gore et al., 2015; Janak and Tye 2015; LeDoux et al., 1990; Paton et al., 2006).

The function above is accomplished through a precise pattern of internal circuitry. Sensory information representing environmental stimuli enters the LA, splits into parallel streams that move into the anterior (BLa) and posterior (BLp) divisions of the BL and activates specific populations of pyramidal neurons (PNs) located in different regions of the BL that project to different brain areas (Beyeler et al., 2018; Janak and Tye 2015; Jimenez and Maren, 2009; Kim et al., 2016; LeDoux 2000; Maren, 2001; Pitkänen et al., 1997). BLa and BLp PNs are reported to preferentially process negative and positive emotions, respectively (Kim et al., 2016, 2017; Pi et al., 2020; Yang et al., 2016; Zhang et al., 2020), suggesting the LA-BLa and LA-BLp pathways do as well.

Internal information streams conveying sensory information from LA to BLa and BLp PNs are modulated by diverse extra-amygdalar inputs (Pitkänen et al., 1997). Therefore, the ability of LA terminals to fire these different PNs and, consequently, the BNC to attribute salience and valence to environmental stimuli is also under their influence. Interestingly, the cholinergic basal forebrain (CBF) innervates the BL more heavily than any of its other targets (Carlsen and Heimer 1986; Muller et al., 2011), highlighting acetylcholine (ACh) as a prime candidate for mediating these effects via its interactions with LA inputs onto BLa and BLp PNs. Our lab has previously shown that the BLa receives a greater cholinergic innervation than the BLp, suggesting ACh could preferentially modulate LA-BLa PN over LA-BLp PN circuits.

ACh is a neuromodulator that alters synaptic transmission and neuronal excitability by activating nicotinic (nAChRs) and muscarinic (mAChRs) receptors

on distinct cell types and circuit components (Crouse et al., 2020; Laszlovszky et al., 2020; Picciotto et al., 2012). ACh has well-established roles in attention and arousal (Everitt and Robbins 1997; Hasselmo and Sarter 2011) and substantial evidence from hippocampus and cortex indicate that nAChRs and mAChRs cooperate to enhance the signal-to-noise ratio of inputs, a postulated mechanism for the cholinergic enhancement of attention to and encoding of salient stimuli (Colangelo et al., 2019; Hasselmo 2006; Lustig and Sarter 2016; Mineur and Picciotto 2021). Interestingly, no studies have determined whether nAChRs and mAChRs cooperate to enhance the signal-to-noise ratio (SNR) of LA inputs to BLa and BLp PNs.

Mounting evidence suggests that ACh can signal rapidly (or phasically) via point-to-point synapses (Colangelo et al., 2019; Dasgupta et al., 2018; Disney and Higley 2020; Hangya et al., 2015; Hedrick and Waters 2015; Joshi et al., 2016; Letzkus et al., 2011; Muñoz and Rudy 2014; Nelson and Mooney 2016; Sarter and Lustig 2020; Urban-Ciecko et al., 2018) and ACh is phasically released during negative and positive emotional experiences (Hangya et al., 2015; Laszlovszky et al., 2020; Sturgill et al., 2020; Teles-Grilo Ruivo et al., 2017). Phasic ACh release in cortex is intimately associated with cue-detection and cue-guided behavior (Gritton et al., 2016; Howe et al., 2017; Lu et al., 2020; Parikh et al., 2007; Sarter and Lustig 2019) – key functions of the amygdala – and phasic activation of cholinergic terminals in BNC in response to salient stimuli facilitates attention to and learning of cue-reward contingencies (Crouse et al., 2020).

Despite the overlapping functions of phasic ACh release and BNC circuits in cue-detection and cue-guided behavior, no studies have examined the impact of phasic ACh on the ability of the LA inputs to fire BLa and BLp PNs. Therefore, this was the focus of our study. We hypothesized phasic ACh would preferentially direct information flow from LA inputs through BLa PNs over BLp PNs by recruiting nAChRs and mAChRs to enhance SNR. We tested this hypothesis with two aims. First, we compared the effects of phasic ACh on BLa and BLp PN membrane potential and excitability in response to LA inputs. Second, we determined the molecular mechanisms underlying these effects. Findings from this study will provide novel insight into the circuit- and molecular- mechanisms by which ACh signaling could modulate attention, learning and memory, and valence processing mediated by the BNC.

4.2. MATERIALS AND METHODS

4.2.1. ANIMAL CARE AND USE PROCEDURES

All animal care, use, and surgical procedures were performed in compliance with the National Institutes of Health guidelines for care and use of laboratory animals and approved by The Institutional Animal Care and Use Committee (IACUC) of the University of South Carolina. All mice were housed in temperature-controlled cages (with maximum of 5 mice per cage) and maintained on a 12-hour light/dark cycle with ad libitum food and water.

4.2.2. ANIMALS

In most experiments, six- to 24-week-old ChAT-Cre/Ai32(ChR2-EYFP) transgenic mice of either sex were used, which express ChR2(H134R)-EYFP in

cholinergic neurons. These were generated by crossing ChAT-Cre animas (#006410, The Jackson Laboratory) with Cre-dependent reporter Ai-ChR2-eYFP animals (#012569, Jackson Labs). In experiments where muscarine was applied (Fig. 4.6.G. and 4.6.H.), male and female ChAT-Cre mice of a similar age were used instead. All mice were group housed in a climate-controlled facility with a 12/12 light/dark cycle and provided with ad libitum access to food and water.

4.2.3. SLICE PREPARATION

Animals were deeply anesthetized with isoflurane and the brain was quickly extracted and submerged in ice-cold artificial cerebrospinal fluid (ACSF) saturated with 95% O_2 and 5% CO_2 and containing the following (in mM): 110 choline chloride, 2.5 KCl, 25 $NaHCO_3$, 1.0 NaH_2PO_4, 20 glucose, 5 $MgCl_2$, 0.5 $CaCl_2$. Coronal brain slices (300μM thick) containing amygdala were sectioned using a vibratome (VT1000S; Leica, Nussloch, Germany) and immediately transferred to ACSF (saturated with 95% O2 and 5% CO2) containing (in mM) 125 NaCl, 2.7 KCl, 25 $NaHCO_3$, 1.25 NaH_2 PO_4, 10 glucose, 5 $MgCl_2$, 0.5 $CaCl_2$. All slices were incubated at 34-36°C for a minimum of 20 minutes before the solution was allowed to equilibrate to room temperature. For recordings, individual slices were transferred to a recording chamber maintained at 32-34°C and continuously perfused with ACSF (saturated with 95% O_2 and 5% CO_2) containing 2 mM calcium and 1 mM magnesium.

4.2.4. SLICE ELECTROPHYSIOLOGY RECORDINGS

PNs were visualized using infrared-differential interference contrast optics through a 40x objective (Olympus BX51WI). For whole cell recordings,

borosilicate glass electrodes of 4-6 MΩ resistance filled with potassium gluconate internal solution consisting of (in mM) 130 K-gluconate, 5 KCl, 10 HEPES, 2 MgCl2, 2 MgATP, 0.3 NaGTP, 0.5 EGTA (pH 7.3) were used. In some cases, biocytin (Sigma, St. Louis, MO) 0.2–0.4% was added to the internal solution for post hoc visualization of the neuron location and morphology. For single unit recordings, the internal solution was replaced with ACSF, the recording electrode was positioned close to the cell membrane, and the holding current was adjusted to a setting resulting in zero output from the amplifier. Phasic and endogenous ACh release was evoked by delivering brief, single flashes of blue light (473nM; Thor Labs) directly over the recorded cells through a 40x lens. Light durations varied from 1-4ms, 7ms, and 10ms and were always applied at 60 sec intervals. Electrical stimulation of glutamatergic LA input was achieved by delivering single or dual (50ms apart) pulses of current (0.1ms) every 20 sec through a monopolar stimulating electrode positioned in LA. All LA EPSCs were recorded at a holding potential of -70mV. In some experiments, ACh was phasically released an early or late interval in relation to single or paired LA stimulation. At the early interval, a single 10ms flash or pair of 10ms flashes (50ms apart) were delivered simultaneously with a single or paired stimulation of LA, respectively. At the late interval, a single 10ms flash was delivered 160ms before a single or paired stimulation of LA. In all experiments combining cholinergic and LA stimulation, light was applied once every third electrical stimulation, or 60 sec apart. In whole cell experiments recording LA EPSCs, a stable EPSC baseline was achieved before starting the experiment. To determine the effect of light on EPSC

amplitude, direct post-synaptic currents produced by optically released ACh alone were recorded and subtracted from evoked EPSC traces where light was also applied. Whenever drugs were used, they were added to ACSF and perfused through recording chamber during recordings.

4.2.5. CONFOCAL IMMUNOFLUORESCENCE

4.2.5.A. Validation of selective expression of ChR2 in cholinergic neurons

In one set of experiments (see Figure 4.1.), we validated the selective expression of ChR2 in the cholinergic neurons of our transgenic ChAT-Cre/Ai32(ChR2-EYFP) mice. To do so, we first perfused them and prepared 50μm thick coronal brain sections containing the horizontal limb of the diagonal band of Broca (HDB), a region of the CBF, which we used for subsequent confocal immunohistochemistry. Images were collected as maximum projected z-stacks. Cholinergic neurons in the HDB were identified via immunolabeling targeting choline acetyltransferase (ChAT), an enzyme that synthesizes ACh. Specifically, we used a goat anti-ChAT primary antibody (Millipore, [1:500]) and a donkey anti-goat IgG secondary antibody conjugated to Alexa Fluor 546 (Thermo Fisher, [1:400]). ChAT positive (ChAT+) and ChR2 positive (ChR2+) cells were defined as cells that were labeled by ChAT immunolabelling (red) and transgenic expression of eYFP (green), respectively. Cells with both markers (ChAT+ ChR2+) appeared orange when imaging. For quantification, cells of each group in the HDB were counted by hand and two definitions of percent overlap were used (depicted in Figure 4.1.B.): ChAT+ cells that also expressed ChR2 (red

cells that were also green) (Figure 4.1.B., Bottom, Left) and ChR2+ cells that also expressed ChAT (green cells that were also red) (Figure 4.1.B., Bottom, Right). We also imaged these same channels in coronal sections containing the BLa (see Figure 4.1.C).

4.2.5.B. Post hoc visualization of recorded cells with biocytin

In some cases, biocytin (Sigma, St. Louis, MO) 0.2–0.4% was added to the internal recording solution to enable later visualization of the neuron morphology. After recordings were performed, slices were transferred from the recording chamber to 4% paraformaldehyde in 0.1 M phosphate buffer, where they remained for a minimum of 24-hours at 4 degrees C for fixation. Later, slices were resectioned at 50-75 µm on a vibratome. Sections were then rinsed in 3 changes of TBS (10 min each) and permeabilized with 0.5% Triton-X100 for 30 min, before incubation in Alexa-488-conjugated streptavidin (1:1,000; Invitrogen, Thermo Fisher) for 2-3 hours. Sections were then rinsed in 3 changes of TBS (10 min each), mounted on glass slides using Vectashield mounting medium (Vector Laboratories, Burlingame, CA) and examined with an Invitrogen EVOS FL Auto 2.0 Imaging system (Thermo Fisher Scientific Inc., USA) or a Leica SP8 Multiphoton Confocal System (Leica Microsystem Inc., IL, USA).

4.2.6. ANALYSES AND STATISTICS

Data from electrophysiological recordings was analyzed using Clampfit 10.7 (Molecular Devices) and figures were made using Origin Lab Pro software. Statistical comparisons were performed using the appropriate t test or ANOVA

with post hoc test. Values are given as mean ± SEM. A minimum of three animals were used for data presented in each figure.

4.3. RESULTS

4.3.1. DEFINING THE RESPONSE TO PHASIC RELEASE OF ENDOGENOUS ACETYLCHOLINE

4.3.1.A. ChR2 is selectively expressed in cholinergic neurons of our ChAT-Cre/Ai32(ChR2-EYFP) mice

Our first goal was to anatomically verify that ChR2 was expressed selectively in the cholinergic neurons of our ChAT-Cre/Ai32(ChR2-EYFP) transgenic mice, as intended. Figure 1A and 1C show significant overlap (orange) between ChAT antibody immunofluorescence (red) and ChAT promoter-driven eYFP-ChR2 fusion protein fluorescence (green). Figure 1C shows cholinergic terminals in the BLa. Figure 1B quantifies the number of ChAT+ HDB cell bodies (877) that also express ChR2 (690) (78.7% overlap) and the number of ChR2+ HDB cell bodies (694) that also express ChAT (690) (99.4% overlap). One hundred and eighty-seven of the 877 ChAT antibody+ cells did not express ChR2, whereas only four of the 694 ChR2+ cells were not labeled by the ChAT antibody (data not shown). Together, these anatomical data suggest ChR2 is selectively expressed in the cholinergic neurons of our ChAT-Cre/Ai32(ChR2-EYFP) transgenic mice.

4.3.1.B. Phasic acetylcholine release produces a biphasic response in BLa pyramidal neurons

To determine the impact of phasic and endogenous ACh release on BLa PN membrane potential, we next performed whole cell recordings from BLa PNs voltage clamped at -60mV while delivering brief flashes of blue light (10ms duration; 473nm; 60 sec apart; Fig. 4.2.A.). We found that phasic ACh release reliably and repeatably evoked a biphasic response in BLa PNs (Fig. 4.2.B.), comprised of a fast depolarization or early EPSC (amplitude = -25.93 ± 2.57 pA, time to peak from light = 22.58 ± 1.53 ms, n = 46 cells; Fig 4.2.C) that always preceded a slower hyperpolarization or late IPSC (amplitude = 38.78 ± 2.45 pA, time to peak from light = 181.2 ± 3.47 ms, n = 46 cells; Fig. 4.2.C.). Our observation of the late IPSC is consistent with earlier reports that also recorded the responses of BLa PNs to optically evoked endogenous ACh release in the amygdala (Aitta-aho et al., 2018; Jiang et al., 2016; Unal et al., 2015). Interestingly, however, our study appears to be the first to report the presence of a faster depolarization (or early EPSC) immediately preceding it.

4.3.2. DEFINING THE MOLECULAR AND CIRCUIT MECHANISMS UNDERLYING EACH COMPONENT OF THE RESPONSE TO PHASIC ACETYLCHOLINE RELEASE

4.3.2.A. The early cholinergic EPSC is mediated by α7 and α4β2 nicotinic receptors located on presynaptic glutamate terminals

Our observation that phasic release of endogenous ACh evokes an early EPSC in BLa PNs is novel and unreported. Therefore, we focused on elucidating its underlying mechanism first. Given the rapid onset of the early EPSC following photostimulation, we suspected it would be mediated by the activation of nicotinic ACh receptors (nAChRs), whereas we suspected the late IPSC would not be. To test these hypotheses, we repeated the photostimulation protocol from Figure 2 (a 10ms flash) and measured the amplitudes of the cholinergic EPSC and IPSC in the absence and presence of the general nAChR antagonist mecamylamine (MEC, 20µM). MEC significantly decreased the amplitude of the early EPSC (ACSF: -34.86 ± 8.67 pA, MEC: -11.63 ± 1.01 pA, 38.98 ± 4.70% of the EPSC remained, n = 9 cells, p = 0.025, two-tailed paired t test; Fig. 4.3.B. and 4.3.E.) and had no effect on the late IPSC (ACSF: 30.98 ± 9.33 pA, MEC: 26.99 ± 7.33 pA, 79.91 ± 8.0% of the IPSC remained, n = 9 cells, p = 0. 0.212, two-tailed paired t test; Fig. 4.3.B. and 4.3.E.), suggesting the early EPSC, but not late IPSC, is mediated by the activation of nAChRs.

Next, we wanted to determine the circuit-level mechanism by which the nAChRs activated by phasic ACh release produce the early EPSC. There is evidence that nAChRs in the BL can evoke GABA release onto PNs (Pidoplichko et al., 2013; Unal et al., 2015; Zhu et al., 2005). To test this possibility, we compared the amplitude of the early EPSC in ACSF with its amplitude in the presence of the $GABA_A$ receptor antagonist picrotoxin (Pic, 50 µM). Pic had no

effect on the amplitude of the early EPSC (ACSF: -20.97 ± 2.81 pA, Pic: -20.17 ± 2.68 pA, 98.89 ± 13.53% of the EPSC remained, n = 5 cells, p = 0.764, two-tailed paired t test; Fig. 4.3.C., middle, and Fig. 4.3.E.) nor the amplitude of the late IPSC (ACSF: 56.37 ± 14.59 pA, Pic: 50.39 ± 13.11. pA, 95.22 ± 10.84% of the IPSC remained, n = 5 cells, p = 0.173, two-tailed paired t test; Fig. 4.3.C., middle, and Fig. 4.3.E.), suggesting the early EPSC is not mediated by the $GABA_A$ receptor. It is also unlikely we would be able to detect $GABA_A$ receptors currents in our recordings because our cells were voltage clamped near $GABA_A$ receptor reversal, at -60mV. Thus, our experimental conditions and results combined suggest that neither the early cholinergic EPSC nor the late cholinergic IPSC are mediated by GABA release onto $GABA_A$ receptors evoked by activation of nAChRs.

The nAChRs responsible for the early cholinergic EPSC could be located postsynaptically on BLa PNs and directly depolarize them via positive current influx (Klein and Yakel, 2006). Alternatively, they could be located presynaptically on glutamate terminals and indirectly depolarize them by evoking glutamate release (Jiang et al., 2013, 2016; Jiang and Role, 2008). We tested both possibilities by first measuring the size of the cholinergic EPSC and IPSC in the absence and presence of the AMPA receptor antagonist 6-cyano-7-nitroquinoxaline-2,3-dione (CNQX, 20 µM). If the nAChRs are located on the postsynaptic cell, we would expect CNQX to have no effect on the early EPSC nor the late IPSC. However, if the nAChRs are located on presynaptic glutamate terminals instead, we would expect CNQX to reduce the size of the early EPSC

to a similar extent as MEC without affecting the size of the late IPSC. We found that CNQX significantly decreased the amplitude of the early EPSC (ACSF: -53.41 ± 7.42 pA, CNQX: -21.38 ± 1.59 pA, 42.01 ± 3.85% of the EPSC remained, n = 5 cells, p = 0.009, two-tailed paired t test; Fig. 4.3.C., left, and Fig. 4.3.E.) and had no effect on the late IPSC (ACSF: 45.04 ± 7.44 pA, CNQX: 51.92 ± 4.71 pA, 120.17 ± 8.43% of the IPSC remained, n = 5 cells, p = 0.137, two-tailed paired t test; Fig. 4.3.C., left, and Fig. 4.3.E.), suggesting the early EPSC, but not the late IPSC, is mediated by AMPA receptors. To verify this finding, we repeated this experiment by replacing CNQX with a cocktail of synaptic blockers (containing CNQX and Pic and sometimes also MK801 and CGP), which eliminates other receptors commonly involved in synaptic transmission potentially contributing to the early EPSC. Cocktail decreased the amplitude of the early EPSC (ACSF: -33.34 ± 5.15 pA, cocktail: -9.81 ± 0.96 pA, n = 19 cells, p = 0.0003, two-tailed paired t test; Fig. 4.3.C., right, and Fig. 4.3.E.) to a similar extent as CNQX alone (37.86 ± 5.66% of the EPSC remained in cocktail versus 42.01 ± 3.85% in CNQX alone; Fig. 4.3.E.), without affecting the late IPSC (ACSF: 45.04 ± 7.44 pA, CNQX: 51.92 ± 4.71 pA, 102.91 ± 4.66% of the IPSC remained, n = 5 cells, p = 0.137, two-tailed paired t test; Fig. 4.3.C., right, and Fig. 4.3.E.), confirming that the early EPSC, but not late IPSC, is mediated by an AMPA receptor. Finally, CNQX alone and cocktail decreased the amplitude of the early EPSC to the same extent as MEC (38.98 ± 4.70% of the EPSC remained in MEC versus 37.86 ± 5.66% in cocktail and 42.01 ± 3.85% in CNQX alone, Fig.

4.3.E.), suggesting the early EPSC, but not late IPSC, is mediated by glutamate release evoked by nAChRs located on presynaptic glutamate terminals.

Next, we were interested in determining which nAChR subtype(s) mediate(s) the early cholinergic EPSC. We suspected a possible contribution of both α4β2 and α7 nAChRs because previous studies have shown that both can evoke glutamate release from cortical inputs in the BLa (Jiang et al., 2013; Jiang and Role, 2008). First, we focused on the α4β2 subtype by measuring the size of the cholinergic EPSC and IPSC in the absence and presence of the α4β2 nAChR antagonist dihydro-β-erythroidine hydrobromide (DHβE, 1 μM). DHβE significantly decreased the amplitude of the early EPSC (ACSF: -42.28 ± 9.78 pA, DHβE: -29.57 ± 7.51 pA, 65.43 ± 11.69% of the EPSC remained, n = 11 cells, p = 0.0087, two-tailed paired t test; Fig. 4.3.D. and 4.3.E.) and had no effect on the late IPSC (ACSF: 48.10 ± 8.76 pA, DHβE: 44.40 ± 4.98 pA, 99.50 ± 5.93% of the IPSC remained, n = 11 cells, p = 0.55, two-tailed paired t test; Fig. 4.3.D. and 4.3.E.), suggesting α4β2 nAChRs contribute to the early EPSC, but not late IPSC. We also repeated this experiment replacing DHβE with the α7 nAChR antagonist methyllycaconitine (MLA, 100 nM) to assess whether α7 nAChRs are also involved in the early EPSC. As we saw with DHβE, MLA significantly decreased the amplitude of the early EPSC (ACSF: -40.48 ± 9.96 pA, MLA: -27.58 ± 6.30 pA, 74.89 ± 8.68% of the EPSC remained, n = 11 cells, p = 0.049, two-tailed paired t test; Fig. 4.3.D. and 4.3.E.) without affecting the late IPSC (ACSF: 46.17 ± 8.68 pA, MLA: 43.13 ± 7.02 pA, 95.04 ± 6.02% of the IPSC remained, n = 11 cells, p = 0.35, two-tailed paired t test; Fig. 4.3.D. and 4.3.E.).

Interestingly, the size of the effects of DHβE alone and MLA alone on the early EPSC were similar (65.43 ± 11.69% of the EPSC remained in DHβE and 74.89 ± 8.68% remained in MLA) but also noticeably smaller than MEC, CNQX alone, and cocktail (38.98 ± 4.70% remained in MEC, 42.01 ± 3.85% of the EPSC remained in CNQX alone, and 37.86 ± 5.66% remained in cocktail), suggesting the early EPSC is mediated by a combination of α4β2 and α7 nAChRs (Fig. 4.3.E.). If true, we would expect the simultaneous application of DHβE and MLA to reduce the early EPSC to a similar extent as MEC, CNQX alone, and cocktail. DHβE and MLA decreased the amplitude of the early EPSC (ACSF: -42.39 ± 10.81 pA, DHβE+MLA: -15.81 ± 4.10 pA, n = 10 cells, p = 0.015, two-tailed paired t test; Fig. 4.3.D. and 4.3.E.) without affecting late IPSC (ACSF: 4 46.76 ± 9.57 pA, DHβE+MLA: 38.38 ± 4.23 pA, 92.47 ± 9.50% of the IPSC remained, n = 10 cells, p = 0.37, two-tailed paired t test; Fig. 4.3.D. and 4.3.E.). Supporting our hypothesis, the size of the effect of DHβE and MLA combined on the early EPSC (40.51 ± 10.72% remained) was similar to MEC (38.98 ± 4.70%), CNQX alone (42.01 ± 3.85% remained), and cocktail (37.86 ± 5.66%) (Fig. 4.3.E.), indicating the early cholinergic EPSC, but not the late cholinergic IPSC, is mediated by both α4β2 and α7 nAChRs.

4.3.2.B. The late cholinergic IPSC is mediated by M1 muscarinic receptors located on postsynaptic pyramidal neurons that are coupled to GIRK channels

It has previously been reported that endogenous ACh release into the BL causes an IPSC mediated by postsynaptic M1 muscarinic ACh receptors

(mAChRs) linked to G protein-gated inwardly rectifying potassium (GIRK) channels (Aitta-aho et al., 2018; Jiang et al., 2016; Unal et al., 2015). Therefore, we sought to determine whether the late IPSC component of the biphasic response to phasic ACh release was mediated by the same mechanism. In these experiments, we applied the same photostimulation protocol from Figures 2 and 3. First, we tested whether the late IPSC was mediated by the activation of postsynaptic mAChRs by measuring the amplitude of the pharmacologically isolated late IPSC in the absence and presence of the general mAChR antagonist atropine (ATR, 5 µM). ATR significantly decreased the amplitude of the late IPSC (cocktail: 39.53 ± 5.05 pA, ATR: 0.689 ± 0.689 pA, 1.089 ± 1.089% of the IPSC remained, n = 12 cells, p = 0.000006, two-tailed paired t test; Fig. 4.4.A.), suggesting it is mediated by the activation of postsynaptic mAChRs. Next, we sought to determine whether the late IPSC was mediated by the M1 mAChR subtype (M1R) by measuring the effect of the M1 mAChR antagonist pirenzepine (PRZ, 1 µM) on size the isolated IPSC. PRZ significantly decreased the amplitude of the late IPSC (cocktail: 36.35 ± 10.02 pA, PRZ: 4.42 ± 1.70 pA, 14.03 ± 5.085% of the IPSC remained, n = 6 cells, p = 0.017, two-tailed paired t test; Fig. 4.4.B.), suggesting the late IPSC is mediated by activation of M1R. Next, we sought to determine the ion conductance underlying the M1R-mediated late IPSC. To do so, we recorded the amplitude of the isolated late IPSC in response to phasic ACh release (a 10ms flash) as the recorded cell was voltage clamped at a range of different membrane potentials (from -110 to -50 mV). The amplitude of the late IPSC was voltage-dependent and reversed around -100 mV

(Fig. 4.4.C.). Linear fit analysis of the late IPSC provided a reversal potential of (-103.09 ± 11.78 mV; n = 7 cells; Fig. 4.4.C.), very close to the calculated reversal potential for the potassium ion under our conditions (-103.20 mV; Nernst Equation), suggesting the late IPSC is mediated by the opening of an inwardly rectifying potassium channel. To determine whether the inwardly rectifying potassium channel mediating the late IPSC is linked to a G protein signaling cascade stemming from M1R activation, we next attempted to occlude the late cholinergic IPSC by comparing its size in the absence of drug (ACSF) with its size in the presence of the $GABA_B$ receptor agonist baclofen (Bac, 20 µM), which stimulates the GIRK channel. If the M1R's activated by phasic ACh release mediate the late IPSC by transiently opening GIRK channels, as suspected, releasing ACh in the presence of Bac should no longer produce the late IPSC since Bac will already be keeping a majority of the GIRK channels constantly open. Bac significantly decreased the amplitude of the late IPSC (ACSF: 47.40 ± 9.90 pA, Bac: 14.12 ± 4.53 pA, 27.62 ± 5.96% of the IPSC remained, n = 9 cells, p = 0.0008, two-tailed paired t test; Fig. 4.4.D.), confirming that the late IPSC, but not early EPSC, is mediated by M1R activation of GIRK channels. Finally, to confirm that the late cholinergic IPSC is mediated by a GIRK channel located on the postsynaptic neuron, we recorded the amplitude of the late IPSC in response to phasic ACh release (a 10ms flash) in ACSF while the internal solution was filled with the selective GIRK-channel blocker QX-314 (5 mM) (Andrade, 1991; Hu et al., 2002). The amplitude of the late IPSC recorded in ACSF and cells filled with QX-314 was significantly smaller than it was in a separate group of cells

recorded in ACSF and regular internal without QX-314 (regular internal (n = 46 cells): 38.78 ± 2.45 pA vs. QX-314 internal (n = 4 cells): 13.75 ± 8.91 pA, p = 0.006, two-tailed unpaired t test; Fig. 4.4.E.), indicating QX-314 blocked the late IPSC and that it is mediated by a postsynaptic GIRK channel.

4.3.3. COMPARING THE RESPONSE OF BLA PYRAMIDAL NEURONS TO PHASIC ACETYLCHOLINE RELEASE WITH PNS IN THE BLP

Recent studies have reported that the BLa and BLp preferentially process negative and positive emotions, respectively (Kim et al., 2016, 2017; Pi et al., 2020; Yang et al., 2016; Zhang et al., 2020) but no studies have attempted to compare the cholinergic modulation of PNs in these two divisions of the BL. Therefore, we wanted to explore this possibility next.

4.3.3.A. BLa and BLp pyramidal neurons can be distinguished by their active and passive electrical properties

Previous studies have reported that BLa and BLp PNs are non-overlapping, morphologically, and electrophysiologically distinct cell types (Kim et al., 2016; McDonald 1982; Sah et al., 2003). Therefore, we first sought to distinguish between BLa and BLp PNs based on their electrophysiological characteristics. We found that BLa and BLp PNs can be distinguished based on numerous passive and active electrical properties (Figure 5 and Table 1). Consistent with a previous report, we found that BLa PNs (n = 20 cells) have a larger membrane capacitances (BLa Cm = 45.9 ± 0.71 pF versus BLp Cm = 34.29 ± 0.5 pF, p = 2.55E-16, two-tailed unpaired t test; Table 1), lower

membrane resistances (BLa Rm = 115.5 ± 5.45 ΩM versus BLp Rm = 147.71 ± 7.4 ΩM, p = 0.0013, two-tailed unpaired t test; Table 1), more negative resting membrane potentials (BLa RMP = -71.35 ± 0.92 mV versus BLp RMP= -68 ± 0.96 pF, p = 0.016, two-tailed unpaired t test; Table 1), and lower spike thresholds (BLa Spike Thresh = -42.26 ± 0.69 mV versus BLp Spike Thresh = -40.19 ± 0.74 mV, p = 0.048, two-tailed unpaired t test; Table 1) compared to BLp PNs (n = 21 cells). The larger membrane capacitances of BLa PNs reflects a larger soma size compared to BLp PNs, which is consistent with the reports mentioned above. We are also the first to report that BLa PNs have a shorter delay to initial spike onset (BLa (n = 20 cells): 318.04 ± 47.92 ms versus BLp (n = 21 cells): 596.67 ± 88.14 ms p = 0.0093, two-tailed unpaired t test; Table 1 and Fig. 4.5.C. and 4.5.G.), have more diverse types of initial spikes (BLa: 10/20 cells (50%) singlet and 10/20 cells (50%) doublet versus BLp: 21/21 cells (100%) singlet; Fig. 4.5.D.), and display a greater frequency of spontaneous synaptic events (BLa (n = 20 cells): 3.23 ± 0.73 Hz versus BLp (n = 10 cells): 13.40 ± 3.81 Hz, p = 0.024, two-tailed unpaired t test; Fig. 4.5.H.). Together, these data verify and build upon previous work demonstrating that BLa and BLp PNs can be distinguished based on their electrophysiological characteristics.

4.3.3.B. Phasic acetylcholine release preferentially impacts BLa over BLp pyramidal neurons

Next, we tested the relative sensitivities of BLa and BLp PNs to phasic and endogenous ACh release by performing whole cell recordings from BLa and BLp PNs while delivering single flashes of blue light that gradually increased in

duration (1-4ms, 7ms, and 10ms; 473nm; 60 seconds apart; Fig. 4.6.A.iii.). We found that a majority of BLa PNs responded to weak cholinergic stimuli (2ms flash: 16/23 cells or 70%, 3ms flash: 20/23 cells or 87%), whereas the same stimuli produced no responses in BLp PNs (2ms and 3ms flashes: 0/13 cells or 0%) (Fig. 4.6.B. and 4.6.C.). When the maximal cholinergic stimulus (a 10ms flash) was applied, it produced responses in all BLa PNs (50/50 cells or 100%; Fig. 4.6.B. and 4.6.C.) but only a minority of BLp PNs (11/36 cells or 31%; Fig. 4.6.B. and 4.6.C.). BLa PNs also had larger response amplitudes than BLp PNs in response to identical cholinergic stimuli (Fig. 4.6.B. and 4.6.D.). At the 4ms duration, BLa PNs had an early EPSC amplitude of -15.78 ± 1.76pA and a late IPSC amplitude of 22.72 ± 1.66 pA (n = 29 cells) compared to an early EPSC amplitude of 0 pA and late IPSC amplitude of 2.11 ± 1.43 pA in BLp PNs (n = 26 cells) (late IPSC: p = 7.71E-13, two-tailed unpaired t test; Fig. 4.6.D.). At the 7ms duration, BLa PNs had an early EPSC amplitude of -17.74 ± 1.95pA and a late IPSC amplitude of 26.46 ± 1.81 pA (n = 29 cells) compared to an early EPSC amplitude of -1.14 ± 0.80 pA and late IPSC amplitude of 3.64 ± 1.73 pA in BLp PNs (n = 25 cells) (early EPSC: p = 1.97E-9, two-tailed unpaired t test; late IPSC: p = 2.231E-12, two-tailed unpaired t test; Fig. 4.6.D.). At the 10ms duration, BLa PNs had an early EPSC amplitude of -38.40 ± 7.10pA and a late IPSC amplitude of 40.52 ± 2.60 pA (n = 50 cells) compared to an early EPSC amplitude of -5.05 ± 1.63 pA and late IPSC amplitude of 7.11 ± 2.05 pA in BLp PNs (n = 36 cells) (early EPSC: p = 2.77E-5, two-tailed unpaired t test; late IPSC: p = 4.02E-16, two-tailed unpaired t test; Fig. 4.6.B. and 4.6.D.). When we compared the effect

of a 10ms flash on spike firing in BLa and BLp PNs, accomplished by continuously injecting positive current into the soma, a similar trend was observed. Phasic ACh release inhibited spike firing in all BLa PNs (7/7 cells or 100%) but only a minority of BLp PNs (2/9 cells or 22%) and the duration of inhibition was significantly longer in the BLa PNs (BLa: 543.63 ± 50.32 ms versus BLp: 543.63 ± 50.32 ms, p = 1.88E-5, two-tailed unpaired t test) (Fig. 4.6.E. and 4.6.F.). Together, these data indicate that BLa PNs are more sensitive phasic release of endogenous ACh compared to BLp PNs.

We have previously shown that the BLa expresses significantly more M1R than the BLp (Fig. 3.2.B. and 3.5.B.). Therefore, it is possible that the greater sensitivity of BLa PNs to phasic ACh release is mediated by a greater expression of GIRK-coupled M1R's on BLa compared to BLp PNs. Here, we would like to emphasize our interest in the M1Rs coupled to GIRK channels – since these are the ones activated by phasic ACh release – as opposed to M1Rs in general, of which there could be distinct subtypes coupled to distinct effectors. To address this possibility, we bath-applied the mAChR agonist muscarine (Musc, 10µM) to brain slices while recording from BLa and BLp PNs voltage clamped at -60mV in the presence of a cocktail blocking synaptic transmission (same as used in Fig. 4.3. and Fig. 4.4. above). Because M1Rs are the predominant mAChR subtype expressed on BL PNs (McDonald and Mascagni 2010; McDonald and Mott 2021; Muller et al., 2013) and any interfering effects from synaptic transmission are blocked, the effects of muscarine are likely to reflect activation of postsynaptic M1Rs on each cell type. Muscarine elicited a biphasic response comprised of an

early muscarinic IPSC and late muscarinic EPSC (Fig. 4.6.H.) in all BLa PNs (11/11 cells or 100%) and 5/11 (45%) BLp PNs, while the remaining 6/11 (55%) BLp PNs only responded with a muscarinic EPSC (data not shown). By measuring the amplitudes of the muscarinic IPSCs in the BLa and BLp PNs that exhibited the muscarinic IPSC, we inferred and compared the relative amounts of GIRK-coupled M1Rs expressed in each cell type. We found that there was no difference in the amplitude of the early muscarinic IPSC between BLa and BLp PNs (BLa (n = 11 cells): 26.03 ± 4.07 pA versus BLp (n = 5 cells): 27.22 ± 6.58 pA, p = 0.88, two-tailed unpaired t test) (Fig. 4.6.I., left), suggesting BLa and BLp PNs express a similar amount of GIRK-coupled M1Rs and that the greater sensitivity of BLa PNs to phasic ACh release is not due to greater GIRK-coupled M1R expression in BLa PNs. Interestingly, we did notice that the amplitude of the slower muscarinic EPSC was significantly larger in BLa PNs compared to BLp PNs (BLa (n = 11 cells): -47.73 ± 4.91 pA versus BLp (n = 11 cells): -27.13 ± 3.12 pA, p = 0.003, two-tailed unpaired t test) (data not shown), suggesting there may be a greater amount of M1R's coupled to non-GIRK channel effectors that depolarize the cell. However, we did not explore this further because our phasic mode of ACh release did not cause a slow depolarization.

We also inferred and compared the relative amounts of overall GIRK channel expression between BLa and BLp PNs by bath-applying baclofen (Bac, 10μM) after Musc in the same cells and comparing the amplitudes of their Bac IPSCs. Bac produced an IPSC in all BLa and BLp PNs (BLa: 11/11 cells or 100%, BLp: 11/11 cells or 100%; Fig. 4.6.I.) and the Bac IPSC amplitudes were

similar in both cell types (BLa (n = 11 cells): 78.57 ± 11.04 pA versus BLp (n = 11 cells): 78.19 ± 8.38 pA, p = 0.98, two-tailed unpaired t test), suggesting BLa and BLp PNs express similar levels of GIRK-coupled $GABA_B$ receptors. Interestingly, the Bac IPSC amplitudes of BLa and BLp PNs were much larger than Musc IPSC amplitudes (Fig. 4.6.I.), suggesting the population of GIRK channels that are coupled to M1Rs in each cell type only represent a fraction of the overall population of GIRK channels each cell type expresses.

4.3.4. PHASIC ACETYLCHOLINE RELEASE ASSOCIATIVELY ENHANCES THE SIGNAL-TO-NOISE RATIO OF APPROPRIATELY TIMED LA INPUTS TO BNC, BUT NOT BLP, PYRAMIDAL NEURONS

4.3.4.A. Acetylcholine receptors activated by phasic ACh release do not influence evoked glutamate release at LA-BLa synapses

Nicotinic and muscarinic receptors located on glutamate terminals can alter the probability of glutamate release from the terminals they reside on. Some studies in the amygdala have shown that mAChR and nAChR agonists can alter the probability of evoked glutamate release from cortical afferents in the amygdala (Jiang et al., 2013; Jiang and Role, 2008; Yajeya et al., 2000). Additionally, a recent study measuring the amplitudes and paired pulse facilitation ratios (PPRs) of glutamate responses evoked from cortical afferents in the amygdala before and after a sustained period of endogenous ACh release reported increased amplitudes of each response without an effect on the PPR,

which they attributed to nAChRs located on the cortical afferents (Jiang et al., 2016). However, no studies have measured the effect of simultaneously present and phasically released endogenous ACh on the amplitudes and PPR of glutamate responses evoked from LA terminals in the BLa. We have shown that phasic ACh release in the BLa activates both mAChRs and nAChRs (Fig. 4.2–4.4. and 4.6.), raising questions as to whether these receptors can influence evoked glutamate release at LA-BLa synapses. We tested this possibility by recording the amplitudes and PPRs of evoked glutamate responses at LA-BLa synapses in the absence and simultaneous presence of endogenous ACh. To assess contributions of nAChRs and mAChRs, we released ACh at two intervals relative to LA stimulation. At the shorter interval, two 10ms light flashes (50ms apart) were applied simultaneously with two electrical stimuli (also 50ms apart) delivered to LA to align the peak of the early nicotinic EPSC with each evoked release of glutamate (Fig. 4.7.A. and 4.7.B.). At the longer interval, a single 10ms light flash was applied 160ms before the two electrical stimuli (50ms apart) were delivered to LA to align the peak of the late muscarinic IPSC with evoked glutamate release (Fig. 4.7.D. and 4.7.E.). ACh was released on every third LA stimulation (60 sec inter-stimulus interval) for both protocols to avoid rundown of the cholinergic response throughout the experiments.

Phasic ACh release did not significantly affect the amplitudes nor the PPRs of the LA-BLa EPSCs at the shorter interval (Fig. 4.7.B-C.). The amplitude of the first EPSC without ACh was 107.66 ± 23.18 pA compared to 96.03 ± 24.01 pA in the presence of ACh (n = 10 cells, p = 0.12, two-tailed paired t test), the

amplitude of the second EPSC without ACh was 162.37 ± 35.61 pA compared to 151.75 ± 37.45 pA in the presence of ACh (n = 10 cells, p = 0.09, two-tailed paired t-test), and the PPR without ACh was 1.54 ± 0.08 compared to 1.62 ± 0.08 in the presence of ACh (n = 10 cells, p = 0.29, two-tailed paired t test) (Fig. 4.7.C.). Interestingly, at the later interval, phasic ACh release significantly decreased the amplitudes of each LA-BLa EPSC without affecting the PPR (Fig. 4.7.E-F.). The amplitude of the first EPSC without ACh was 157.83 ± 49.79 pA compared to 112.52 ± 35.84 pA in the presence of ACh (n = 7 cells, p = 0.048, two-tailed paired t test), the amplitude of the second EPSC without ACh was 225.78 ± 64.16 pA compared to 163.47 ± 49.75 pA in the presence of ACh (n = 7 cells, p = 0.034), and the PPR without ACh was 1.64 ± 0.18 compared to 1.56 ± 0.14 in the presence of ACh (n = 7 cells, p = 0.64, two-tailed paired t test) (Fig. 4.7.F.). The percent decrease between the two EPSCs were strikingly similar (30.67 ± 4.7% first EPSC versus 32.68 ± 6.94% second EPSC, p = 0.67, two-tailed paired t test; data shown in Fig. 5.3.F., right), explaining no change in the PPR and suggesting the effect is mediated through a postsynaptic mechanism. Overall, these results suggest that neither the nicotinic nor muscarinic receptors activated by phasic ACh release alter the probability of glutamate release from LA-BLa terminals. Importantly, because we know the nAChRs are presynaptic (Fig. 4.3.), this indicates they are located on glutamate terminals other than those belonging to the LA.

4.3.4.B. Activation of α7 and α4β2 nAChRs does not influence evoked glutamate release at LA-BLa synapses

It has previously been shown that pharmacological activation of nicotinic receptors alters the probability of evoked glutamate release from cortical inputs to BL PNs and that these effects are mediated by α7 or α4β2 nicotinic receptors (Jiang et al., 2013; Jiang and Role, 2008). It is therefore possible that LA-BLa terminals do express nicotinic receptors that can alter the probability of evoked glutamate release, but that the spread of ACh from phasic release is inadequate to reach and activate them. Therefore, we tested this possibility by recording the amplitudes and PPRs of evoked glutamate responses at LA-BLa synapses in the absence and presence of the α7 agonist PNU-282987 (300nM) and the α4β2 agonist RJR-2403 (100nM). These concentrations have been successful in earlier studies (Garduño et al., 2012; Hajós et al., 2005). Like with ACh release, we found that neither PNU-282987 nor RJR-2403 affected the LA-BLa EPSC amplitudes nor their PPRs. The amplitude of the first EPSC in ACSF/control was 144.7 ± 28.39 pA compared to 152.89 ± 30.21 pA in the presence of PNU-282987, 139.18 ± 22.93 pA in the additional presence of RJR-2403, and 147.57 ± 22.2 pA in the additional presence of MEC (n = 5 cells, p = 0.99, one-way ANOVA) (Fig. 4.8.C., left). The amplitude of the second EPSC in ACSF (control) was 245.42 ± 52.07 pA compared to 241.73 ± 40.14 pA in the presence of PNU-282987, 229.56 ± 30.94 pA in the additional presence of RJR-2403, and 229.77 ± 26.47 pA in the additional presence of MEC (n = 5 cells, p = 0.99, one-way ANOVA) (Fig. 4.8.C., left). The PPR of the two LA-BLa EPSCs in ACSF (control)

was 1.79 ± 0.10 compared to 1.69 ± 0.08 in the presence of PNU-282987, 1.82 ± 0.08 in the additional presence of RJR-2403, and 1.79 ± 0.09 in the additional presence of MEC (n = 5 cells, p = 0.76, one-way ANOVA) (Fig. 4.8.C., right). This data suggests that LA-BLa inputs do not express functional α7 or α4β2 nicotinic receptors.

4.3.4.C. Phasic acetylcholine release associatively enhances the ability of appropriately timed LA inputs to fire BLa, but not BLp, pyramidal neurons

Next, we determined whether the early nicotinic depolarizing response to phasic ACh release associatively increases a baseline action potential (AP) probability driven by LA inputs to BLa and BLp PNs. The term “associatively” refers to the simultaneous depolarization of the recorded cell by electrically recruited LA terminals and non-LA terminals recruited by ACh (Fig. 4.7. and Fig. 4.8.). To align the peak of the early nicotinic depolarization with the arrival of LA glutamatergic EPSPs (Fig. 4.9.B., right), we implemented a modified Figure 4.7. protocol that simultaneously presents a single 10ms flash with every third, single stimulation of LA (Fig. 4.9.A-B., left). Single unit recordings were performed to maintain intracellular composition and support longer experiment durations. We hypothesized ACh would preferentially enhance LA-driven BLa PN output since BLa PNs are more sensitive than BLp PNs to phasic ACh release (Fig. 4.6.). Phasic ACh significantly increased the LA-driven BLa PN output (48.57 ± 15.86% increase, No ACh probability: 0.46 ± 0.028, ACh probability: 0.63 ± 0.056, n = 21 cells, p = 0.017, two-tailed paired t test; Fig. 4.9.C-D.) but did not affect LA-driven

BLp PN output (1.89 ± 8.57% increase, 0.48 ± 0.026 without ACh versus 0.48 ± 0.034 with ACh, n = 10 cells p = 0.96, two-tailed paired t test; Fig. 4.9.C-D.), supporting our hypothesis that phasic ACh preferentially enhances LA-driven output of BLa over BLp PNs when LA inputs are appropriately timed (p = 0.015, two-tailed unpaired t test; Fig. 4.9.D., right). To confirm the increase was mediated by nAChRs, we repeated the experiment in BLa PNs in the absence and subsequent presence of MEC (20 μM) (Fig. 4.9.E-H.). MEC blocked the cholinergic increase in LA-driven AP probability that was observed in control, indicating it was mediated by nAChRs as expected (Fig. 4.9.G-H.). As above, phasic ACh significantly increased the LA-driven BLa PN output in ACSF/control (70.13 ± 15.94% increase, No ACh probability: 0.45 ± 0.046, ACh probability: 0.74 ± 0.021 with ACh, n = 4 cells, p = 0.010, two-tailed paired t test), whereas the probability did not significantly change in MEC (80.86 ± 14.15% of baseline, No ACh probability: 0.52 ± 0.023, ACh probability 0.42 ± 0.076 with ACh, n = 4 cells, p = 0.076) (Fig. 4.9.G-H.). Together, these data suggest that phasic ACh release associatively enhances the ability of appropriately timed LA inputs to fire BLa, but not BLp, PNs.

4.3.4.D. Phasic acetylcholine release reduces the ability of inappropriately timed LA inputs to fire BLa and BLp pyramidal neurons

We also wanted to know whether the late muscarinic hyperpolarizing response to phasic ACh release directly reduces a baseline LA-driven AP probability in BLa and BLp PNs. Here, we use the term “directly” because the

GIRK-coupled M1Rs responsible for the muscarinic hyperpolarization in response to phasic ACh release are located postsynaptically on the recorded cells in BL (Fig. 4.3. and Fig. 4.4.). We tested this possibility by repeating the Figure 8 procedure, except that the 10ms flash was delivered 160ms before LA stimulation to align the peak of the late muscarinic hyperpolarization with the arrival of the LA glutamatergic EPSPs (Fig. 4.10.A-B.). Like above, we hypothesized ACh would preferentially reduce LA-driven BLa PN output since BLa PNs are more sensitive than BLp PNs to phasic ACh release (Fig. 4.6.). Surprisingly, phasic ACh significantly reduced the probability of LA-driven APs in BLa and BLp PNs (Fig. 4.10.C-D.). However, supporting our hypothesis, this effect was significantly greater in BLa PNs ($p = 0.001$, two-tailed unpaired t test; Fig. 4.10.D., right). Phasic ACh reduced baseline AP probability in BLa PNs by 86.34 ± 4.94% (No ACh probability: 0.79 ± 0.052, ACh probability: 0.13 ± 0.049, $n = 15$ cells, $p = 1.10E-9$, two-tailed paired t test; Fig. 4.10.C-D.), whereas phasic ACh only reduced baseline AP probability in BLp PNs by 39.50 ± 15.33% (No ACh probability: 0.81 ± 0.049, ACh probability: 0.50 ± 0.14, $n = 5$ cells, $p = 0.049$, two-tailed paired t test) (Fig. 4.10.C-D.). $GABA_B$ receptors activate the same GIRK channels as the M1Rs activated by phasic ACh. Therefore, in addition to confirming that the reduction in LA-driven BL PN output observed above is mediated by mAChRs, we also wanted to rule out the possibility that it was mediated by $GABA_B$ receptors. To do so, we repeated this experiment in BLa PNs in the absence and subsequent presence of CGP (2 μM) in one set of cells and ATR (5 μM) in a separate set of cells (Fig. 4.10.E-H.). As expected, ATR, but

not CGP, blocked the cholinergic decrease in LA-driven AP probability observed in BLa PNs, indicating it was mediated by mAChRs, not $GABA_B$ receptors (Fig. 4.10.F.). In the CGP cells, phasic ACh significantly decreased the LA-driven BLa PN output in ACSF/control (91.87 ± 3.64% decrease, No ACh probability: 0.88 ± 0.040, ACh probability: 0.072 ± 0.032, n = 6 cells, p = 0.00002, two-tailed paired t test) to a similar extent as it did in CGP (80.93± 7.47% decrease, No ACh probability: 0.87 ± 0.034, ACh probability: 0.17 ± 0.068, n = 6 cells, p = 0.0002, two-tailed paired t test) (Fig. 4.10.G-H., Top). When ATR was tested, phasic ACh significantly decreased the LA-driven AP probability of BLa PNs in ACSF/control (90.20 ± 6.00% decrease, No ACh probability: 0.86 ± 0.062, ACh probability: 0.096 ± 0.059 with ACh in ACSF, n = 5 cells, p = 0.00005, two-tailed paired t test), whereas the baseline probability did not significantly change in ATR (105.70 ± 21.53% of baseline, No ACh probability: 0.75 ± 0.093, ACh probability: 0.73 ± 0.068 with ACh, n = 5 cells, p = 0.86) (Fig. 4.10.G-H., Bottom). Together, these data suggest that phasic ACh release directly reduces the ability of inappropriately timed LA inputs to fire both BLa and BLp PNs, but that this effect is significantly greater in BLa PNs.

4.4. DISCUSSION

The core finding of this study is that phasic ACh release indirectly and associatively enhances the ability of appropriately timed LA glutamatergic inputs to fire BLa PNs, while also directly reducing the ability of inappropriately timed LA glutamatergic inputs to fire the same cells. This is accomplished via the slightly staggered activation of nicotinic and muscarinic receptors on different circuit

components that together generate a biphasic response in the membrane potential. Presynaptic α7 and α4β2 nAChRs depolarize the cell by evoking glutamate release from terminals that do not belong to LA. Previous studies by Lorna Role's lab have shown cortical inputs to BLa express functional α7 and α4β2 nAChRs (Jiang et al., 2013, 2016; Jiang and Role, 2008), indicating these inputs could be cortical. This effect precedes the activation of postsynaptic M1Rs that hyperpolarize the cell by opening postsynaptic GIRK channels. The latter component has been reported before (Aitta-aho et al., 2018; Jiang et al., 2016; Unal et al., 2015), but we are the first to report the former, although previous pharmacological studies suggest the α7 and α4β2 nAChRs could be located on cortical inputs (Jiang et al., 2013; Jiang and Role, 2008). Whether phasic ACh makes BLa PN spike firing more or less likely depends on which component of this biphasic response is active when LA inputs arrive, as the nicotinic and muscarinic components bring the cell closer to and farther away from AP threshold, respectively.

The nicotinic enhancement of LA-driven BLa PN output is associative because the nAChRs that evoke glutamate release are not present on the LA terminals driving the baseline AP probability. Thus, by depolarizing BLa PNs via nAChRs on non-LA terminals while LA terminals unaffected by ACh are simultaneously depolarizing the same cells, the two sets of inputs associate in time to boost BLa PN AP probability. To our knowledge, we are the first to report such a mechanism for presynaptic nAChRs, although a recent study reported a similar phenomenon in cortex (Urban-Ciecko et al., 2018), which we will discuss

in more detail below. This effect is also indirect because ACh must involve different cells to influence the membrane potential of the recorded cell. In contrast, the muscarinic reduction of LA-driven BLa PN output is direct because ACh produces the effect by activating M1Rs located directly on the recorded cell itself. These findings layer a novel mechanism onto a well-established body of literature in the cortex that nAChRs and mAChRs cooperate to enhance the signal-to-noise ratio of inputs to enhance attention to and encoding of important stimuli (Colangelo et al., 2019; Hasselmo 2006; Lustig and Sarter 2016; Mineur and Picciotto 2021).

We also compared the effect of phasic ACh on the membrane potential and LA-driven excitability between BLa and BLp PNs. Interestingly, we found that the effects of ACh in BLp PNs were muted compared to those in the BLa. BLa PNs were more sensitive to phasic ACh release and had significantly larger response amplitudes than BLp PNs in response to the same cholinergic stimuli. It should be noted that BLp PNs that did respond to ACh displayed both components of the biphasic response observed in the BLa. In terms of phasic ACh's impact on LA-driven BLp PN output, the nicotinic facilitating effect was not detected and the muscarinic reductive effect, while significant, was smaller. Our results suggest that differences in the muscarinic effect are not due to differences in the postsynaptic expression of GIRK-coupled M1Rs because the amplitudes of the hyperpolarizing responses to bath-applied muscarine in BLa and BLp PNs were not significantly different. Instead, based on previous anatomical data from our lab (not shown), the more likely explanation for differences in the nicotinic

and muscarinic effects is a greater cholinergic innervation of the BLa. However, a differential expression of nAChRs between the two regions could explain the former difference because no studies have quantitatively compared nAChR expression between the BLa and BLp. Future studies should explore this possibility further.

Interestingly, we also found that BLa PNs had significantly larger slow depolarizing responses to muscarine compared to BLp PNs. We did not focus much on this difference because phasic ACh release did not reproduce this response. However – because our 10ms flash likely creates a brief and small ACh spread zone of only tens to hundreds of nanometers from presynaptic release sites (Sarter and Lustig 2020), whereas muscarine ubiquitously activates all M1Rs in the slice, including those beyond phasic ACh's reach – this observation could reflect the existence of distinct sets of M1Rs coupled to different effectors that are activated by different modes of ACh release: "synaptic" GIRK-coupled M1Rs that hyperpolarize the cell and respond to phasic ACh release, and "extrasynaptic" M1Rs coupled to depolarizing effectors (like KCNQ channels that mediate the M-current) that respond to sustained ACh release via a farther-reaching zone of ACh spread. Indeed, there is much ongoing debate over the nature of ACh signaling in vivo and how ACh spreads in target regions (Disney and Higley 2020; Sarter and Lustig 2020) and the presence of synaptic versus extrasynaptic mAChRs has been proposed before (Aitta-aho et al., 2018; Hasselmo and Sarter 2011, Unal et al., 2015). If true, perhaps the differences in M1R expression between the BLa and BLp from our previous work (Chapter 3)

reflect a greater expression of extrasynaptic M1Rs in the BLa. Future studies should explore this possibility further. (Hasselmo and Sarter 2011)

4.4.1. FUNCTIONAL IMPLICATIONS

Phasic ACh release in cortex is necessary for behaviors reporting cue detection (Gritton et al., 2016); the BL – a cortex-like region – is the most densely innervated target of the cholinergic basal forebrain (CBF) (Carlsen and Heimer 1986; Muller et al., 2011); salient emotional experiences elicit phasic ACh release in the BNC (Crouse et al., 2020) and other regions (Hangya et al., 2015; Laszlovszky et al., 2020; Sturgill et al., 2020; Teles-Grilo Ruivo et al., 2017); and the BNC detects biologically important environmental stimuli and orchestrates appropriate behavioral responses to their implied meaning (Adolphs et al., 1994; Blanchard and Blanchard 1972; Brown and Schafer 1888; Klüver and Bucy 1937; LeDoux et al., 1990; McDonald 2020; Pitkänen et al., 1997; Weiskrantz 1956). Despite the overlap of these observations, no studies have searched for circuit-level and molecular mechanisms by which salient stimulus-driven phasic ACh release could shape attentional computations performed by the BNC.

Our results suggest that LA inputs – simulating sensory information flowing into the BL – are more likely to fire BLa PNs when they arrive at the precise moment when ACh is released due to the additional depolarization provided by the nicotinic recruitment of extra-amygdalar glutamatergic inputs. This could be a mechanism by which ACh ensures behaviorally relevant stimuli – defined as those represented by LA terminals signaling in the BNC when ACh is initially released – are detected and responded to. This process could also

facilitate the acquisition of associative emotional memories at the LA-BLa pathway by promoting spike-timing dependent long term-potentiation of LA-BLa synapses. Supporting this, a recent study showed that the formation of associative emotional memories requires ACh transients in the BL that peak around 500ms after reward retrieval (Crouse et al., 2020), which is relatively close to the duration our 10ms light flash. Further supporting the physiological nature of our stimulus, a recent review suggests ACh may signal along multiple spatiotemporal zones, with one zone corresponding to a region that is tens to hundreds of nanometers surrounding cholinergic release sites and accomplished by signaling lasting tens of milliseconds (Sarter and Lustig 2020).

Our results also suggest that these same LA inputs are less likely to fire the same BLa PNs if they arrive merely tens of milliseconds later. This could be a means by which ACh ensures behaviorally irrelevant or distracting stimuli – defined as those represented by LA terminals signaling in the BNC at a delayed interval after initial ACh release – are not noticed or responded to. Together, both components of the biphasic response to phasic ACh could represent a temporal signal-to-noise ratio (SNR) filter. Indeed, ACh has long been postulated to enhance the SNR of sensory inputs to cortex (Sarter et al., 2005) and a study in the BNC reported that phasic ACh enhances the SNR of BLa PNs by bidirectionally modulating their excitability depending on their level of activity when ACh impacts the cells (Unal et al., 2015). Our findings reveal an additional mechanism by which phasic ACh could enhance the SNR in the BLa, in this case

in response to internal sensory inputs. To our knowledge, we are the first to report a such an effect.

Intriguingly, a temporally specific facilitation of glutamatergic signaling via presynaptic nAChRs activated by phasic ACh (generated by the same 10ms flash used here) was recently reported in the cortex and its authors suggested it could represent a potential mechanism by which ACh enhances sensory processing in the attentive, cued state (Urban-Ciecko et al., 2018). This raises the interesting question of whether transient recruitment of presynaptic nAChRs on glutamate terminals represents a common synaptic motif by which stimulus driven phasic ACh release facilitates attentional performance throughout the brain. In support of this, nAChRs have been implicated in enhancing attention and deficits in nAChR signaling are associated with attentional deficits in schizophrenia and Alzheimer's disease (Freedman, 2014; Guillem et al., 2011; Hahn, 2015; Parikh et al., 2007; Sarter et al., 2005). It will be interesting to see whether future studies continue to reveal this mechanism in other brain areas.

Finally, there is evidence that negative and positive emotions are preferentially processed by the BLa and BLp. We have observed a more heightened influence of phasic ACh signaling in the BLa, suggesting ACh could differentially contribute to the BNC's processing of negative and positive emotion. Since phasic ACh signaling is increasingly appreciated to correspond to attentional performance and the early nicotinic facilitation of LA-driven BLa PN output was not observed in the BLp, our results could suggest that the brain is wired to perceive with an attentional bias to negative stimuli. However, it should

again be noted that the nicotinic response was detected in BLp PNs, suggesting a similar role for these receptors could emerge under different circumstances. Although this possibility awaits further experimental verification, it does tempt speculation. Perhaps defaulting to negative valence and defensive behavior over positive valence and appetitive behavior is evolutionally advantageous and more beneficial for survival, as an example.

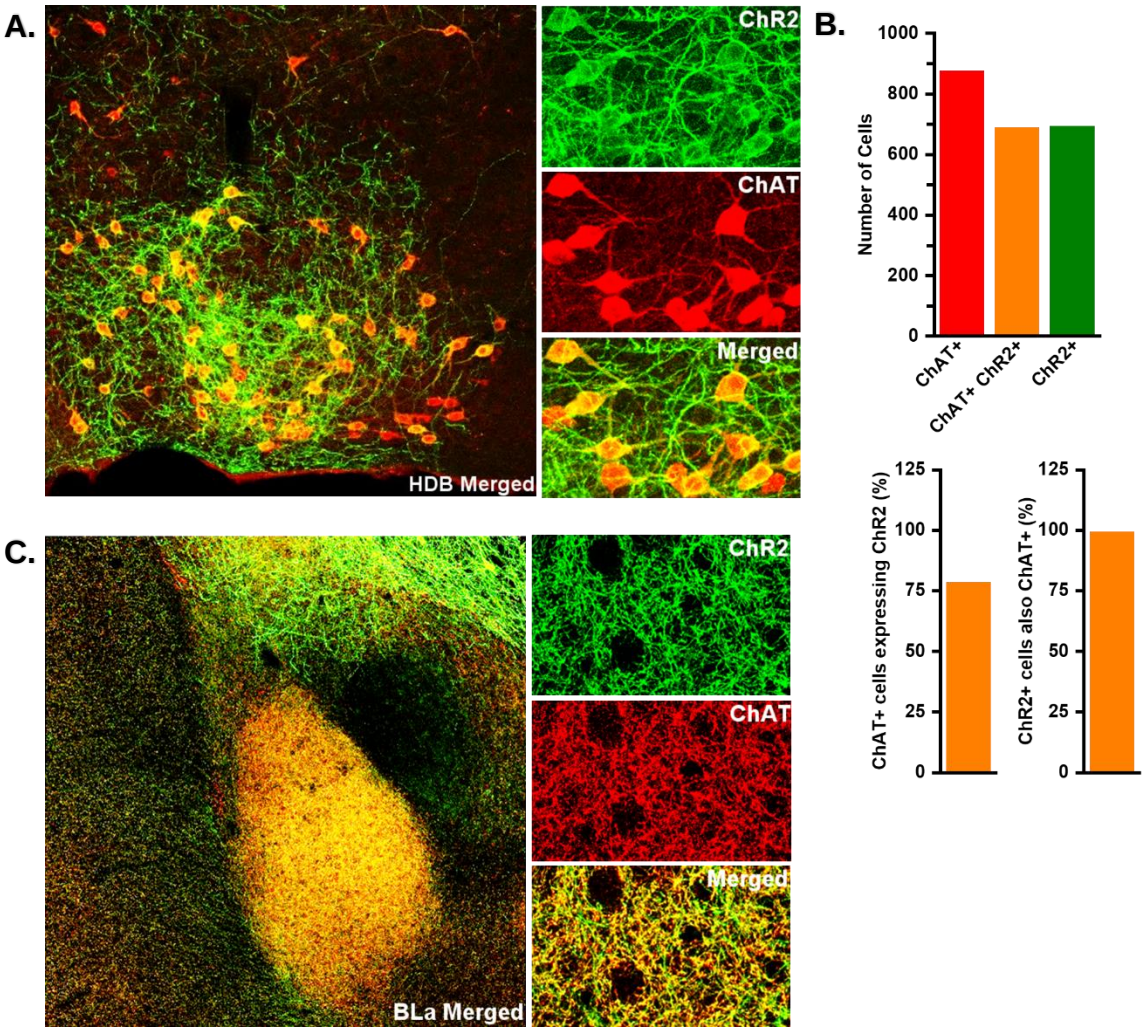

Figure 4.1. ChR2 is selectively expressed in cholinergic neurons. **A.** Representative images of ChR2 expression (green) and ChAT antibody immunoreactivity (red) in the horizontal limb of the diagonal band of Broca (HDB), one source of cholinergic terminals to the BLa. Overlap is depicted in yellow. **B. Top.** The total number of ChAT antibody+ cells (left bar), ChR2+ cells (right bar), and overlapping (ChR2+ and ChR2+) cells in the HDB. **Bottom, Left.** The percentage of ChAT antibody+ cells in the HDB that also express ChR2. **Bottom, Right.** The percentage of ChR2+ cells in the HDB that are also ChAT antibody+. **C.** Representative images of ChR2 expression (green) and ChAT antibody immunoreactivity (red) in the BLa. Overlap is depicted in yellow.

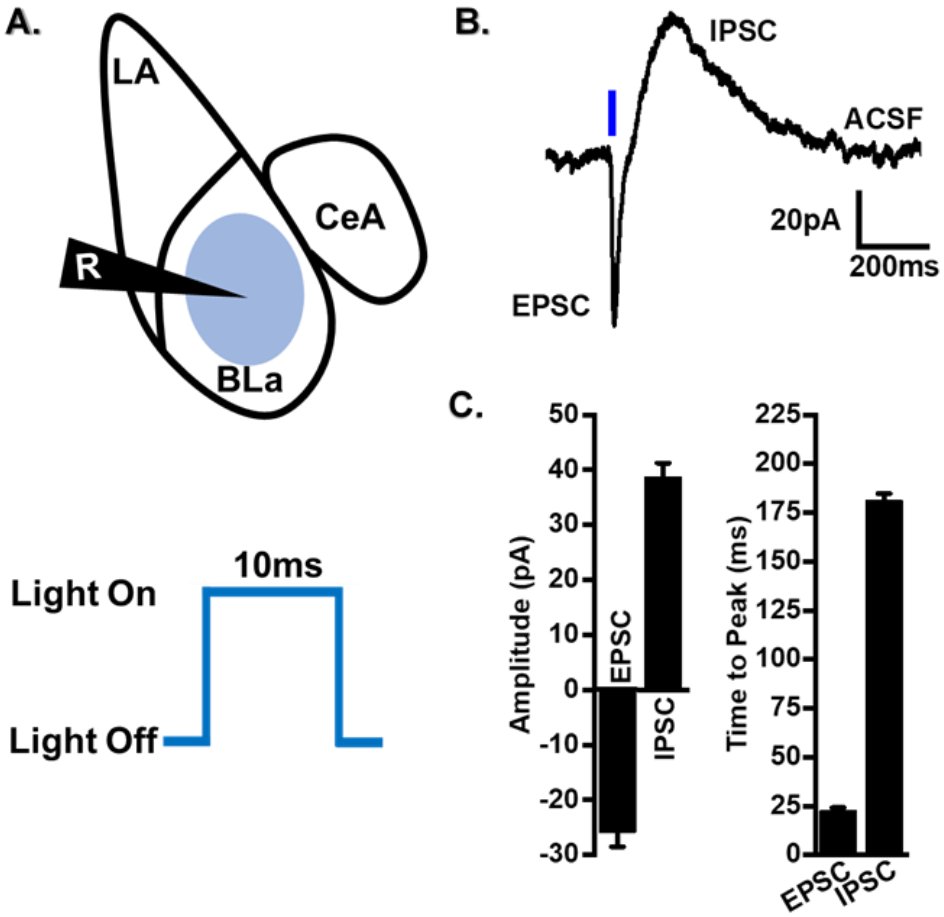

Figure 4.2. Phasic acetylcholine release produces a biphasic response in BLa pyramidal neurons. **A. Top.** Schematic of the experimental setup depicting the positioning of the recording electrode in the BLa and the targeting of the BLa with the blue light flash. **Bottom.** Illustration of the 10ms blue light flash that was used to evoke phasic acetylcholine release into the BLa during recordings. **B.** Representative trace depicting the biphasic membrane potential response of a BLa PN to a 10ms flash (blue bar). Both components are labelled. **C. Left.** Bar graph showing the average amplitudes of the EPSC and IPSC components of the biphasic response to phasic ACh in BLa PNs in ACSF. **Right.** Bar graph showing the average time it took from the start of a 10ms flash to reach the peak of the EPSC and IPSC components of the biphasic response.

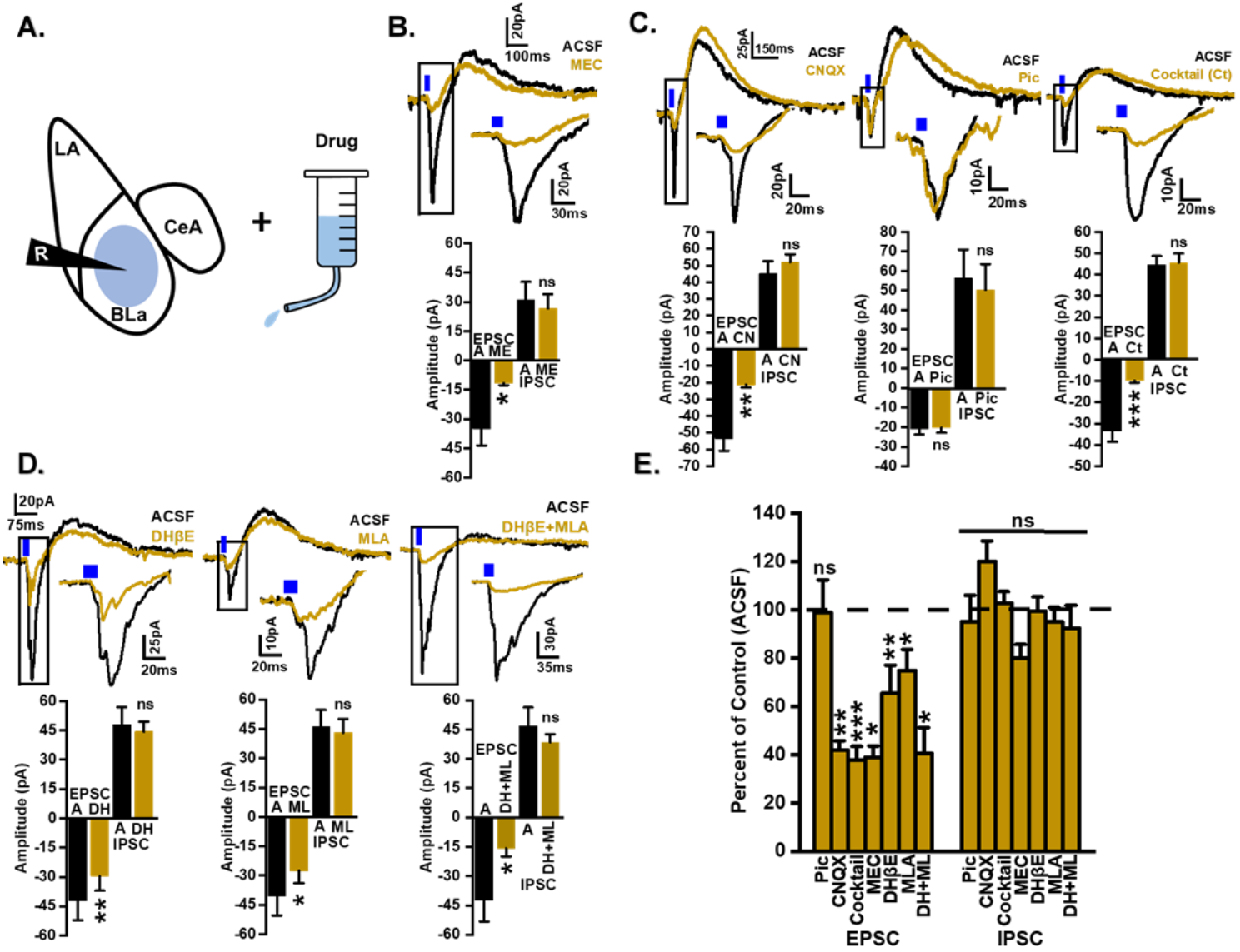
A.
LA
CeA
R
BLa
Drug
B.
20pA
100ms
ACSF
MEC
20pA
30ms
Amplitude (pA)
EPSC
A ME
A ME
IPSC
ns
*
C.
25pA
150ms
ACSF
CNQX
20pA
20ms
ACSF
Pic
10pA
20ms
ACSF
Cocktail (Ct)
10pA
20ms
EPSC
A CN
A CN
IPSC
EPSC
A Pic
A Pic
IPSC
EPSC
A Ct
A Ct
IPSC
**
***
ns
D.
20pA
75ms
ACSF
DHβE
25pA
20ms
ACSF
MLA
10pA
20ms
ACSF
DHβE+MLA
30pA
35ms
EPSC
A DH
A DH
IPSC
EPSC
A ML
A ML
IPSC
EPSC
A
DH+ML
A
DH+ML
IPSC
**
*
E.
Percent of Control (ACSF)
ns
ns
Pic
CNQX
Cocktail
MEC
DHβE
MLA
DH+ML
EPSC
IPSC

Figure 4.3. The faster cholinergic depolarization is mediated by α7 and α4β2 nicotinic receptors located on presynaptic glutamate terminals. **A.** Schematic of the experimental setup depicting the positioning of the recording electrode in the BLa, the targeting of the BLa with a blue light flash, and the occasional application of drug to probe the transmitters and receptors mediating the early EPSC. **B. Top.** Representative traces depicting the membrane potential responses of a BLa PN to a 10ms flash (blue bar) in ACSF (black trace) and the subsequent addition of 20μM MEC (gold trace). The inset shows a zoomed view of the early EPSC. Its boundaries are defined by the adjacent black box. **Bottom.** Bar graph showing the average amplitudes of the EPSC and IPSC components of the biphasic response to phasic ACh in BLa PNs in ACSF (black bars) and MEC (gold bars). **C. Top.** Representative traces depicting the membrane potential responses of a BLa PNs to a 10ms flash (blue bars) in ACSF (all black traces) and the subsequent addition of 20μM CNQX (left gold trace), 50μM Pic (middle gold trace), and cocktail (CNQX + Pic and sometimes also MK801 and CGP) (right gold trace). The insets show zoomed views of the early EPSCs in each drug condition. Their boundaries are defined by the adjacent black boxes. **Bottom.** Bar graphs showing the average amplitudes of the EPSC and IPSC components of the biphasic response to phasic ACh in BLa PNs in ACSF (black bars of all bar graphs) and CNQX (gold bars of left bar graph), Pic (gold bars of middle bar graph), and cocktail (gold bars of right bar graph). **D. Top.** Representative traces depicting the membrane potential responses of a BLa PNs to a 10ms flash (blue bars) in ACSF (all black traces) and the subsequent addition of 1μM DHβE (left gold trace), 100nM MLA (middle gold trace), and DHβE + MLA (right gold trace). The insets show zoomed views of the early EPSCs in each drug condition. Their boundaries are defined by the adjacent black boxes. **Bottom.** Bar graphs showing the average amplitudes of the EPSC and IPSC components of the biphasic response to phasic ACh in BLa PNs in ACSF (black bars of all bar graphs) and DHβE (gold bars of left bar graph), MLA (gold bars of middle bar graph), and DHβE + MLA (gold bars of right bar graph). **E.** Bar graph showing the average amplitude of the early EPSC and late IPSC in the presence of each drug expressed as a percentage of the average amplitude of the same response component recorded in control conditions (or ACSF). A = ACSF, ME = MEC, CN = CNQX, Ct = Cocktail, DH = DHβE, ML = MLA. * = $p < 0.01$, ** = $p < 0.01$, *** $p < 0.001$.

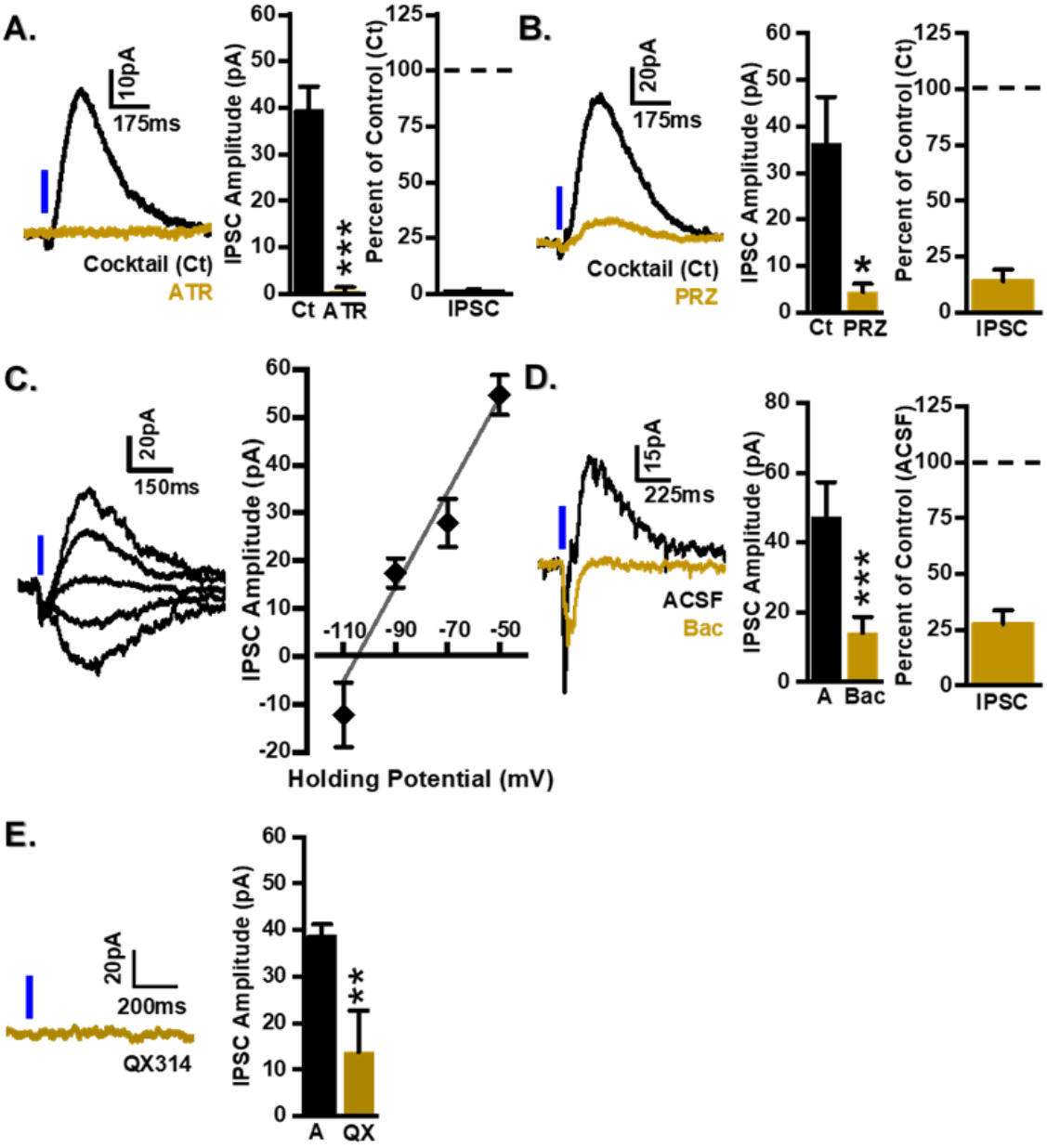

Figure 4.4. The slower cholinergic hyperpolarization is mediated by postsynaptic M1Rs coupled to GIRK channels. **A. Left.** Representative traces depicting the membrane potential responses of a BLa PN to a 10ms flash (blue bar) in cocktail (black trace) and the subsequent addition of 5μM ATR (gold trace). **Middle.** Bar graph showing the average amplitudes of the EPSC and IPSC components of the biphasic response to phasic ACh in BLa PNs in cocktail (black bar) and ATR (gold bar). **Right.** Bar graph showing the average amplitude of the late IPSC in the presence of ATR expressed as a percentage of the average amplitude of the late IPSC recorded in control conditions (or cocktail). **B. Left.** Representative traces

depicting the membrane potential responses of a BLa PN to a 10ms flash (blue bar) in cocktail (black trace) and the subsequent addition of 1µM PRZ (gold trace). **Middle.** Bar graph showing the average amplitudes of the EPSC and IPSC components of the biphasic response to phasic ACh in BLa PNs in cocktail (black bar) and PRZ (gold bar). **Right.** Bar graph showing the average amplitude of the late IPSC in the presence of PRZ expressed as a percentage of the average amplitude of the late IPSC recorded in control conditions (or cocktail). **C. Left.** Representative traces depicting the membrane potential responses of a BLa PN to a 10ms flash (blue bar) in ACSF and held at -110mV, -90mV, -70mV, and -50mV. **Right.** Graph showing the direction and average amplitudes of the late IPSCs recorded at -110mV, -90mV, -70mV, and -50mV. **D. Left.** Representative traces depicting the membrane potential responses of a BLa PN to a 10ms flash (blue bar) in ACSF (black trace) and the subsequent addition of 20µM Bac (gold trace). **Middle.** Bar graph showing the average amplitudes of the EPSC and IPSC components of the biphasic response to phasic ACh in BLa PNs in ACSF (black bar) and Bac (gold bar). **Right.** Bar graph showing the average amplitude of the late IPSC in the presence of Bac expressed as a percentage of the average amplitude of the late IPSC recorded in control conditions (or ACSF). **E. Left.** Representative trace depicting the membrane potential response of a BLa PN to a 10ms flash (blue bar) in ACSF and internal solution containing 5mM QX-314 (gold trace). **Right.** Bar graph showing the average amplitude of the late IPSC in one set of cells that had regular internal solution (black bar) and a separate set of cells that had intracellular QX-314 (gold bar). Responses in both sets of cells were recorded in ACSF. * = $p < 0.01$, ** = $p < 0.01$, *** $p < 0.001$.

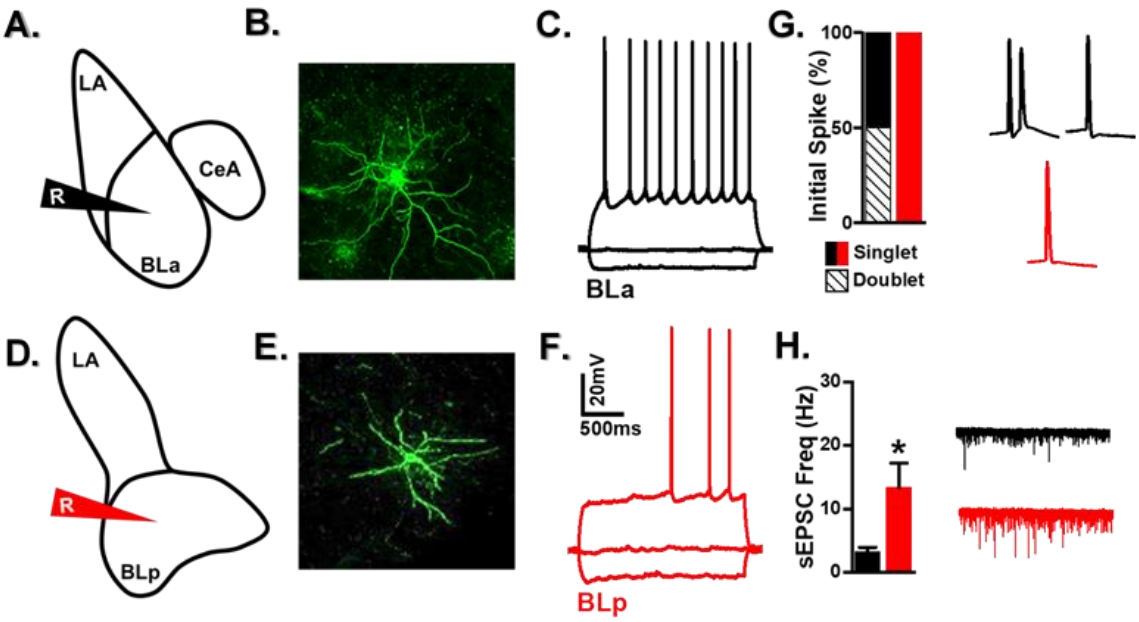

Figure 4.5. BLa and BLp pyramidal neurons can be distinguished by their passive and active electrical properties. A. Schematic of the experimental setup depicting the positioning of the recording electrode in the BLa. **B.** Representative image depicting a biocytin-filled BLa PN. **C.** Voltage response of a BLa PN to hyperpolarizing and depolarizing current pulses. **D.** Schematic of the experimental setup depicting the positioning of the recording electrode in the BLp. **E.** Representative image depicting a biocytin-filled BLp PN. **F.** Voltage response of a BLp PN to hyperpolarizing and depolarizing current pulses. **G. Left.** Bar graph showing the percentage of BLa (left bar) and BLp (right bar) PNs that had initial spikes in response to depolarizing current pulses characterized as a singlet (solid bar) or doublet (diagonal lines). **Right.** Representative traces depicting a BLa PN singlet (top, left), BLa PN doublet (top, right), and a BLp PN singlet (bottom). **H. Left.** Bar graph showing the average frequency of spontaneous depolarizing synaptic events (sEPSCs) in BLa PNs (left bar) and BLp PNs (right bar). **Right.** Representative traces depicting sEPSCs in a BLa PN (top) and BLp PN (bottom). * = $p < 0.01$, ** = $p < 0.01$, *** $p < 0.001$.

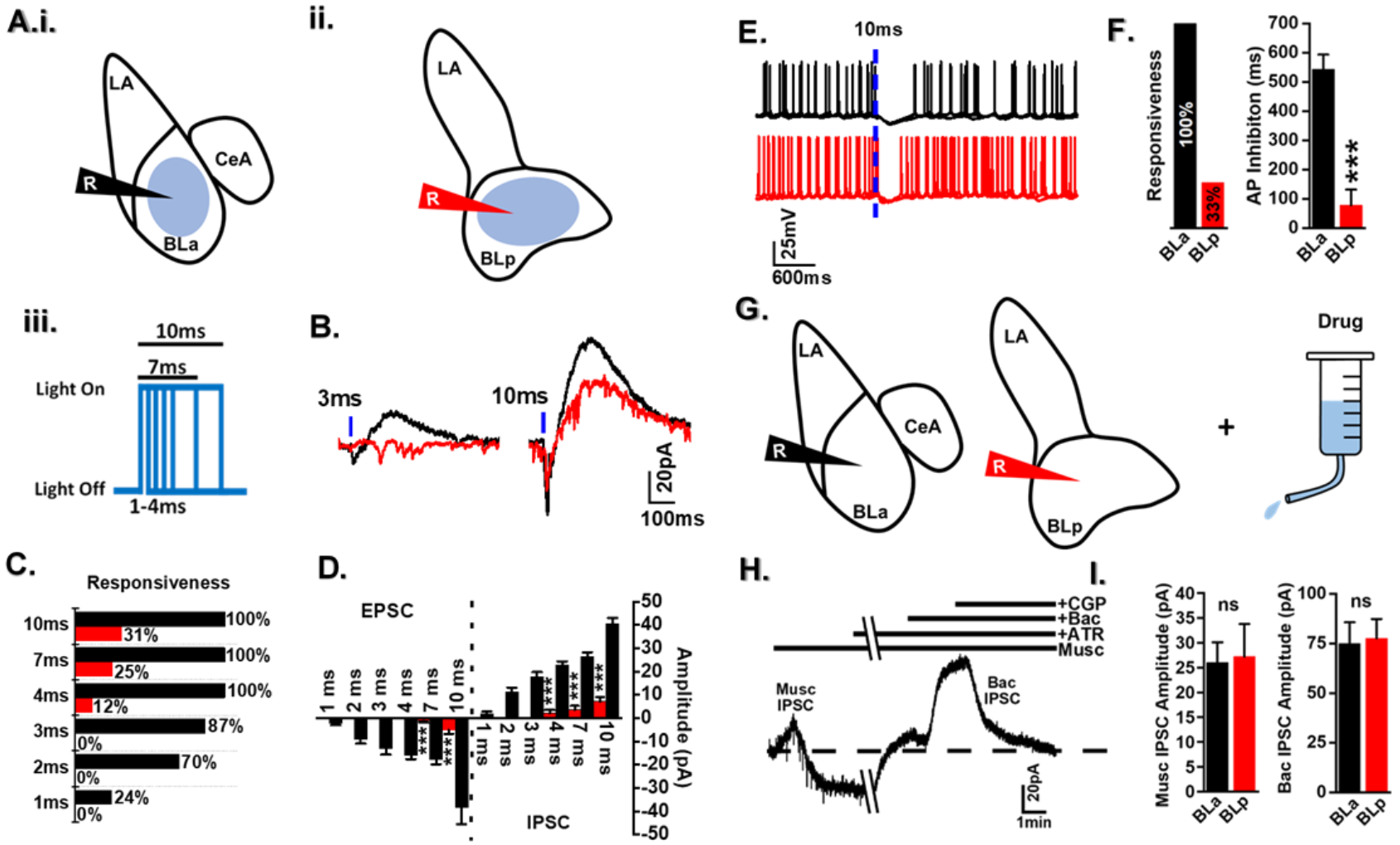
A.i.
LA
CeA
R
BLa
ii.
LA
R
BLp
iii.
10ms
7ms
Light On
Light Off
1-4ms
B.
3ms
10ms
20pA
100ms
C.
Responsiveness
10ms
7ms
4ms
3ms
2ms
1ms
100%
31%
100%
25%
100%
12%
87%
0%
70%
0%
24%
0%
D.
EPSC
IPSC
1 ms
2 ms
3 ms
4 ms
7 ms
10 ms
Amplitude (pA)
E.
10ms
25mV
600ms
F.
Responsiveness
100%
33%
BLa
BLp
AP Inhibiton (ms)
***
G.
LA
CeA
R
BLa
LA
R
BLp
Drug
+
H.
+CGP
+Bac
+ATR
Musc
Musc IPSC
Bac IPSC
20pA
1min
I.
Musc IPSC Amplitude (pA)
ns
Bac IPSC Amplitude (pA)
ns
BLa
BLp

Figure 4.6. Phasic acetylcholine release preferentially impacts BLa over BLp pyramidal neurons. A. Schematic of the experimental setup depicting **(i.)** the positioning of the recording electrode in the BLa and the targeting of the BLa with blue light flashes or **(ii.)** the positioning of the recording electrode in the BLp and the targeting of the BLp with blue light flashes. **iii.** Illustration of the blue light flash protocol that was used to evoke increasing amounts of phasic acetylcholine into the BLa and BLp during recordings from BLa and BLp PNs. 1ms, 2ms, 3ms, 4ms, 7ms, and 10ms flashes were presented in successive order to every cell recorded. **B.** Representative traces depicting the membrane potential responses of BLa (black traces) and BLp (red traces) PNs to a **(Left)** 3ms flash (blue bar) in ACSF or **(Right)** 10ms flash (blue bar) in ACSF. **C.** Bar graph showing the percentage of BLa (black bars) and BLp (red bars) PNs that displayed responses to each light flash duration. **D.** Bar graph showing the average amplitudes of the EPSC and IPSC components of the biphasic response to phasic ACh in BLa (black bars) and BLp (red bars) PNs in ACSF at each light duration. **E.** Representative traces depicting the responses of BLa (black traces) and BLp (red traces) PNs to a 10ms flash (blue bar) in ACSF during spiking in response to steady depolarizing current injection. **F. Left.** Bar graph showing the percentage of spiking BLa (black bar) and BLp (red bar) PNs that responded to a 10ms flash in ACSF with a brief pause in action potential firing. **Right.** Bar graph showing the average duration of AP inhibition produced by a 10ms flash in BLa (black bar) and BLp (red bar) PNs in ACSF. **G.** Schematic of the experimental setup depicting the positioning of the recording electrode in the BLa or BLp and the application of drug to compare the responses between BLa and BLp PNs. **H.** Representative trace depicting the membrane potential responses of a BLa PN to the successive application of 10μM muscarine, 10μM ATR, 10μM Bac, and 2μM CGP in the presence of cocktail. **I. Left.** Bar graph showing the average amplitude of the IPSC component of the biphasic response to muscarine in BLa (black bars) and BLp (red bars) PNs in cocktail. **Right.** Bar graph showing the average amplitude of the Bac IPSC in BLa (black bars) and BLp (red bars) PNs in cocktail. * = $p < 0.01$, ** = $p < 0.01$, *** $p < 0.001$.

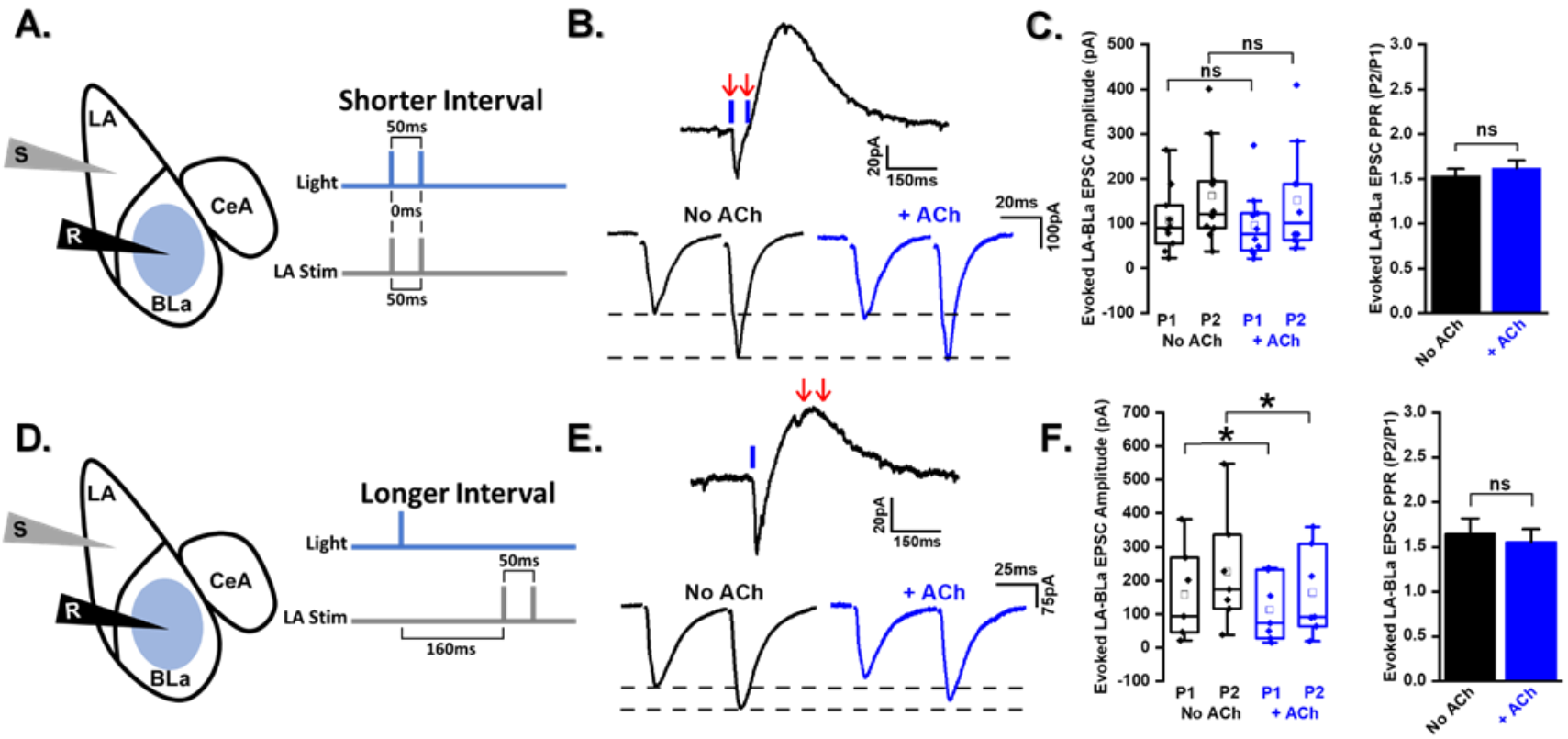
A.
LA
S
CeA
R
BLa
Shorter Interval
50ms
Light
0ms
LA Stim
50ms
B.
20pA
150ms
No ACh
+ ACh
20ms
100pA
C.
Evoked LA-BLa EPSC Amplitude (pA)
ns
ns
P1
P2
P1
P2
No ACh
+ ACh
Evoked LA-BLa EPSC PPR (P2/P1)
ns
No ACh
+ ACh
D.
LA
S
CeA
R
BLa
Longer Interval
Light
50ms
LA Stim
160ms
E.
20pA
150ms
No ACh
+ ACh
25ms
75pA
F.
Evoked LA-BLa EPSC Amplitude (pA)
*
*
P1
P2
P1
P2
No ACh
+ ACh
Evoked LA-BLa EPSC PPR (P2/P1)
ns
No ACh
+ ACh

Figure 4.7. Acetylcholine receptors activated by phasic acetylcholine release do not influence evoked glutamate release at LA-BLa synapses. A. Left. Schematic of the experimental setup depicting the positioning of the recording electrode in the BLa, the simulating electrode in the LA, and the targeting of the BLa with two blue light flashes. **Right.** The timing relationship between the paired stimulation of LA (50ms apart) and the presentation of two 10ms flashes (also 50ms apart). **B. Top.** Representative trace depicting the membrane potential response of a BLa PN to two successive 10ms flashes (blue bars) in ACSF. Although LA is not stimulated in this trace, the timing of LA inputs with respect to this response is illustrated by two red arrows. **Bottom.** Representative traces depicting the membrane potential response to paired stimulation of LA in the absence **(Left)** and presence **(Right)** of phasic ACh evoked by two 10ms flashes. Note that the membrane potential response to ACh is subtracted from the right trace. The left and right traces were recorded in ACSF. **C. Left.** Graph showing the amplitude of the first LA-BLa EPSC (Pulse 1 or P1) and the second LA-BLa EPSC (P2) evoked by paired LA stimulation in the absence (black, left half of graph) and presence (blue, right half of graph) of phasic ACh evoked by two 10ms flashes. **Right.** Bar graph showing the paired-pulse facilitation ratio (P2 amplitude/P1 amplitude) of the LA-BLa EPSCs in the absence (black bar) and presence (right bar) of phasic ACh evoked by two 10ms flashes. **D. Left.** Schematic of the experimental setup depicting the positioning of the recording electrode in the BLa, the simulating electrode in the LA, and the targeting of the BLa with individual blue light flashes. **Right.** The timing relationship between the paired stimulation of LA (50ms apart) and the presentation of a single 10ms flash. **E. Top.** Representative trace depicting the membrane potential response of a BLa PN to a single 10ms flash (blue bar) in ACSF. Although LA is not stimulated in this trace, the timing of LA inputs with respect to this response is illustrated by two red arrows. **Bottom.** Representative traces depicting the membrane potential response to paired stimulation of LA in the absence **(Left)** and presence **(Right)** of phasic ACh evoked by a single 10ms flash. Note that the membrane potential response to ACh is subtracted from the right trace. The left and right traces were recorded in ACSF. **F. Left.** Graph showing the amplitude of the first LA-BLa EPSC (P1) and the second LA-BLa EPSC (P2) evoked by paired LA stimulation in the absence (black, left half of graph) and presence (blue, right half of graph) of phasic ACh evoked by a single 10ms flash. **Right.** Bar graph showing the paired-pulse facilitation ratio (P2 amplitude/P1 amplitude) of the LA-BLa EPSCs in the absence (black bar) and presence (right bar) of phasic ACh evoked by a single 10ms flash. * = $p < 0.01$, ** = $p < 0.01$, *** $p < 0.001$.

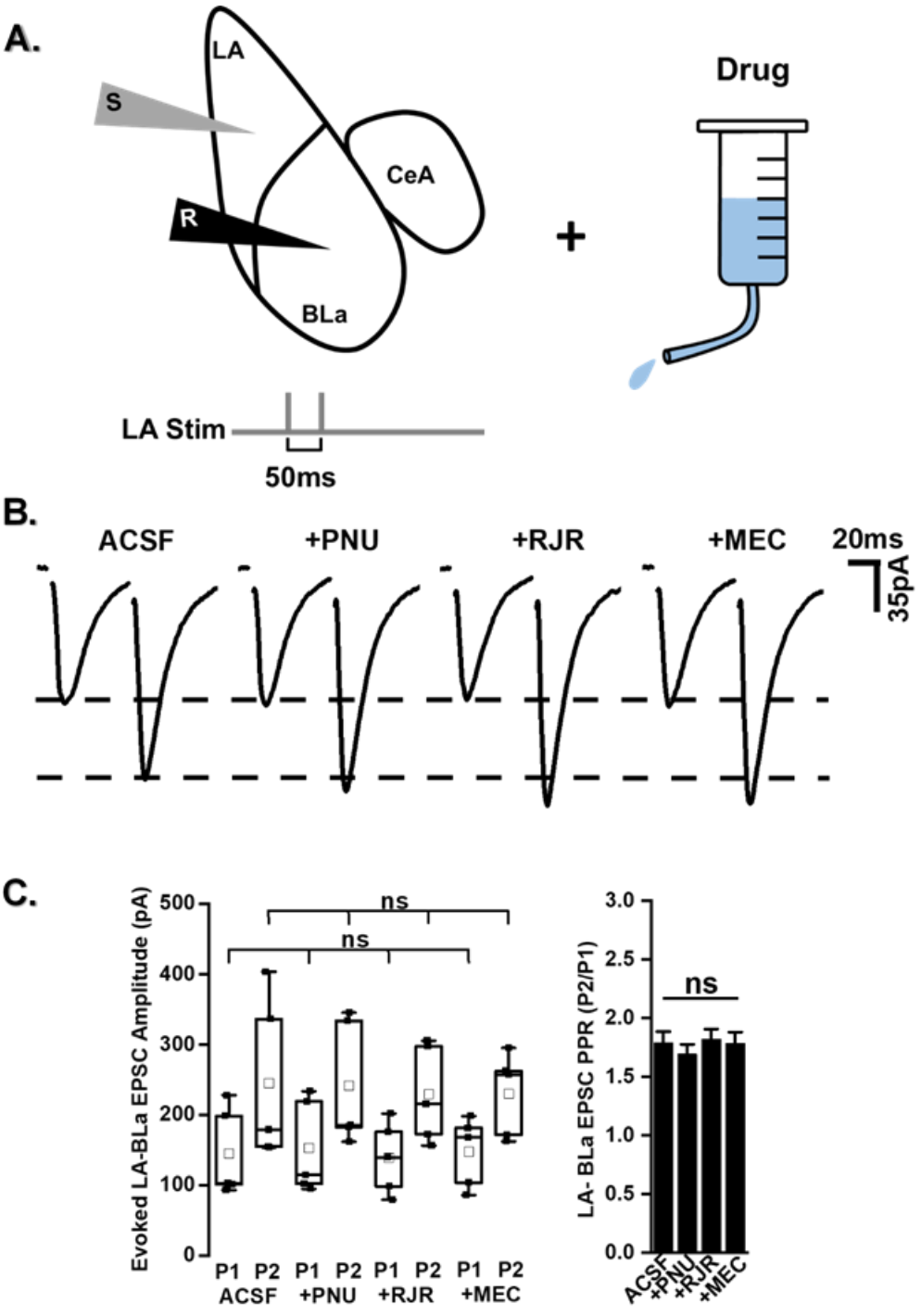
A.
LA
S
CeA
R
BLa
Drug
+
LA Stim
50ms
B.
ACSF
+PNU
+RJR
+MEC
20ms
35pA
C.
Evoked LA-BLa EPSC Amplitude (pA)
500
400
300
200
100
0
ns
ns
P1 P2 P1 P2 P1 P2 P1 P2
ACSF +PNU +RJR +MEC
LA- BLa EPSC PPR (P2/P1)
3.0
2.5
2.0
1.5
1.0
0.5
0.0
ns
ACSF
+PNU
+RJR
+MEC

Figure 4.8. Activation of α7 and α4β2 nicotinic acetylcholine receptors does not influence evoked glutamate release at LA-BLa synapses. A. Schematic of the experimental setup depicting the positioning of the recording electrode in the BLa, the simulating electrode in the LA, and the application of drug. The LA stimulation protocol is also depicted, which involves a paired stimulation of LA (50ms apart). **B.** Representative traces depicting the membrane potential responses of a BLa PN to paired LA stimulation in ACSF and the subsequent and successive application of 300nM PNU-282987, 100nM RJR-2403, and 20μM MEC. **C. Left.** Graph showing the amplitude of the first LA-BLa EPSC (Pulse 1 or P1) and the second LA-BLa EPSC (P2) evoked by paired LA stimulation in ACSF (far left) and the subsequent addition of PNU-282987 (middle left), RJR-2403 (middle right), and MEC (far right). **Right.** Bar graph showing the paired-pulse facilitation ratio (P2 amplitude/P1 amplitude) of the LA-BLa EPSCs in ACSF (far left) and the subsequent addition of PNU-282987 (middle left), RJR-2403 (middle right), and MEC (far right). * = $p < 0.01$, ** = $p < 0.01$, *** $p < 0.001$.

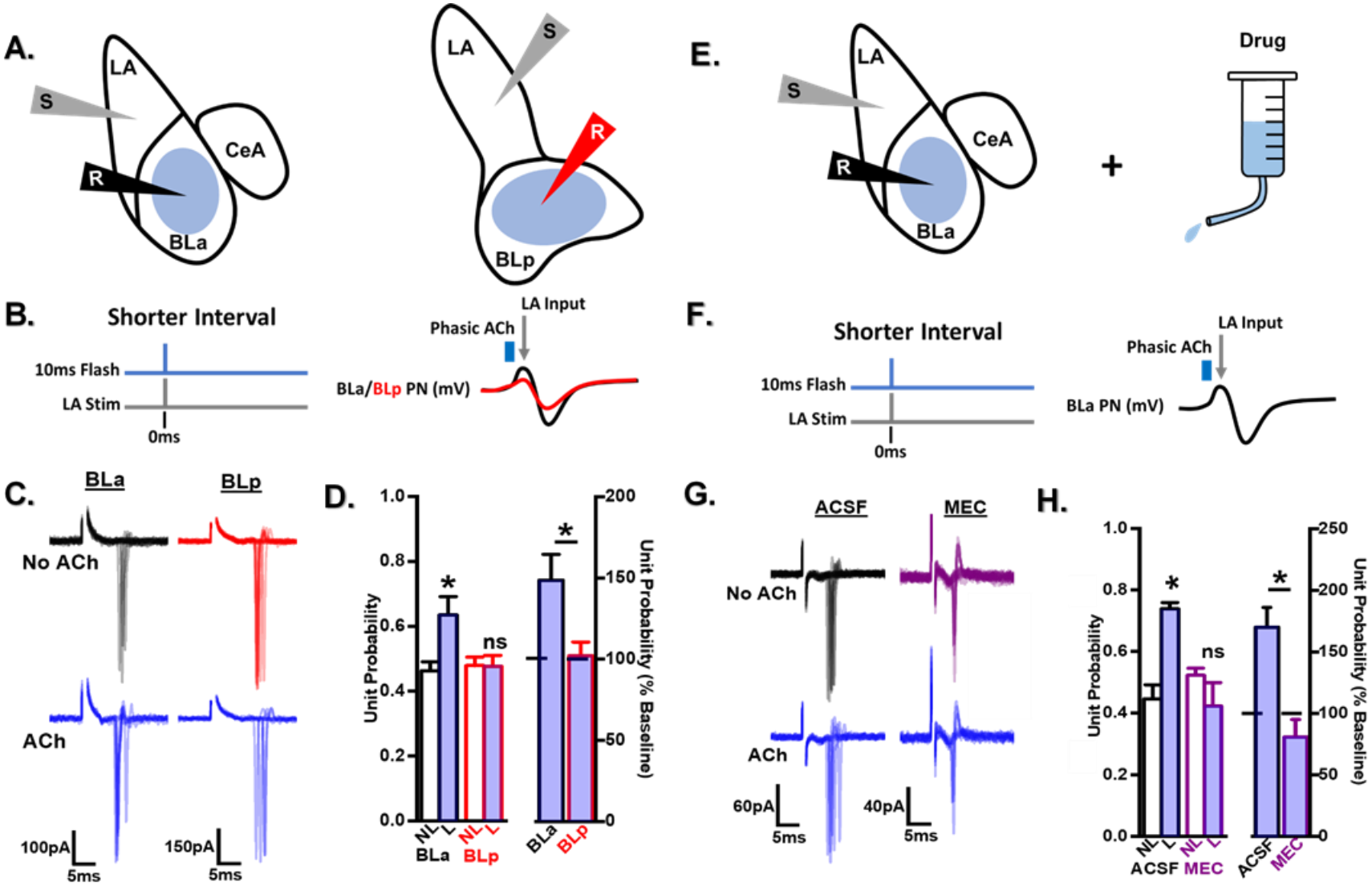
A.
LA
S
R
CeA
BLa
BLp
B.
Shorter Interval
10ms Flash
LA Stim
0ms
LA Input
Phasic ACh
BLa/BLp PN (mV)
C.
BLa
BLp
No ACh
ACh
100pA
5ms
150pA
5ms
D.
Unit Probability
Unit Probability (% Baseline)
ns
NL
L
BLa
BLp
E.
Drug
F.
Shorter Interval
10ms Flash
LA Stim
0ms
LA Input
Phasic ACh
BLa PN (mV)
G.
ACSF
MEC
No ACh
ACh
60pA
5ms
40pA
5ms
H.
Unit Probability
Unit Probability (% Baseline)
ns
ACSF
MEC

Figure 4.9. Phasic acetylcholine release associatively enhances the ability of appropriately timed LA inputs to fire BLa, but not BLp, pyramidal neurons. A. Schematic of the experimental setup depicting **(Left)** the positioning of the recording electrode in the BLa, the simulating electrode in the LA, and the targeting of the BLa with individual blue light flashes or **(Right)** the positioning of the recording electrode in the BLp, the simulating electrode in the LA, and the targeting of the BLp with individual blue light flashes. **B. Left.** The timing relationship between the single stimulation of LA and the presentation of individual 10ms flashes. **Right.** Showing how the protocol on the left is designed to align the peak of the early nicotinic depolarization with the arrival of LA input. The nicotinic depolarization and muscarinic hyperpolarization of BLa PNs (black trace) are drawn with larger amplitudes than those of the BLp (red trace) based on findings from Figure 4.6. **C.** Representative traces depicting recordings of single units from consecutive sweeps (overlaid) in BLa (top left and bottom left) and BLp (top right and bottom right) PNs in the absence (top left and top right) and presence (bottom left and bottom right) of phasic ACh. **D. Left.** Bar graph showing the average probability of observing LA-driven single units in BLa (black bars, left half) and BLp (red bars, right half) PNs in the absence (colorless bars) and presence (blue shaded bars) of phasic ACh. **Right.** Bar graph showing the average probability of observing LA-driven single units in BLa (black bar, left half) and BLp (red bar, right half) PNs in the presence of ACh expressed as a percentage of baseline (the average probability of observing single units in either cell type without ACh). No drugs were present in these experiments. **E.** Schematic of the experimental setup depicting the positioning of the recording electrode in the BLa, the simulating electrode in the LA, the targeting of the BLa with individual blue light flashes, and the application of drug (MEC) to assess the contribution of nicotinic receptors to the effect of phasic ACh at this interval. **F. Left.** The timing relationship between the single stimulation of LA and the presentation of individual 10ms flashes. **Right.** Showing how the protocol on the left is designed to align the peak of the early nicotinic depolarization with the arrival of LA input. **G.** Representative traces depicting recordings of single units from consecutive sweeps (overlaid) in BLa PNs in ACSF (top left and bottom left) and 20μM MEC (top right and bottom right) in the absence (top left and top right) and presence (bottom left and bottom right) of phasic ACh. **H. Left.** Bar graph showing the average probability of observing an LA-driven single unit in BLa PNs in ACSF (black bars, left half) and MEC (purple bars, right half) in the absence (colorless bars) and presence (blue shaded bars) of phasic ACh.

Right. Bar graph showing the average probability of observing an LA-driven single unit in BLa PNs in ACSF (black bar, left half) and MEC (purple bar, right half) in the presence of ACh expressed as a percentage of baseline (the average probability of observing single units in BLa PNs without ACh). NL = no light (or no ACh), L = light (ACh is present). * = $p < 0.01$, ** = $p < 0.01$, *** $p < 0.001$.

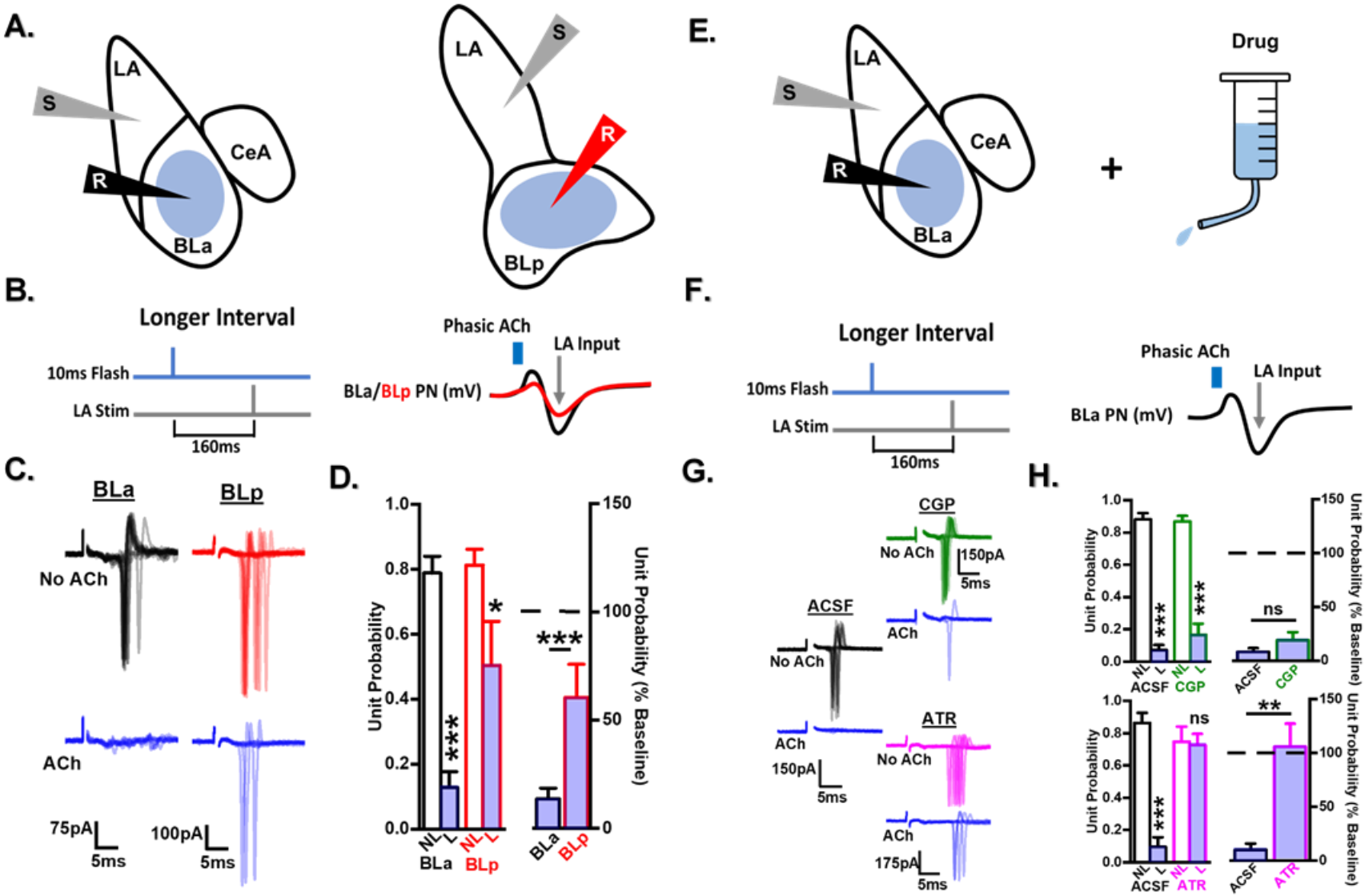
A.
LA
S
CeA
R
BLa
LA
S
R
BLp
E.
LA
S
CeA
R
BLa
+
Drug
B.
Longer Interval
10ms Flash
LA Stim
160ms
Phasic ACh
LA Input
BLa/BLp PN (mV)
F.
Longer Interval
10ms Flash
LA Stim
160ms
Phasic ACh
LA Input
BLa PN (mV)
C.
BLa
BLp
No ACh
ACh
75pA
5ms
100pA
5ms
D.
Unit Probability
Unit Probability (% Baseline)
NL
L
BLa
BLp
*
***
***
G.
CGP
No ACh
150pA
5ms
ACSF
ACh
No ACh
ATR
ACh
150pA
5ms
No ACh
ACh
175pA
5ms
H.
Unit Probability
Unit Probability (% Baseline)
***
***
ns
ACSF
CGP
ns
**
ACSF
ATR

Figure 4.10. Phasic acetylcholine release reduces the ability of inappropriately timed LA inputs to fire BLa and BLp pyramidal neurons. A. Schematic of the experimental setup depicting **(Left)** the positioning of the recording electrode in the BLa, the simulating electrode in the LA, and the targeting of the BLa with individual blue light flashes or **(Right)** the positioning of the recording electrode in the BLp, the simulating electrode in the LA, and the targeting of the BLp with individual blue light flashes. **B. Left.** The timing relationship between the single stimulation of LA and the presentation of individual 10ms flashes. **Right.** Showing how the protocol on the left is designed to align the peak of the late muscarinic hyperpolarization with the arrival of LA input. The nicotinic depolarization and muscarinic hyperpolarization of BLa PNs (black trace) are drawn with larger amplitudes than those of the BLp (red trace) based on findings from Figure 4.6. **C.** Representative traces depicting recordings of single units from consecutive sweeps (overlaid) in BLa (top left and bottom left) and BLp (top right and bottom right) PNs in the absence (top left and top right) and presence (bottom left and bottom right) of phasic ACh. **D. Left.** Bar graph showing the average probability of observing LA-driven single units in BLa (black bars, left half) and BLp (red bars, right half) PNs in the absence (colorless bars) and presence (blue shaded bars) of phasic ACh. **Right.** Bar graph showing the average probability of observing LA-driven single units in BLa (black bar, left half) and BLp (red bar, right half) PNs in the presence of ACh expressed as a percentage of baseline (the average probability of observing single units in either cell type without ACh). No drugs were present in these experiments. **E.** Schematic of the experimental setup depicting the positioning of the recording electrode in the BLa, the simulating electrode in the LA, the targeting of the BLa with individual blue light flashes, and the application of drug (CGP or ATR) to assess the contribution of $GABA_B$ and muscarinic receptors to the effect of phasic ACh at this interval. **F. Left.** The timing relationship between the single stimulation of LA and the presentation of individual 10ms flashes. **Right.** Showing how the protocol on the left is designed to align the peak of the late muscarinic hyperpolarization with the arrival of LA input. **G.** Representative traces depicting recordings of single units from consecutive sweeps (overlaid) in BLa PNs in ACSF (left traces), 2 µM CGP (top right traces), and 5 µM ATR (bottom right traces) in the absence (black traces for ACSF, green traces for CGP, pink traces for ATR) and presence (blue traces for all drug conditions) of phasic ACh. **H. Top Left.** Bar graphs showing the average probability of observing an LA-driven single unit in BLa PNs in ACSF (black bars, left half) and CGP (green bars, right half) in the absence (colorless bars) and presence (blue shaded bars) of phasic ACh. **Top Right.** Bar graph showing the average probability of observing an LA-driven single unit in BLa PNs in ACSF (black bar, left half) and

CGP (green bar, right half) in the presence of ACh expressed as a percentage of baseline (the average probability of observing single units in BLa PNs without ACh). **Bottom Left.** Bar graphs showing the average probability of observing an LA-driven single unit in BLa PNs in ACSF (black bars, left half) and ATR (pink bars, right half) in the absence (colorless bars) and presence (blue shaded bars) of phasic ACh. **Bottom Right.** Bar graph showing the average probability of observing an LA-driven single unit in BLa PNs in ACSF (black bar, left half) and ATR (pink bar, right half) in the presence of ACh expressed as a percentage of baseline (the average probability of observing single units in BLa PNs without ACh). * = $p < 0.01$, ** = $p < 0.01$, *** $p < 0.001$.

Table 4.1. Active and passive electrical properties of BLa and BLp pyramidal neurons. Cm = membrane capacitance, Rm = membrane resistance, RMP = resting membrane potential, spike onset delay = time from start of depolarizing current pulse until initial spike, spike thresh = spike threshold = the membrane potential at which the cell spikes, rheobase = the amount of current required to reach spike threshold. * = p < 0.01, ** = p < 0.01, *** p < 0.001.

		BLa (n=20)	BLp (n=21)	2-Sample T-Test	
	Cell Property	Mean ± SEM	Mean ± SEM	P-Value	Significance
Passive	Cm (pF)	45.9 ± 0.71	34.29 ± 0.5	2.55E-16	***
	Rm (ΩM)	115.5 ± 5.45	147.71 ± 7.4	0.0013	**
	RMP (mV)	-71.35 ± 0.92	-68 ± 0.96	0.016	*
Active	Spike Onset Delay (ms)	318.04 ± 47.92	596.67 ± 88.14	0.0093	**
	Spike Thresh (mV)	-42.26 ± 0.69	-40.19 ± 0.74	0.048	*
	Rheobase (pA)	99 ± 6.24	107.62 ± 4.87	0.28	ns

Table 4.2. Drugs used in Chapter 4.

Drug Name	Drug Type	Target	Method	Dose	Citation
6-cyano-7-nitroquinoxaline-2,3-dione (CNQX)	Selective Antagonist	AMPA Receptors	Bath	20µM	Lee et al., 2010
Dizocilpine Maleate (MK-801)	Selective Antagonist	NMDA Receptors	Bath	20µM	Sison and Gerlai 2011
Picrotoxin (Pic)	Selective Antagonist	$GABA_A$ Receptors	Bath	50µM	Power and Sah 2008
Baclofen (Bac)	Selective Agonist	$GABA_B$ Receptors	Bath	20µM	Skov et al., 2011
CGP	Selective Antagonist	$GABA_B$ Receptors	Bath	2µM	Bony et al. 2013
Mecamylamine (MEC)	Non-Selective Antagonist	nAChRs	Bath	20µM	Shen and Horn, 1998
RJR-2403	Selective Agonist	α4β2 nAChRs	Bath	100nM	Garduño et al., 2012
Dihydro-β-erythroidine Hydrobromide (DHβE)	Selective Antagonist	α4β2 nAChRs	Bath	1µM	Brusco et al., 2015
PNU-282987	Selective Agonist	α7 nAChRs	Bath	300nM	Hajós et al., 2005
Methyllycaconitine (MLA)	Selective Antagonist	α7 nAChRs	Bath	100nM	van Goethem et al., 2019
Muscarine (Musc)	Non-Selective Agonist	mAChRs	Bath	10µM	Meng et al., 2017
Atropine (ATR)	Non-Selective Antagonist	mAChRs	Bath	5µM	Yang et al., 2014
Pirenzepine (PRZ)	Selective Antagonist	M1 mAChRs	Bath	1µM	Unal et al., 2015
QX-314	Selective Antagonist	GIRK Channels	Intracellular	5mM	Smirnov et al., 1999

CHAPTER 5

OPPOSITE IMPACT OF OPTICALLY AND PHARMACOLOGICALLY STIMULATED M1 MUSCARINIC RECEPTORS ON SYNAPTIC NMDA CURRENTS IN PYRAMIDAL NEURONS OF THE BASOLATERAL NUCLEAR COMPLEX OF THE AMYGDALA

5.1. INTRODUCTION

The basolateral nuclear complex of the amygdala (BNC) – consisting of the lateral (LA), basolateral (BL), and basomedial nuclei (BM) – detects biologically relevant environmental stimuli and orchestrates appropriate behavioral responses to their implied meaning (Adolphs et al., 1994; Blanchard and Blanchard 1972; Brown and Schafer 1888; Klüver and Bucy 1937; LeDoux et al., 1990; McDonald 2020; Pitkänen et al., 1997; Weiskrantz 1956). The BNC is also a crucial storage site for associative emotional memories (Bocchio et al., 2017; Pape and Pare 2010). Like the cortex, the BNC is comprised of local inhibitory interneurons that release gamma-aminobutyric acid (GABA) and long-range excitatory pyramidal neurons (PNs) that release glutamate (McDonald 2020; Sah et al., 2003). Sensory information enters the LA, and its PNs send heavy projections to the PNs in the ventrally-adjacent (Bazelot et al., 2015; Jolkkonen and Pitkänen 1998; Pitkänen et al., 1997; Pu et al., 2009; Wang et al.,

2002), the output of which are important for mediating BNC function (Ambroggi et al., 2008; Baxter and Murray 2002; Beyeler et al., 2016, 2018; Goosens and Maren 2001; Gore et al., 2015; Janak and Tye 2015; Killcross, Robbins, and Everitt 1997; Kim et al., 2016, 2017; Namburi et al., 2015; Paton et al., 2006; Pignatelli and Beyeler 2019; Stuber et al., 2011; Tye 2018; Tye et al., 2008; Zhang et al., 2020).

Associative emotional memories are formed in the BNC through long-term potentiation (LTP) (Bocchio et al., 2017; Carrere and Alexandre 2015; Maren 1999; Pape and Pare 2010), the cellular and molecular correlate of learning (Luscher and Malenka 2012; Lynch 2004). LTP is a process whereby the communication strength between neurons activated during experience becomes and remains enhanced for a prolonged period (Luscher and Malenka 2012; Yang and Calakos 2013). At the cellular level, synapses of weak sensory inputs representing neutral stimuli that are unable to activate BNC behavioral output neurons alone become strengthened via their coincident signaling onto the same postsynaptic cells as strong sensory inputs representing salient stimuli (Johansen et al., 2011; Sigurdsson et al., 2007). The synaptic modifications that result from this pairing (i.e., LTP) enable the initially neutral stimuli to activate the same BNC circuitry (and generate the same emotional behaviors) as the salient stimuli they were paired with during the original emotional experience (Johansen et al., 2011; Sigurdsson et al., 2007). This process enables the BNC to assign meaning to stimuli through experience and predict biologically relevant outcomes that promote organismal survival (Janak and Tye 2015).

N-Methyl-D-aspartic acid (NMDA) receptors are essential for the LTP underlying associative emotional learning in the BNC (Campeau et al., 1992; Fanselow and Kim 1994; Lee et al., 2001; Maren 1999; Maren et al., 1996; Miserendino et al., 1990) because their activation during emotional experiences enables calcium influx into BNC PNs, which initiates intracellular mechanisms underlying LTP expression (Luscher and Malenka 2012). The size of NMDA receptor currents, and therefore the amount of calcium entry they permit, can be controlled via numerous molecular mechanisms (Bazzari and Parri 2019; Kantamneni 2015; Luján et al., 2009; MacDonald et al., 2007).

The BL is heavily innervated by cholinergic fibers originating in the basal forebrain (Carlsen and Heimer 1986; Muller et al., 2011) and acetylcholine (ACh) has important roles in learning in memory (Drever et al., 2011; Hasselmo 2006). ACh is transiently released during significant emotional experiences and muscarinic ACh receptors (mAChRs) are a major class of receptors by which ACh is known to influence learning and memory (Wilson and Fadel, 2017). mAChRs are G protein-coupled receptors (GCPRs) and GCPRs are known to modulate postsynaptic NMDA receptor expression and function (Bazzari and Parri 2019; Kantamneni 2015; MacDonald et al., 2007). In fact, pharmacological activation of the M1 mAChR (M1R) subtype has been shown to potentiate NMDA receptor currents in hippocampal PNs by preventing the normal opening of nearby small conductance calcium-activated potassium (SK) channels that negatively regulate NMDA receptor currents (Buchanan et al., 2010; Calabresi et al., 1998; Dennis et al., 2016; Giessel and Sabatini 2010; Marino et al., 1998; Sur

et al., 2003; Tigaret et al., 2018). This mechanism has also been shown to underlie the facilitation of LTP induction in hippocampal neurons elicited by electrically induced trains of endogenous ACh release (Buchanan et al., 2010).

Surprisingly, very few studies have explored the role of ACh in LTP or learning in the BNC (Crouse et al., 2020; Jiang et al., 2016; Park et al., 2004; Watanabe et al., 1995). Among these, there was substantial variation in the techniques used, study focus, and findings. Two were older studies that used exogenous cholinergic agonists that fail to closely mimic endogenously released ACh, with one reporting a unique form of presynaptic LTP and the other focusing on structures other than the BL (Park et al., 2004; Watanabe et al., 1995). The other two studied explored the effects of endogenous ACh signaling on learning, but each reported different results and only one looked at the underlying LTP (Crouse et al., 2020; Jiang et al., 2016). The study that only looked at learning reported a necessary role for mAChR activation but did not identify the mAChR subtype nor molecular mechanism by which the mAChRs exerted their effects (Crouse et al., 2020). The other study, which also looked at LTP, reported that sustained ACh signaling in BNC is sufficient to elicit LTP and strengthen emotional learning but, contrary to the first study, said this effect was mediated by a presynaptic mechanism that did not depend on mAChRs (Jiang et al., 2016). Neither study assessed the impact of ACh signaling on postsynaptic NMDA receptors in BNC PNs, warranting future studies examining such possibilities.

In the present study, we hypothesized that M1Rs activated by phasic ACh and muscarine would potentiate NMDA receptor currents at LA-BLa synapses by blocking SK channels. We focused on the BLa due to its exceptionally high cholinergic innervation and M1R expression (Chapter 3; Muller et al., 2011, 2013). We tested this hypothesis with three aims. First, we determined whether M1Rs activated by phasic ACh release potentiate glutamate responses at LA synapses onto BLa PNs. Second, we compared the effects of M1Rs activated by phasic ACh release and bath-applied muscarine on LA-BLa NMDA responses. Third, we determined the molecular mechanisms underlying the effects of M1Rs activated by each mode on LA-BLa NMDA responses. If M1Rs potentiate NMDA receptor currents in amygdala, this could lower the threshold for LTP induction and represent a means by which ACh strengthens the acquisition of emotional memories.

5.2. MATERIALS AND METHODS

5.2.1. ANIMAL CARE AND USE PROCEDURES

All animal care, use, and surgical procedures were performed in compliance with the National Institutes of Health guidelines for care and use of laboratory animals and approved by The Institutional Animal Care and Use Committee (IACUC) of the University of South Carolina. All mice were housed in temperature-controlled cages (with maximum of 5 mice per cage) and maintained on a 12-hour light/dark cycle with ad libitum food and water

5.2.2. ANIMALS

In most experiments, six- to 24-week-old ChAT-Cre/Ai32(ChR2-EYFP) transgenic mice of either sex were used, which express ChR2(H134R)-EYFP in cholinergic neurons. These were generated by crossing ChAT-Cre animas (#006410, The Jackson Laboratory) with Cre-dependent reporter Ai-ChR2-eYFP animals (#012569, Jackson Labs). All mice were group housed in a climate-controlled facility with a 12/12 light/dark cycle and provided with ad libitum access to food and water.

5.2.3. SLICE PREPARATION FOR ELECTROPHYSIOLOGY RECORDINGS

Animals were deeply anesthetized with isoflurane and the brain was quickly extracted and submerged in ice-cold artificial cerebrospinal fluid (ACSF) saturated with 95% O2 and 5% CO2 and containing the following (in mM): 110 choline chloride, 2.5 KCL, 25 NaHCO3, 1.0 NaH2PO4, 20 glucose, 5 MgCl2, 0.5 CaCl2. Coronal brain slices (300μM thick) containing amygdala were sectioned using a vibratome (VT1000S; Leica, Nussloch, Germany) and immediately transferred to ACSF (saturated with 95% O2 and 5% CO2) containing (in mM) 125 NaCl, 2.7 KCl, 25 NaHCO3, 1.25 NaH2 PO4, 10 glucose, 5 MgCl2, 0.5 CaCl2. All slices were incubated at 34-36°C for a minimum of 20 minutes before the solution was allowed to equilibrate to room temperature. For recordings, individual slices were transferred to a recording chamber maintained at 32-34°C and continuously perfused with ACSF (saturated with 95% O2 and 5% CO2) containing 2 mM calcium and 1 mM magnesium.

5.2.4. SLICE ELECTROPHYSIOLOGY RECORDINGS

PNs were visualized using infrared-differential interference contrast optics through a 40x objective (Olympus BX51WI). For whole cell recordings, borosilicate glass electrodes of 4-6 MΩ resistance filled with potassium gluconate internal solution consisting of (in mM) 130 K-gluconate, 5 KCl, 10 HEPES, 2 MgCl2, 2 MgATP, 0.3 NaGTP, 0.5 EGTA (pH 7.3) were used. Phasic and endogenous ACh release was evoked by delivering brief, single flashes of blue light (473nM; Thor Labs) directly over the recorded cells through a 40x lens. Light flashes were always applied at 60 sec intervals. Electrical stimulation of glutamatergic LA input was achieved by delivering single pulses of current (0.1ms) every 20 sec through a monopolar stimulating electrode positioned in LA. All LA EPSCs were recorded at a holding potential of -70mV. To assess the influence of phasic ACh release on glutamate receptor responses (Fig. 5.1–5.4.), we implemented a protocol whereby glutamate release at LA-BLa synapses (or NMDA puffs in Fig. 5.4.) was periodically evoked and ACh was additionally released 160ms before every third LA stimulation (or every second NMDA puff in Fig. 5.4.) by presenting a 10ms blue light flash, which we know evokes ACh release because cholinergic agonists block the responses they evoke (Chapter 4) and we have previously shown ChR2 is selectively expressed in the cholinergic neurons of the ChAT-Cre/Ai32(ChR2-EYFP) transgenic mice we used in this study (Fig. 4.1.). We chose the 160ms interval for two primary reasons. First, we have previously shown that phasic ACh release at this interval does not influence glutamate release from LA terminals at LA-BLa synapses and

we were interested in studying ACh's postsynaptic effects on glutamate receptor responses. Second, previous studies have shown that postsynaptic M1Rs can influence glutamate receptor responses (Buchanan et al., 2010; Calabresi et al., 1998; Dennis et al., 2016; Giessel and Sabatini 2010; Marino et al., 1998; Sur et al., 2003; Tigaret et al., 2018) and we have previously shown that M1Rs are activated by phasic ACh release at this interval. In whole cell experiments measuring the effects of muscarine and apamin on the amplitude of LA EPSCs (Fig. 5.5.– 5.7.), drugs were added to the recording ACSF and only applied to slices in the recording chamber after a stable EPSC baseline was achieved in a prior condition.

5.2.5. ANALYSES AND STATISTICS

Data from electrophysiological recordings was analyzed using Clampfit 10.7 (Molecular Devices) and figures were made using Origin Lab Pro software. Statistical comparisons were performed using the appropriate t test or ANOVA with post hoc test. Values are given as mean ± SEM. A minimum of three animals were used for data presented in each figure.

5.3. RESULTS

5.3.1. THE POSTSYNAPTIC IMPACT OF PHASIC AND ENDOGENOUS ACETYLCHOLINE RELEASE ON GLUTAMATE RESPONSES IN BL PYRAMIDAL NEURONS

5.3.1.A. Acetylcholine decreases the size of glutamate responses at LA-BLa synapses when it is phasically released 160ms before LA stimulation

We first assessed whether phasic ACh release alters the size of glutamate responses from LA terminals innervating BLa PNs (Fig. 5.1.), which has not been done before. To accomplish this, we implemented a protocol whereby glutamate release was periodically evoked at LA-BLa synapses and ACh was additionally released 160ms before every third LA stimulation via a 10ms flash of blue light (Fig. 5.1.A.). We know that ACh is released by the 10ms flash based on our previous work (Chapter 4). We also know that, at this interval, ACh does not alter glutamate release from LA terminals and that postsynaptic M1Rs are active (Chapter 4). We hypothesized that ACh would increase the size of LA-BLa EPSPs because postsynaptic M1Rs can increase the size of NMDA receptor currents in hippocampus (Buchanan et al., 2010; Calabresi et al., 1998; Dennis et al., 2016; Giessel and Sabatini 2010; Marino et al., 1998; Sur et al., 2003; Tigaret et al., 2018). We optimized our ability to detect NMDA receptor contributions to our LA-BLa EPSPs by lowering extracellular Mg^{2+} levels to 0.1mm (alleviating Mg^{2+} block) and prevented $GABA_A$ receptor interference by adding the $GABA_A$ receptor antagonist picrotoxin (Pic, 50 μM) to the recording ACSF. We identified BLa PNs based on their passive and active electrical properties (Fig. 4.5. and Table 4.1.; Fig. 5.1.B.) and characteristic biphasic response to phasic ACh release (Chapter 4; Fig. 5.1.B.). In contrast to our hypothesis, phasic ACh release decreased, rather than increased, the amplitude

of LA-BLa EPSPs (Fig. 5.1.D. and 5.1.E.). The amplitude of the EPSP without ACh was 4.83±0.17 mV compared to 4.0±0.3 mV in the presence of ACh ($p = 0.041$, two-tailed paired t-test) (Fig. 5.1.E., left), translating to a decrease of 17.2±4.07% (n= 3 cells).

Next, we determined whether phasic ACh release can also reduce the size of LA-BLa AMPA and/or NMDA receptor responses (Fig. 5.2.). To do so, we repeated the protocol from Figure 5.1. while pharmacologically isolating AMPA and NMDA receptors. First, we isolated AMPA receptor responses by adding the NMDA receptor antagonist dizocilpine maleate (MK-801 maleate, 20µM) to the recording ACSF while keeping the other conditions the same. Consistent with above, phasic ACh release significantly decreased the amplitude of LA-BLa AMPA EPSPs (Fig. 5.2.B. and 5.2.C., left). The amplitude of the AMPA EPSP without ACh was 4.17±0.34 mV compared to 3.62±0.42 mV in the presence of ACh ($n = 3$ cells, $p = 0.034$, two-tailed paired t-test; Fig. 5.2.C., left). The percent decrease of the LA-BLa AMPA EPSPs (13.56±3.66%; Fig. 5.2.C., right) was close to the percent decrease of LA-BLa EPSPs reported above (17.2±4.07%; Fig. 5.1.E., right).

Next, we isolated NMDA receptor responses by removing all Mg^{2+} from the recording ACSF and replacing MK-801 maleate with the AMPA receptor antagonist 6-cyano-7-nitroquinoxaline-2,3-dione (CNQX, 20µM). Once again, phasic ACh release significantly decreased the amplitude of LA-BLa NMDA EPSCs (Fig. 5.2.E. and 5.2.F., left). The amplitude of the NMDA EPSC without ACh was 100.05±16.65 pA compared to 60.34±10.49 pA in the presence of ACh

(n = 4 cells, p = 0.04, two-tailed paired t-test; Fig. 5.2.F., left). Interestingly, the percent decrease of the LA-BLa NMDA EPSCs (37.81±7.06%; Fig. 5.2.F., right) was noticeably larger than it was for LA-BLa AMPA EPSPs (13.56±3.66%; Fig. 5.2.C., right) and LA-BLa EPSPs (17.2±4.07%; Fig. 5.1.E., right). Together, these results indicate that ACh decreases, rather than increases, the size of AMPA and NMDA receptor responses at LA-BLa synapses when it is phasically released 160ms before LA stimulation.

5.3.1.B. Intracellular GIRK channel blocker QX-314 prevents phasic acetylcholine release from decreasing LA-BLa NMDA EPSCs

Next, we wanted to determine the cause of the inhibitory effects of ACh reported above. We suspected postsynaptic GIRK channels could be responsible because, in the protocol above, LA inputs arrive at the peak of postsynaptic, M1R-mediated GIRK currents (Fig. 4.4.; Fig. 5.1.A., Fig. 5.2.A. and 5.2.D.). Studies have shown the hyperpolarizing current produced by postsynaptic GIRK channels reduce NMDA receptor currents by facilitating Mg^{2+} block (Chalifoux and Carter 2010; Morrisett et al., 1991; Mott et al., 1999; Otmakhova and Lisman 2004), but this mechanism cannot explain the reduced LA-BLa NMDA EPSCs above because our cells were voltage-clamped and Mg^{2+} was not present in our recordings. It also cannot explain the decrease in isolated AMPA receptor responses that we observed (Mott et al., 1999). Postsynaptic GIRK channels can also provide local shunting inhibition of AMPA receptor currents (Chalifoux and Carter 2010; Takigawa and Alzheimer 2002, 2003). We suspected this mechanism to underlie ACh's effects above and focused on NMDA receptor

currents moving forward because this mechanism has never been shown to impact NMDA receptor currents before and NMDA receptors are central to LTP and learning.

To determine whether postsynaptic GIRK channels activated by phasic ACh release reduce LA-BLa NMDA EPSCs via shunting inhibition, we repeated the experiment in Figure 2C and 2D above with the GIRK channel blocker QX-314 (5 mM) (Andrade, 1991; Hu et al., 2002) added to the intracellular solution (Fig. 5.3.). This technique allows us to block GIRK channels in only recorded cells without affecting the surrounding circuitry. QX-314, also a voltage-gated sodium channel blocker, inhibited spiking in every cell (data not shown; n=4, representative trace: Fig. 5.3.A., left), verifying it has a positive effect. In these same cells, the amplitude of the late, GIRK channel-mediated IPSC (13.75±8.91 pA, n = 4 cells) was significantly smaller (p = 0.006, two-tailed unpaired t test) than the amplitude of the late IPSC recorded under control conditions (38.78±2.45 pA, n = 46 cells) (data shown in Fig. 4.4.E.), suggesting GIRK channels were blocked by QX-314 (representative trace: Fig. 5.3.A., right). Contrary to above, phasic ACh release did not significantly decrease the amplitude of LA-BLa NMDA EPSCs under these conditions (Fig. 5.3.B.). We have previously shown that, at the 160ms interval, phasic ACh release does not affect the paired pulse facilitation ratio (PPR) of LA-BLa EPSCs (Fig. 4.7.F., right; Fig. 5.3.C., right), suggesting it does not alter glutamate release from LA terminals. The PPR without ACh was 1.64±0.18 compared to 1.56±0.14 in the presence of ACh (n = 7 cells, p = 0.64, two-tailed paired t test; Fig. 5.3.C., right).

At this interval, ACh did, however, significantly decrease the amplitudes of both paired EPSCs (Fig. 4.7.F., left; Fig. 5.3.C., left). The amplitude of the first EPSC without ACh was 157.83±49.79 pA compared to 112.52±35.84 pA in the presence of ACh (n = 7 cells, p = 0.048, two-tailed paired t test) and the amplitude of the second EPSC without ACh was 225.78±64.16 pA compared to 163.47±49.75 pA in the presence of ACh (n = 7 cells, p = 0.034) (Fig. 5.3.C., left). ACh reduced both EPSCs in the PPR paradigm equally, suggesting a postsynaptic mechanism (Fig. 5.3.D-E.). The amplitudes of the first and second EPSCs recorded in ACh were 0.69±0.047 and 0.67±0.069 of the amplitudes of the first and second EPSCs recorded in control (no ACh), respectively (p = 0.67, two-tailed paired t test; Fig. 5.3.E.). Interestingly, ACh decreased both EPSCs in the PPR paradigm (n= 7 cells) and the single NMDA EPSC with regular internal (n = 4 cells) by a similar amount (P1 = 31.47±5.0 percent decrease, P2 = 29.21±6.27 percent decrease, control NMDA EPSC = 37.81±7.06 percent decrease), and the reduction of these was significantly greater than the 4.32±5.11 percent decrease of single NMDA EPSCs with intracellular QX-314 (n = 5 cells) (QX-314 NMDA vs. P1 EPSC: p = 0.004, two-tailed unpaired t test; QX-314 NMDA vs. P2 EPSC: p = 0.013, two-tailed unpaired t test; QX-314 NMDA vs. control NMDA: p = 0.006, two-tailed unpaired t test) (Fig. 5.3.F.). Together, these data suggest that ACh shunts LA-BLa NMDA EPSCs by activating postsynaptic GIRK channels when it is phasically released 160ms before LA stimulation.

5.3.1.C. Phasic acetylcholine release does not affect the size of the NMDA current evoked by NMDA puffs in BLa or BLp pyramidal neurons

We have previously shown that BLa and BLp PNs are differentially impacted by phasic ACh release (Fig. 4.6.). Therefore, we next determined whether phasic ACh release differentially impacts NMDA currents in BLa and BLp PNs. We have not assessed whether phasic ACh release influences glutamate released from LA terminals in the BLp. Therefore, to avoid this potential confounding factor, we evoked NMDA currents by puffing NMDA onto BLa and BLp PNs instead of stimulating LA. We used the same protocol as above, except that ACh was released 160ms before every second NMDA puff (instead of every third LA stimulation) (Fig. 5.4.A.). Interestingly, despite a slightly increasing trend in BLa and BLp PNs, ACh had no significant effect on the amplitude of puffed NMDA EPSCs in either cell type (Fig. 5.4.B-E.). In BLa PNs, the amplitude of the puffed NMDA EPSC without ACh was 160.42±50.68 pA compared to 173.36±59.4 pA in the presence of ACh (n = 4 cells, p = 0.24, two-tailed paired t test) (Fig. 5.4.D., left). In BLp PNs, the amplitude of the puffed NMDA EPSC without ACh was 287.85±91.56 pA compared to 290.49±85.55 pA in the presence of ACh (n = 4 cells, p = 0.76, two-tailed paired t test) (Fig. 5.4.D., right). The amount by which ACh increased the amplitude of the puffed NMDA EPSCs was also not significantly different between the same BLa and BLp PNs (BLa = 3.31±6.34 percent increase vs. BLp = 5.1±4.49 percent increase, p = 83, two-tailed unpaired t test; Fig. 5.4.E.). MK-801 maleate (20μM) applied at the end

of the recording completely blocked the response to puffed NMDA in every cell it was applied to, indicating the responses were mediated by selective NMDA receptor activation (data not shown; representative traces: Fig. 5.4.B., left and Fig. 5.4.C., left). Together, these data suggest that ACh does not affect NMDA puff-evoked NMDA EPSCs in BLa or BLp PNs when it is phasically released 160ms before NMDA is puffed.

5.3.2. THE IMPACT OF MUSCARINE ON NMDA RECEPTOR CURRENTS IN BL PYRAMIDAL NEURONS

5.3.2.A. Bath-applied muscarine potentiates isolated LA-BLa NMDA EPSCs

ACh phasically released 160ms before LA stimulation reduces the size of LA-BLa glutamate responses in PNs via M1R-coupled postsynaptic GIRK channels, but M1Rs stimulated by cholinergic agonists can also potentiate NMDA receptor currents in hippocampal PNs (Buchanan et al., 2010; Calabresi et al., 1998; Dennis et al., 2016; Giessel and Sabatini 2010; Marino et al., 1998; Sur et al., 2003; Tigaret et al., 2018). We explored this possibility next, as it has not been done in the amygdala. To do so, we reverted to LA stimulation and compared the amplitude of periodically evoked LA-BLa NMDA EPSCs at baseline with their amplitudes in the presence of the general muscarinic acetylcholine receptor (mAChR) agonist muscarine (Musc, 100nM) (Fig. 5.5.). Just as with Figure 5.2.D-F. and Figures 5.3.–5.4. above, NMDA current responses were isolated by using recording ACSF containing zero Mg^{2+}, 50µM Pic, and 20µM CNQX. Consistent with the previous report in hippocampus, Musc

significantly increased the amplitude of LA-BLa NMDA EPSCs. The amplitude of the LA-BLa NMDA EPSC without Musc was 41.65±6.42 pA compared to 65.34±10.28 pA in the presence of Musc (n = 6 cells, p = 0.012, two-tailed paired t test) (Fig. 5.5.A-B.). The percent increase of the baseline LA-BLa NMDA EPSC amplitude produced by Musc (muscarinic NMDA potentiation) was 57.58±12.19 (Fig. 5.5.D.). MK-801 applied at the end of each recording completely blocked the response to LA stimulation in every cell, indicating the EPSCs were mediated by NMDA receptors (Fig. 5.5.A-B.).

5.3.2.B. Pirenzepine prevents muscarine from potentiating isolated LA-BLa NMDA EPSCs

Next, we determined whether the muscarinic potentiation of LA-BLa NMDA EPSCs was mediated by the activation of M1Rs. To do so, we repeated the experimental protocol from Figure 5 in the presence of the M1R antagonist pirenzepine dihydrochloride (PRZ, 1μM). Under these conditions, Musc did not significantly affect the amplitude of the LA-BLa NMDA EPSCs (Fig. 5.6.A-B.). The amplitude of the LA-BLa NMDA EPSC in PRZ without Musc was 74.29±29.75 pA compared to 72.19±23.52 pA in the presence of Musc and PRZ (n = 5 cells, p = 0.78, two-tailed paired t test) (Fig. 5.6.A-B.). The percent increase of the baseline LA-BLa NMDA EPSC amplitude (in PRZ) produced by Musc (muscarinic NMDA potentiation) was 4.53±7.51 percent (Fig. 5.6.C., left), which was significantly lower than the 57.58±12.19% muscarinic NMDA potentiation of LA-BLa NMDA EPSCs observed in the absence of PRZ (p = 0.007, two-tailed unpaired t-test; Fig. 5.5.C. and Fig. 5.6.C., right). MK-801

applied at the end of each recording completely blocked the response to LA stimulation in every cell, indicating the EPSCs were mediated by NMDA receptors (Fig. 5.6.A-B.).

5.3.2.C. Apamin minimizes the muscarinic potentiation of pharmacologically isolated LA-BLa NMDA EPSCs

Studies have reported that calcium entry through NMDA receptors activates nearby SK channels that, in turn, limit the size of those NMDA receptor currents by shunting them (Babiec et al., 2017; Bloodgood and Sabatini 2007; E. S. L. Faber 2010; E S Louise Faber, Delaney, and Sah 2005; Ngo-Anh et al., 2005). Studies have also reported that M1Rs potentiate NMDA receptor currents by preventing these SK channels from opening (Buchanan et al., 2010; Dennis et al., 2016; Giessel and Sabatini 2010; Tigaret et al., 2018). We determined whether this mechanism was responsible for the potentiating effects of Musc on LA-BLa NMDA EPSCs reported above by repeating the protocol from Figures 5 and 6 but applying the selective SK channel blocker apamin (100nM) before applying Musc. If Musc potentiates LA-BLa NMDA EPSCs by preventing SK channels from opening, we would expect: 1) apamin alone to potentiate the NMDA receptor currents to a similar extent as Musc alone and 2) Musc to produce minimal potentiation of the NMDA receptor currents after apamin has been previously applied.

Apamin alone significantly increased the amplitude of baseline LA-BLa NMDA EPSCs recorded under control conditions (Fig. 5.7.A-B.). The amplitude of the LA-BLa NMDA EPSCs without apamin was 51.61±13.46 pA compared to

80.92±26.58 pA in the presence of apamin (n = 5 cells, p = 0.05, one-tailed paired t test) (Fig. 5.7.A-B.). In line with our first expectation, the amount by which apamin potentiated these control LA-BLa NMDA EPSCs (47.26±13.16 percent increase, n = 5 cells) and the amount by which Musc alone potentiated LA-BLa NMDA EPSCs under the same control conditions in Figure 5.5. above (57.58±12.1 percent increase, n = 6 cells) were similar (p = 0.58, two-tailed unpaired t-test) (Fig. 5.7.C.), suggesting a shared mechanism could be involved. Despite an increasing trend, Musc plus apamin did not significantly increase the amplitude of LA-BLa NMDA EPSCs recorded in the presence of apamin alone (Fig. 5.7.A-B.). The amplitude of the LA-BLa NMDA EPSCs in the presence of apamin alone was 80.92±26.58 pA compared to 99.45±36.89 pA in the presence of Musc and apamin (n = 5 cells, p = 0.23, two-tailed paired t test) (Fig. 5.7.A-B.). In line with our second expectation, this translates to a minimal muscarinic potentiation of LA-BLa NMDA EPSCs recorded in the presence of apamin (21.9±10.91 percent increase, n = 5 cells) (Fig. 5.7.D.), suggesting both drugs potentiate control LA-BLa NMDA EPSCs by acting on the same effector. MK-801 maleate (20μM) applied after Musc + apamin completely blocked the LA EPSCs, indicating they were mediated by NMDA receptors (Fig. 5.7.A-B.). Together, these results suggest that Musc potentiates LA-BLa NMDA EPSCs by preventing SK channels from opening.

5.4. DISCUSSION

Our first goal was to determine whether phasic ACh release affects the size of glutamate responses at LA synapses onto BLa PNs at the 160ms interval

used in Chapter 4. We used this interval because we wanted to study the postsynaptic mechanisms of any potential effects and we knew that, at this interval, 1) ACh does not alter glutamate release from LA terminals and 2) postsynaptic M1Rs, which can modulate glutamate receptor responses in other brain areas (Buchanan et al., 2010; Calabresi et al., 1998; Dennis et al., 2016; Giessel and Sabatini 2010; Marino et al., 1998; Sur et al., 2003; Tigaret et al., 2018), are activated by ACh. We hypothesized we would see an increase in the size of LA-BLa EPSPs because pharmacological activation of postsynaptic M1Rs in hippocampal PNs can potentiate NMDA receptor currents (Marino et al., 1998). However, to our surprise, phasic ACh release reduced LA-BLa EPSPs instead. This reduction was observed even when we repeated the experiments while isolating the AMPA and NMDA receptor components of LA-BLa responses. Equivalent reductions of paired LA-BLa EPSCs and an unaffected PPR coupled with no reduction of LA-BLa NMDA EPSCs in the presence of intracellular GIRK channel blocker QX-314, both at the 160ms interval, confirmed the effect is mediated by postsynaptic GIRK channels that provide shunting inhibition of the LA-BLa NMDA EPSCs. This is further supported by a greater amount of reduction of individual LA-BLa NMDA receptor responses compared to individual LA-BLa AMPA receptor responses, as a presynaptic effect would be expected to reduce both equally. Importantly, the lack of increase in LA-BLa NMDA EPSC size in the presence of phasic ACh and QX-314 – the latter of which blocks potential GIRK-channel interference – suggests that phasic ACh also does not block SK channel opening at the 160ms interval via the activated M1Rs, as

predicted. To name a few possible explanations for this: 1) phasic ACh does block SK channels but this occurs before or after the 160ms LA input arrival timepoint, 2) phasic ACh does block SK channels but we could not observe the effect because the subset of NMDA receptors recruited by LA stimulation are not positioned adjacent to them (whereas cortical or other inputs could be), or 3) phasic ACh does block SK channels but we do not observe its effect because the spread zone of ACh from the activated cholinergic terminals is small and ACh only reaches M1Rs coupled to GIRK channels. There are surely other possibilities as well, which future studies should explore. Although postsynaptic GIRK channel-mediated shunting inhibition of AMPA receptor currents has been reported before (Chalifoux and Carter 2010; Takigawa and Alzheimer 2002, 2003), we are the first to report the same for NMDA receptor currents. We are also the first to show that GIRK channels activated by endogenous ACh can do so for AMPA and NMDA currents.

Intriguingly, postsynaptic M1Rs on BLa PNs can potentiate LA-BLa NMDA receptor currents when they are pharmacologically activated by muscarine instead. This effect is consistent with previous studies in other areas (Buchanan et al., 2010; Calabresi et al., 1998; Dennis et al., 2016; Giessel and Sabatini 2010; Marino et al., 1998; Sur et al., 2003; Tigaret et al., 2018) that motivated our hypothesis above that M1Rs activated by ACh release in the BLa would do the same. This discrepancy raises interesting questions about differences between the effects of endogenous ACh signaling and cholinergic agonists.

Indeed, there is strong and ongoing debate over the nature of ACh release from presynaptic cholinergic terminals (Disney and Higley 2020; Sarter and Lustig 2020). The advent of improved technologies has enabled our ability to detect multiple modes of ACh release in vivo and it is now becoming appreciated that ACh can be released rapidly and tonically under different behavioral circumstances (Crouse et al., 2020; Hangya et al., 2015; Laszlovszky et al., 2020; Sarter et al., 2014; Sturgill et al., 2020; Teles-Grilo Ruivo et al., 2017). It is speculated that the spread of endogenous ACh from cholinergic terminals, and therefore the effects it has on its cellular targets, could depend on the strength and/or mode of cholinergic signaling, with there being multiple spatiotemporal "zones" spanning an underlying continuum (Disney and Higley 2020). This spread is expected to be further restricted by the rapid activity of the powerful degradative enzyme acetylcholinesterase (AChE), which is expressed at very high concentrations in the BLa (Ben-Ari et al., 1977; McDonald and Mascagni 2010). Our 10ms flash represents a phasic mode of ACh release that is said to have a spread zone of only tens to hundreds of nanometers from presynaptic cholinergic release sites (Sarter and Lustig 2020). Bath-applied muscarine, on the other hand, would be present everywhere and not degraded by AChE; lingering and constantly stimulating all muscarinic receptors in the slice for as long as it is present. Therefore, a possible explanation for the differences we observe between phasic release of endogenous ACh and bath-applied muscarine could be that the former transiently activates and opens a distinct set of "synaptic" M1Rs coupled to GIRK channels, while the latter constantly

stimulates those M1Rs in addition to “extrasynaptic” M1Rs coupled to SK channels near NMDA receptors, which they prevent from normally opening in the presence of calcium. Indeed, the existence of synaptic and extrasynaptic M1Rs has been postulated before (Aitta-aho et al., 2018; Unal, Pare, and Zaborszky 2015). The fact that we didn’t observe a GIRK channel-mediated reduction of LA-BLa NMDA EPSCs in the presence of muscarine could be explained by temporal differences in GIRK channel activation between the two modes of M1R stimulation. It would be interesting to see whether stronger modes of endogenous ACh stimulation and/or the addition of AChE inhibitors could replicate the potentiation observed by muscarine, which would presumably activate “extrasynaptic” M1Rs coupled to SK channels.

Phasic ACh release at the 160ms interval does not affect the size of NMDA receptor currents evoked by NMDA puffs in BLa or BLp PNs, despite our observation that GIRK channels activated by phasic ACh release shunt LA-BLa NMDA EPSCs. The ability of GIRK channels to shunt NMDA receptor currents depends on where on the BLa PNs they are positioned with respect to the activated NMDA receptors (e.g., between the depolarizing wave and soma) (Spruston et al., 2016) and NMDA puffs and LA stimulation likely recruit different populations of NMDA receptors with different distribution patterns on the cell, likely explaining the discrepancy. Indeed, NMDA puffs recruit both synaptic and extrasynaptic NMDA receptors (Dasgupta, Seibt, and Beierlein 2018; Pallas-Bazarra et al., 2019), the latter of which are more abundant (Hardingham and Bading, 2010), distributed throughout the cell, whereas LA stimulation, in

contrast, would be expected to primarily recruit synaptic NMDA receptors in the dendrites. Therefore, the differential effect of phasic ACh release between these two modes of NMDA receptor stimulation likely reflects that the GIRK channels activated by phasic ACh (and the cholinergic terminals responsible for its release) are positioned between the synaptic NMDA receptors activated by LA terminals and the soma of BLa PNs. Somatic GIRK channel expression would be expected to equally shunt both types of NMDA currents since they would be integrated in the soma (Spruston et al., 2016) and can therefore be ruled out. The lack of an effect in the BLp, on the other hand, is consistent with other comparisons of cholinergic modulation we have made between the BLa and BLp, and, as postulated in those cases, could reflect a weaker cholinergic innervation of the BLp, which our lab has shown before (data not included). Future studies should explore these interesting possibilities further.

A study in amygdala (Power and Sah 2008) demonstrated that bath muscarine causes a transient, SK channel mediated hyperpolarization of BLa PNs. This response occurs when calcium is released from the endoplasmic reticulum in or near the soma via a mAChR and IP3-mediated mechanism, which then activates calcium-sensitive SK channels in or near the soma. It is likely this effect occurred in our experiments but was unobserved due to its transient and desensitizing nature coupled with the constant presence of muscarine (i.e., the effect would not regenerate while muscarine remains present). Importantly, this effect does not occur in the dendrites, where our effect of M1R on SK channels (i.e., to block them) simultaneously occurs.

5.4.1. FUNCTIONAL IMPLICATIONS

The core finding of the present study is that M1Rs can either reduce or enhance the size of NMDA receptor currents evoked at synapses between LA terminals and BLa PNs, depending on how they are stimulated. The M1Rs that mediate these opposite effects may represent discrete populations that are coupled to different potassium channel effectors. The limited spread zone and transient presence of phasic ACh release (Sarter and Lustig 2020) and its dampening effect on LA-BLa NMDA EPSCs could suggest that cholinergic terminals are preferentially positioned near “synaptic” GIRK channel-coupled M1Rs, whereas the uniform and lingering presence and opposite potentiating effect of muscarine seem to suggest that SK channel-coupled M1Rs may be located farther away from these terminals. If true, the former type would be preferentially activated by weaker modes of ACh signaling while the latter type would be recruited under conditions of stronger and more sustained cholinergic signaling, when the spread of ACh can reach them. This scenario might also suggest that the effect of ACh on NMDA receptor dependent long-term potentiation (LTP) and learning depends upon the strength of cholinergic signaling and the timing of LA input arrival with respect to ACh release. For example, LTP may be reduced or prevented at LA-BLa synapses when ACh is phasically released and glutamate is also released during the peak of the M1R-mediated GIRK channel current, whereas it may be facilitated by a stronger mode of ACh signaling at these synapses by a different set of M1Rs coupled to SK-channels. Here, however, the timing of LA input arrival would likely need to

be later so that ACh will have been able to spread far enough to reach the appropriate M1Rs. A final possibility is that, based on our work from Chapter 4, LTP may be facilitated at LA-BLa synapses when ACh is phasically released and glutamate is released during the peak of the presynaptic nicotinic receptor mediated response, as the additional depolarization might facilitate spike-timing dependent plasticity by boosting the removal of Mg^{2+} block at the NMDA receptor and therefore the amount of calcium entry into spines. Future studies will need to explore these possibilities further.

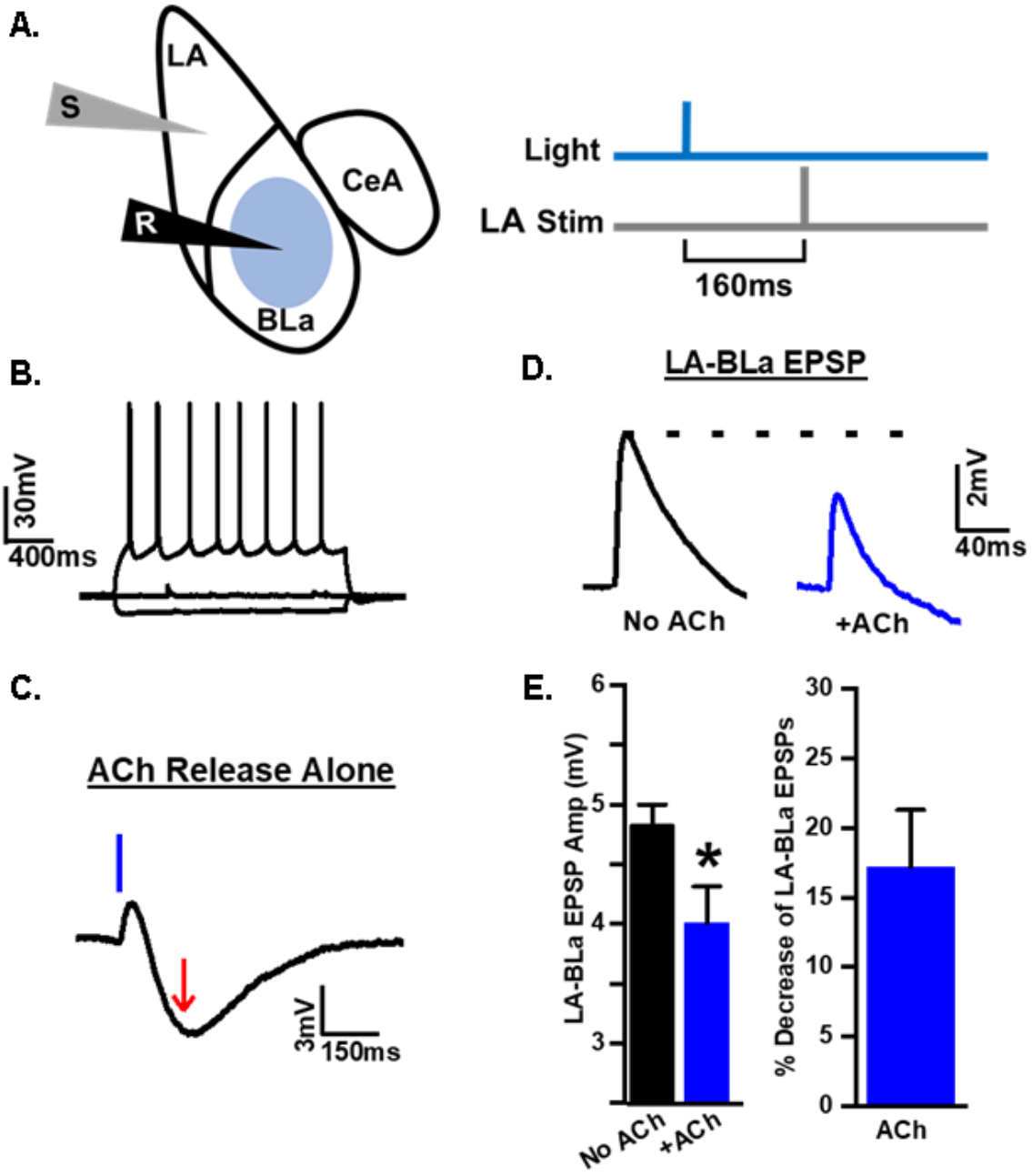

Figure 5.1. Phasic acetylcholine release decreases the size of LA-BLa EPSPs when phasically released 160ms after LA stimulation. A. Left. Schematic of the experimental setup depicting the positioning of the recording electrode in the BLa, the simulating electrode in the LA, and the targeting of the BLa with individual blue light flashes. **Right.** The timing relationship between the single stimulation of LA and the presentation of individual 10ms flashes. **B.** Voltage response of a BLa PN to hyperpolarizing and depolarizing current pulses. **C.** Representative trace depicting the membrane potential response of a BLa PN to a single 10ms flash (blue bar) in ACSF. Although LA is not stimulated in this trace, the timing of LA input with respect to this response is illustrated by a red arrow. **D.** Representative traces depicting the

membrane potential response of a BLa PN to LA stimulation in the absence **(Left)** and presence **(Right)** of phasic ACh evoked by a single 10ms flash. Note that the membrane potential response to ACh is subtracted from the right trace. The left and right traces were recorded in ACSF. **E. Left.** Bar graph showing the average amplitudes of LA-BLa EPSPs recorded in the absence (black bar) and presence (blue bar) of phasic ACh in ACSF. **Right.** Bar graph showing the average percent by which phasic ACh decreased the amplitude of LA-BLa EPSPs recorded in the absence of ACh in ACSF. * = $p < 0.01$, ** = $p < 0.01$, *** $p < 0.001$.

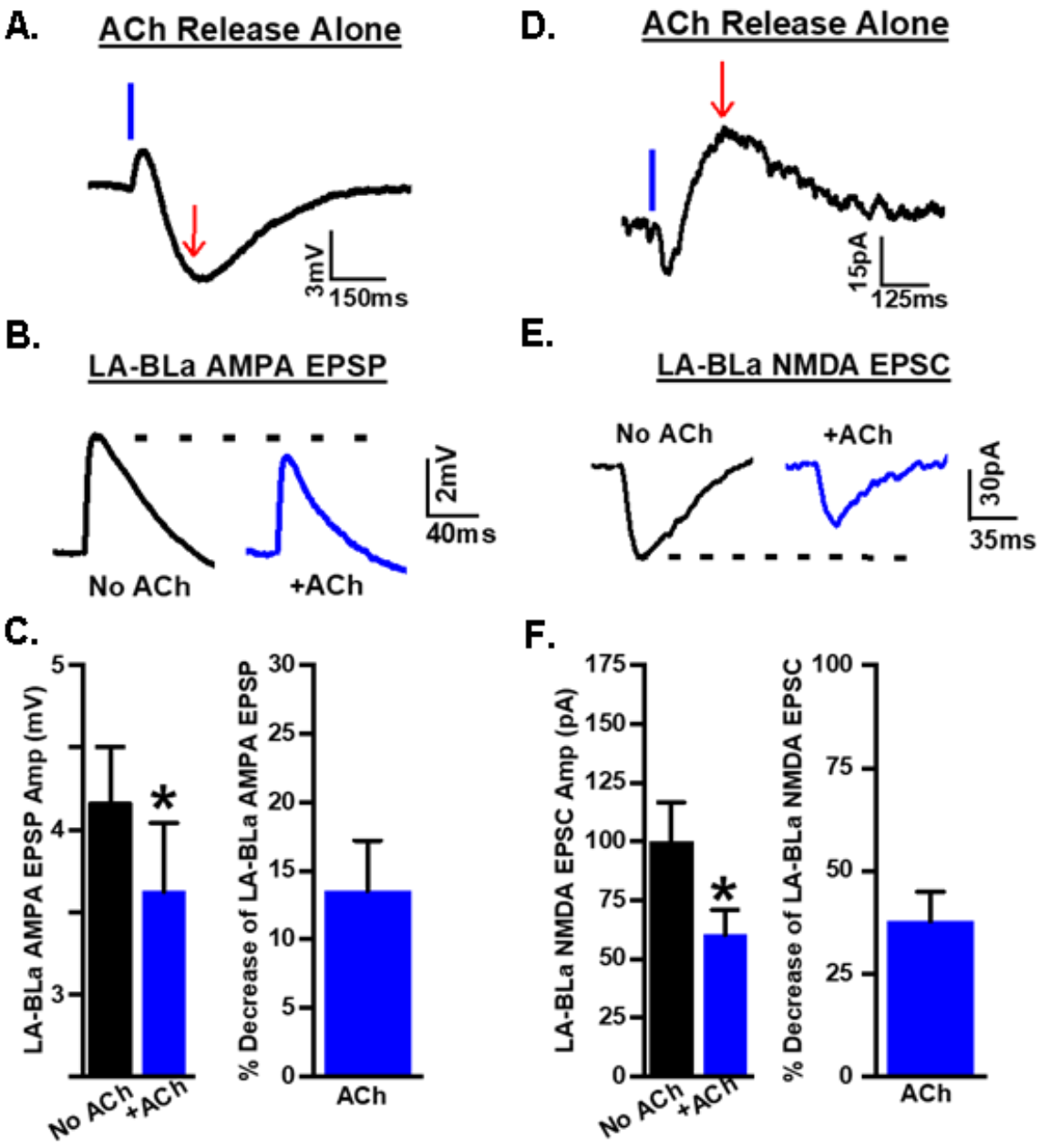

Figure 5.2. Acetylcholine decreases the size of isolated LA-BLa AMPA and NMDA responses when phasically released 160ms after LA stimulation. A. Representative trace depicting the membrane potential response of a BLa PN to a single 10ms flash (blue bar) in ACSF. Although LA is not stimulated in this trace, the timing of LA input with respect to this response is illustrated by a red arrow. **B.** Representative traces depicting pharmacologically isolated AMPA receptor responses in BLa PNs to LA stimulation in the absence **(Left)** and presence **(Right)** of phasic ACh evoked by a single 10ms flash. Note that the membrane potential response to ACh is subtracted from the right trace. The left and right traces were recorded in

ACSF. **C. Left.** Bar graph showing the average amplitudes of LA-BLa AMPA EPSPs recorded in the absence (black bar) and presence (blue bar) of phasic ACh in ACSF. **Right.** Bar graph showing the average percent by which phasic ACh decreased the amplitude of LA-BLa AMPA EPSPs recorded in the absence of ACh in ACSF. **D.** Representative trace depicting the membrane potential response of a BLa PN to a single 10ms flash (blue bar) in ACSF. Although LA is not stimulated in this trace, the timing of LA input with respect to this response is illustrated by a red arrow. **E.** Representative traces depicting pharmacologically isolated NMDA receptor responses in BLa PNs to LA stimulation in the absence **(Left)** and presence **(Right)** of phasic ACh evoked by a single 10ms flash. Note that the membrane potential response to ACh is subtracted from the right trace. The left and right traces were recorded in ACSF. **F. Left.** Bar graph showing the average amplitudes of LA-BLa NMDA EPSCs recorded in the absence (black bar) and presence (blue bar) of phasic ACh in ACSF. **Right.** Bar graph showing the average percent by which phasic ACh decreased the amplitude of LA-BLa NMDA EPSCs recorded in the absence of ACh in ACSF. * = $p < 0.01$, ** = $p < 0.01$, *** $p < 0.001$.

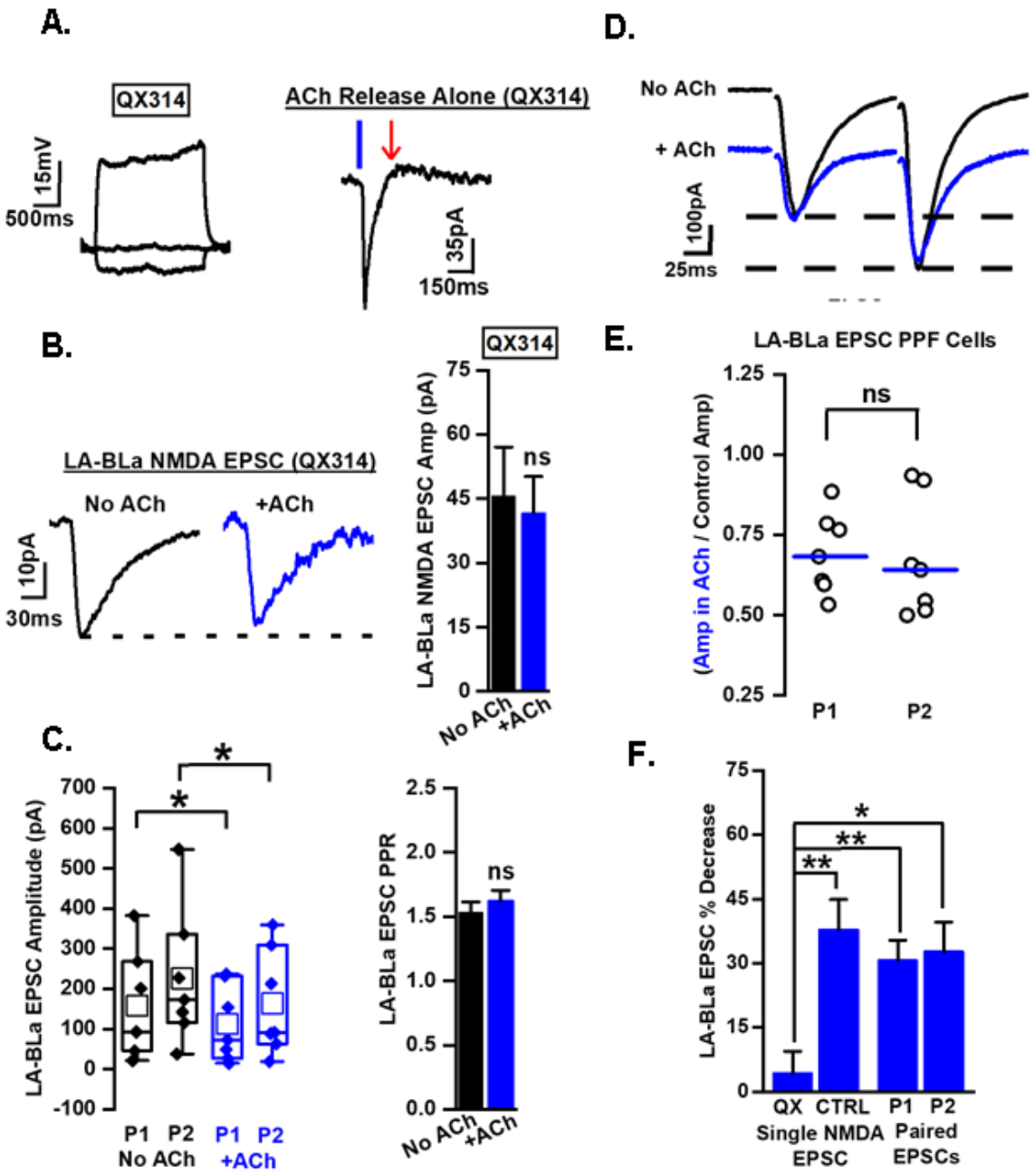

Figure 5.3. Intracellular GIRK channel blocker QX-314 prevents phasic acetylcholine release from decreasing LA-BLa NMDA EPSCs. A. Left. Voltage response of a BLa PN to hyperpolarizing and depolarizing current pulses. Note the absence of spiking at the maximum level of depolarization (which normally produces strong spiking), reflecting QX-314 is exerting intended effects in the recorded cell. **Right.** Representative trace depicting the membrane potential response of a BLa PN filled with QX-314 to a single 10ms flash (blue bar) in ACSF. Note a smaller late IPSC, suggesting QX-314 is blocking the GIRK channels that mediate it. Although LA is not stimulated in this trace, the timing of LA input with respect to this response is illustrated by a red arrow. **B. Left.** Representative traces depicting pharmacologically isolated

NMDA receptor responses in BLa PNs filled with QX-314 to LA stimulation in the absence **(Left)** and presence **(Right)** of phasic ACh evoked by a single 10ms flash. Note that the amplitudes of the NMDA receptor responses are similar in both conditions. Also note that the membrane potential response to ACh is subtracted from the right trace. The left and right traces were recorded in ACSF. **Right.** Bar graph showing the average amplitudes of LA-BLa NMDA EPSCs recorded in the absence (black bar) and presence (blue bar) of phasic ACh in ACSF and the presence of intracellular QX-314. **C. Left.** Graph showing the amplitude of the first LA-BLa EPSC (P1) and the second LA-BLa EPSC (P2) evoked by paired LA stimulation in the absence (black, left half of graph) and presence (blue, right half of graph) of phasic ACh evoked by a single 10ms flash. **Right.** Bar graph showing the paired-pulse facilitation ratio (P2 amplitude/P1 amplitude) of the LA-BLa EPSCs in the absence (black bar) and presence (right bar) of phasic ACh evoked by a single 10ms flash. When considering B. and C. together, note that the individual LA-BLa NMDA EPSCs of B. and the paired LA-BLa EPSCs of C. are evoked at the same 160ms interval following phasic ACh release. **D.** Representative traces depicting the paired LA-BLa EPSCs in the absence (black trace) and presence (blue trace) of phasic ACh release overlaid with the peaks of each response overlapping. Note that each peak is equally reduced by ACh, suggesting the effect is not presynaptic. **E.** Graph showing the average amplitude of P1 in ACh divided by the average amplitude of P1 without ACh (left side) and the average amplitude of P2 in ACh divided by the average amplitude of P1 without ACh (right side). Note the similarity between them, suggesting the effect is not presynaptic. **F.** Bar graph comparing the average percent by which phasic ACh decreased the amplitude of LA-BLa NMDA EPSCs in ACSF and the presence of intracellular QX-314 (far left bar), the amplitude of LA-BLa NMDA EPSCs in ACSF and regular intracellular solution (middle left bar), the first of the paired LA-BLa EPSCs (P1) in ACSF and regular intracellular solution (middle right bar), and the second of the paired LA-BLa EPSCs (P2) in ACSF and regular intracellular solution (far right bar). Note the similar effect of ACh on the three responses recorded with regular internal solution compared to a substantially smaller effect of ACh on the responses recorded with the presence of intracellular QX-314. * = $p < 0.01$, ** = $p < 0.01$, *** $p < 0.001$.

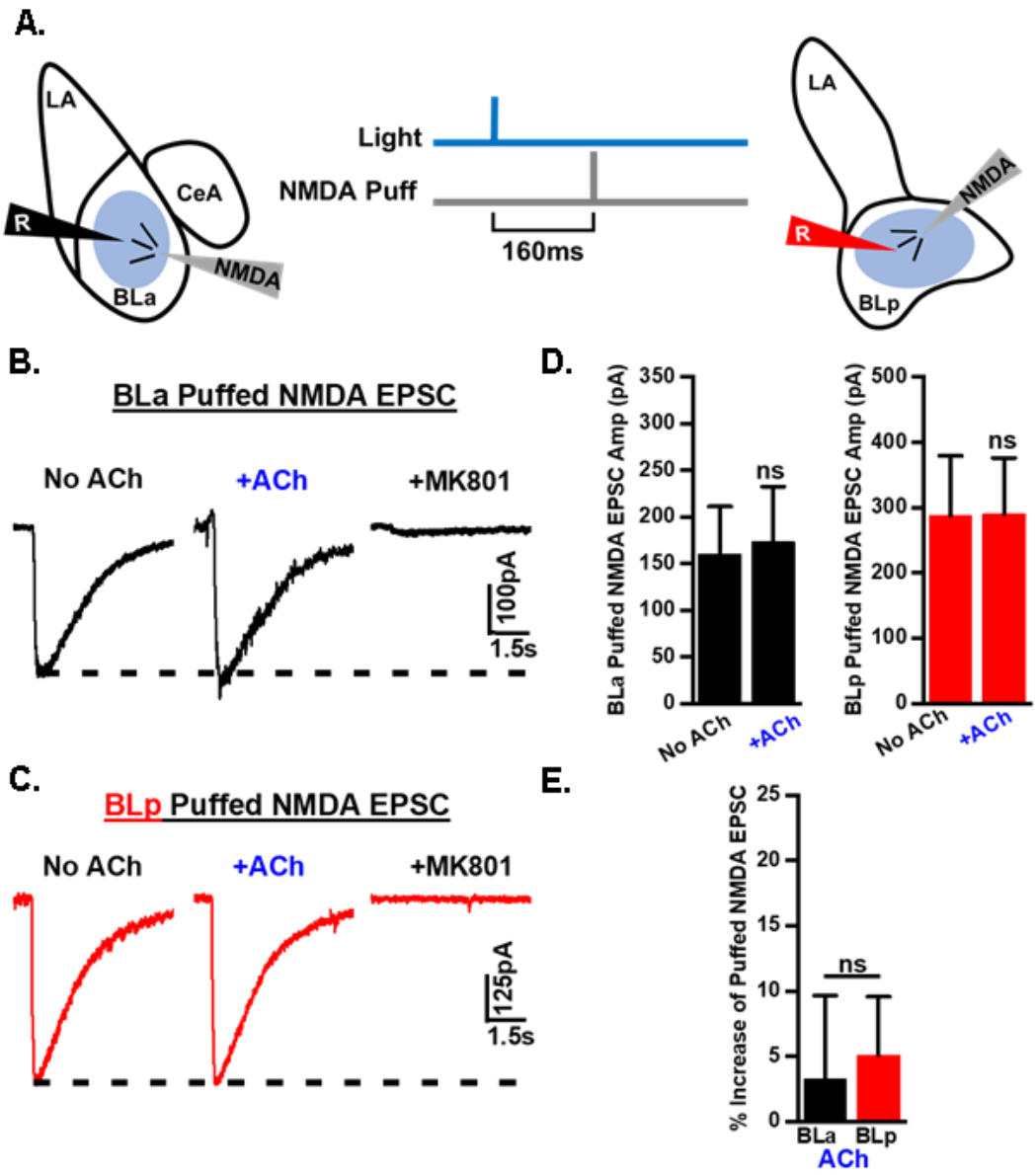

Figure 5.4. Phasic acetylcholine release does not affect the size of the NMDA current evoked by NMDA puffs in BLa or BLp pyramidal neurons. **A.** Schematic of the experimental setup depicting **(Left)** the positioning of the recording electrode and NMDA puffer pipette in the BLa and the targeting of the BLa with blue light flashes or **(Right)** the positioning of the recording electrode and NMDA puffer pipette in the BLp and the targeting of the BLp with blue light flashes. **Middle.** The timing relationship between the single puff of NMDA and the presentation of individual 10ms flashes. **B.** Representative traces depicting NMDA receptor responses evoked by NMDA puffs in BLa PNs. The left and middle traces were recorded in ACSF and the absence (left trace) and presence (middle trace) of phasic ACh. The right trace was recorded in the presence of the NMDA receptor antagonist MK-801 (20 μM)

and absence of phasic ACh. Note that the membrane potential response to ACh is subtracted from the middle trace. **C.** Same as B. but all responses were recorded in a BLp PN. **D. Left.** Bar graph showing the average amplitudes of puffed NMDA EPSCs in BLa PNs recorded in the absence (left bar) and presence (blue bar) of phasic ACh in ACSF. **Right.** Bar graph showing the average amplitudes of puffed NMDA EPSCs in BLp PNs recorded in the absence (left bar) and presence (blue bar) of phasic ACh in ACSF. **E.** Bar graph showing the average percent by which phasic ACh increased the amplitude of puffed NMDA EPSCs in BLa (black bar) and BLp (red bar) PNs in ACSF. * = $p < 0.01$, ** = $p < 0.01$, *** $p < 0.001$.

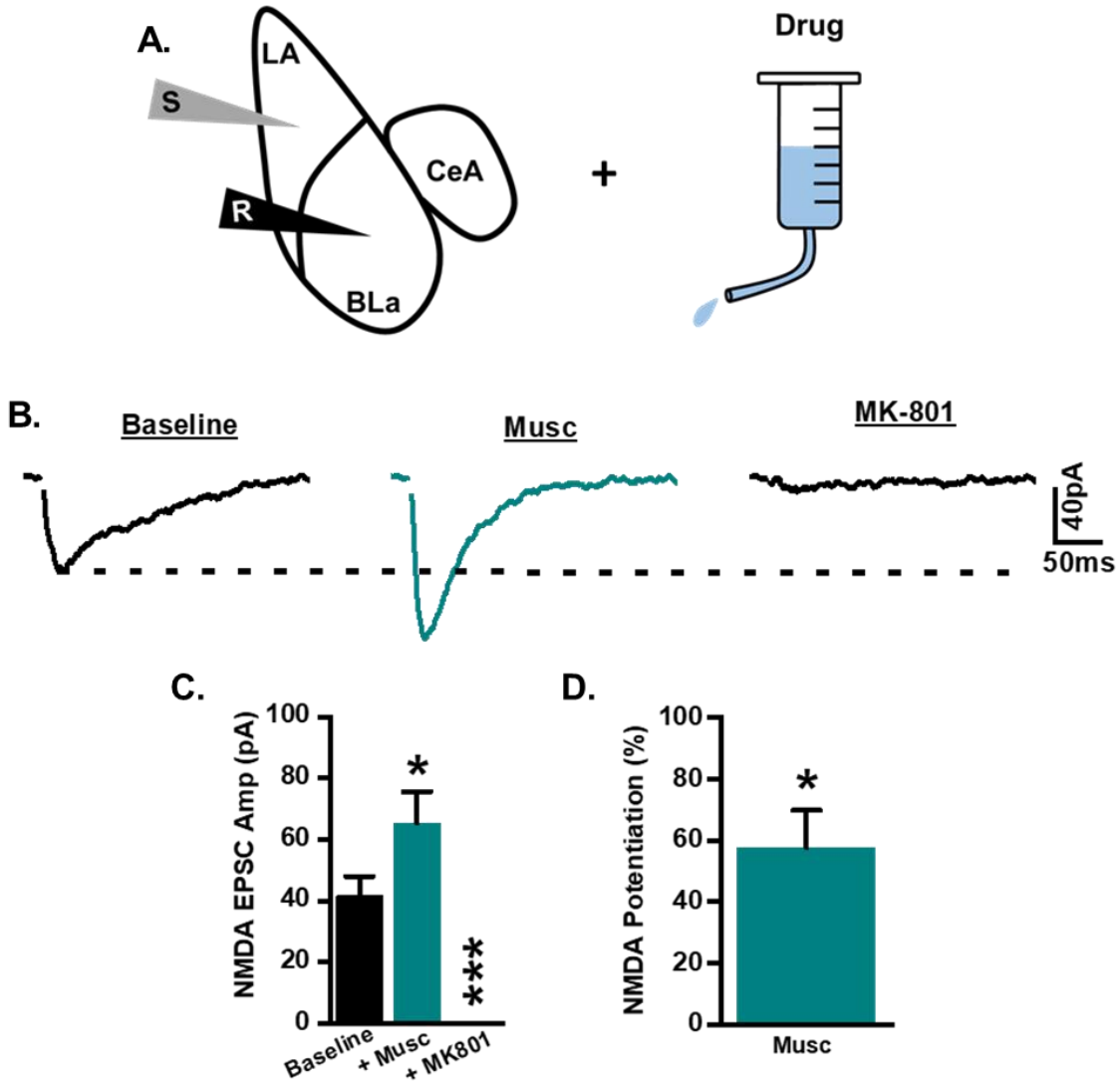

Figure 5.5. Bath-applied muscarine potentiates isolated LA-BLa NMDA EPSCs. A. Schematic of the experimental setup depicting the positioning of the recording electrode in the BLa, the simulating electrode in the LA, and the application of drug. **B.** Representative traces depicting pharmacologically isolated NMDA receptor responses in BLa PNs to LA stimulation in baseline (ACSF) and the subsequent and successive application of 10 µM muscarine and 20 µM MK-801. **C.** Bar graph showing the average amplitudes of LA-BLa NMDA EPSCs in ACSF (black bar), muscarine (cyan bar), and MK-801 (far right). **D.** Bar graph showing the average percent by which muscarine increased the average amplitude of LA-BLa NMDA EPSCs recorded in ACSF. * = $p < 0.01$, ** = $p < 0.01$, *** $p < 0.001$.

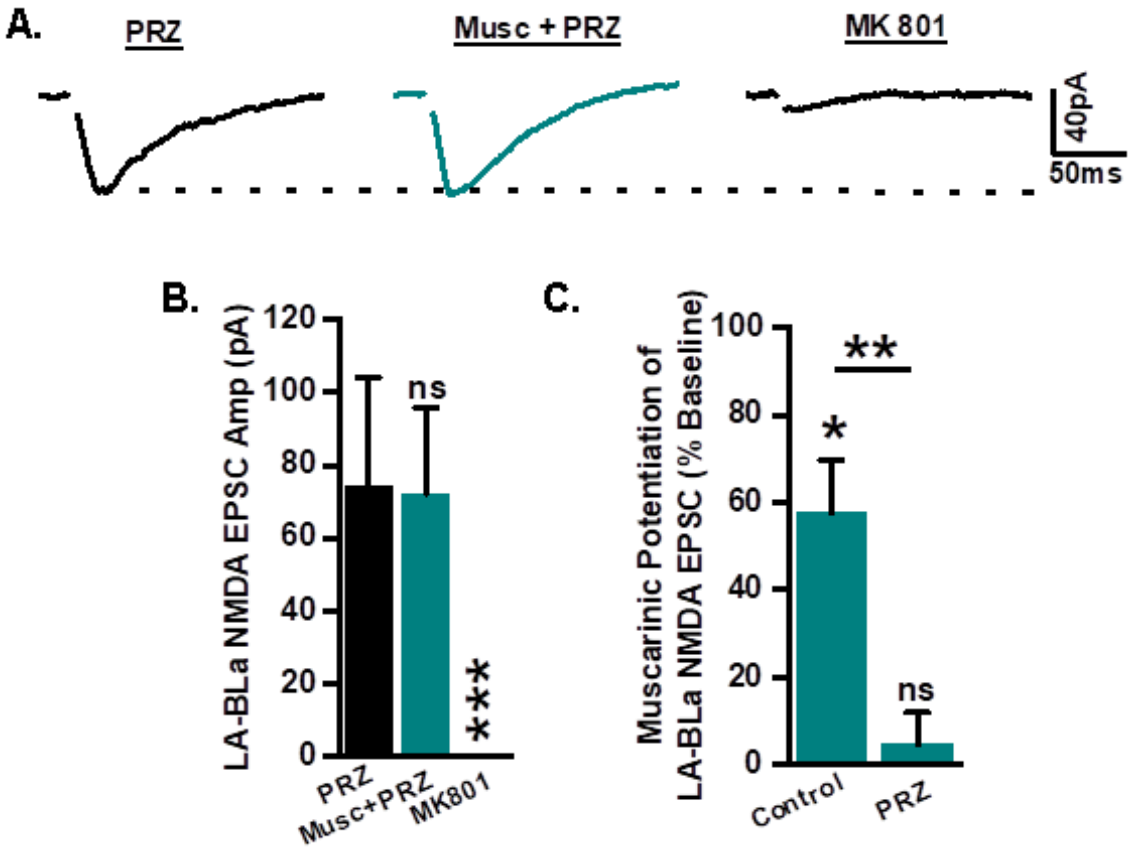

Figure 5.6. Pirenzepine prevents muscarine from potentiating isolated LA-BLa NMDA EPSCs. A. Representative traces depicting pharmacologically isolated NMDA receptor responses in BLa PNs to LA stimulation in PRZ and the subsequent and successive application of 10 µM muscarine and 20 µM MK-801. **B.** Bar graph showing the average amplitudes of LA-BLa NMDA EPSCs in PRZ (black bar), muscarine (cyan bar), and MK-801 (far right). **C.** Bar graph showing the average percent by which muscarine increased the average amplitude of LA-BLa NMDA EPSCs recorded in ACSF (left bar) compared to the average percent by which muscarine increased the average amplitude of LA-BLa NMDA EPSCs recorded in PRZ (right bar). * = $p < 0.01$, ** = $p < 0.01$, *** $p < 0.001$.

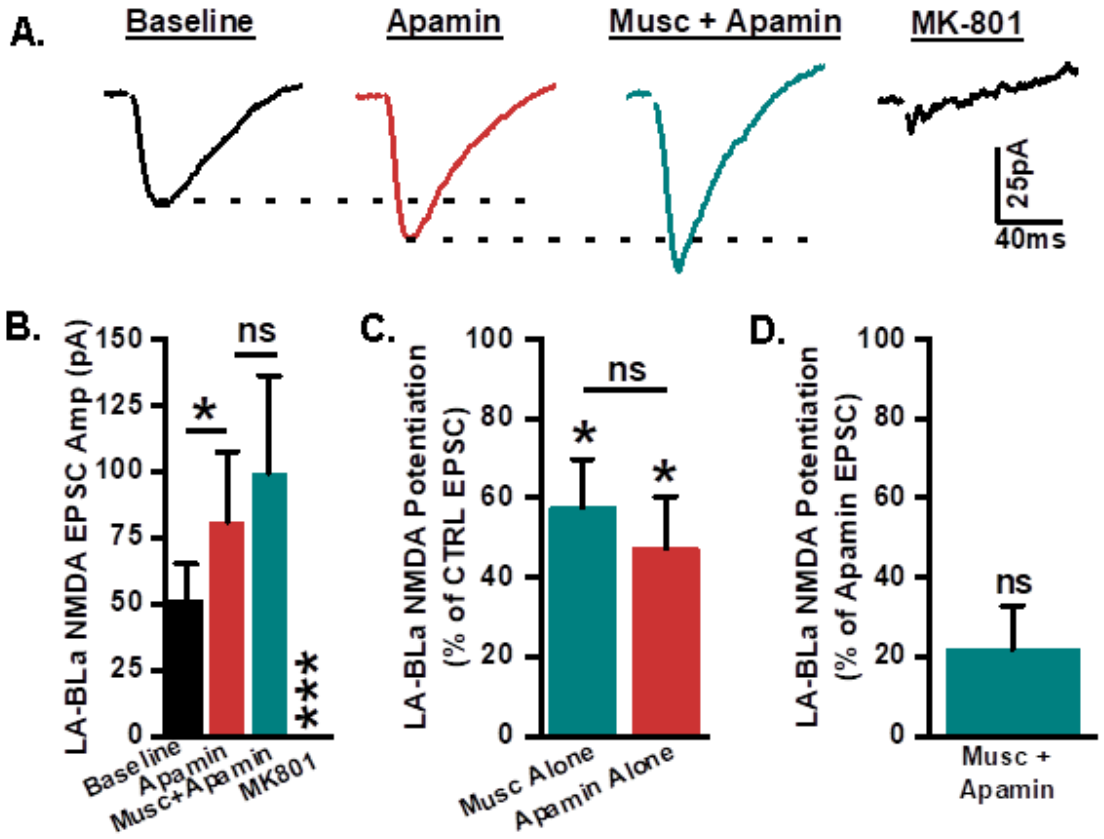

Figure 5.7. Apamin minimizes the muscarinic potentiation of pharmacologically isolated LA-BLa NMDA EPSCs. **A.** Representative traces depicting pharmacologically isolated NMDA receptor responses in BLa PNs to LA stimulation in baseline (ACSF) and the subsequent and successive application of 100nM apamin, 10 µM muscarine, and 20 µM MK-801. **B.** Bar graph showing the average amplitudes of LA-BLa NMDA EPSCs in ACSF (black bar) and the subsequent addition of apamin (red bar), muscarine (cyan bar), and MK-801 (far right). **C.** Bar graph showing the average percent by which muscarine increased the average amplitude of LA-BLa NMDA EPSCs recorded in ACSF in one set of cells (cyan bar) compared to the average percent by which apamin increased the average amplitude of LA-BLa NMDA EPSCs recorded in ACSF in a different set of cells (right bar). Note that the effects of muscarine and apamin on the size of baseline LA-BLa NMDA EPSCs are similar. **D.** Bar graph showing the average percent by which muscarine increased the average amplitude of LA-BLa NMDA EPSCs recorded in apamin. Note how small the effect is compared to the values depicted in C. * = $p < 0.01$, ** = $p < 0.01$, *** $p < 0.001$.

Table 5.1. Drugs used in Chapter 5.

Drug Name	Drug Type	Target	Method	Dose	Citation
6-cyano-7-nitroquinoxaline-2,3-dione (CNQX)	Selective Antagonist	AMPA Receptors	Bath	20µM	Lee et al., 2010
N-methyl-D-aspartate (NMDA)	Selective Agonist	NMDA Receptors	Bath	100µM	Faber et al., 2005
MK-801 Maleate	Selective Antagonist	NMDA Receptors	Puff	20µM	Sison and Gerlai 2011
Picrotoxin (Pic)	Selective Antagonist	$GABA_A$ Receptors	Bath	50µM	Power and Sah 2008
Apamin	Selective Antagonist	SK Channels	Bath	100nM	Ngo-Anh et al., 2005
Muscarine (Musc)	Non-Selective Agonist	mAChRs	Bath	10µM	Meng et al., 2017
Pirenzepine (PRZ)	Selective Antagonist	M1 mAChRs	Bath	1µM	Unal et al., 2015
QX-314	Selective Antagonist	GIRK Channels	Intracellular	5mM	Smirnov et al., 1999

CHAPTER 6

GENERAL DISCUSSION AND SIGNIFICANCE

6.1. KEY FINDINGS OF THE STUDY

Chapter 3:

1) M1R expression in the BLa is significantly higher than it is in the BLp and other nuclei of the BNC.

2) Because of #1, the distribution of projection-defined populations of pyramidal neurons (PNs) in relation to BLa determines their overall M1R expression, whereas their projection target does not appear to be as important in this regard. This is demonstrated in three examples below.

A) NAc projectors in the entire BNC and only the BL express more M1R than CeA projectors in the same regions. This is most likely explained by the fact that a greater fraction of NAc projectors in the entire BNC or only BL reside in the BLa, where M1R expression is highest.

B) NAc and CeA projectors in the BLa express more M1R than NAc and CeA projectors in the BLp.

C) Even though NAc projectors in the entire BNC and only the BL express more M1R than CeA projectors the same regions, NAc projectors in the BLp do not express more M1R the CeA projectors in the BLa.

3) In addition to #2, there also appears to be trending, although not statistically significant, differences between M1R expression on NAc and CeA projectors within BLa and BLp. Within each BL division, NAc projectors express slightly more M1R than CeA projectors.

4) M1R expression levels on BL-residing projector populations is as follows, in order from highest to lowest. M1R expression on NAc projectors in BLa is > M1R expression on CeA projectors in BLa, which is > M1R expression on NAc projectors in BLp, which is > M1R expression on CeA projectors in BLp.

Chapter 4:

1) Phasic release of endogenous ACh elicits a biphasic response in BLa and BLp PNs. The faster cholinergic depolarization is mediated by α7 and α4β2 nicotinic receptors located on presynaptic glutamate terminals. The slower cholinergic hyperpolarization is mediated by postsynaptic M1Rs located coupled to GIRK channels. The former finding has not been reported before.

2) Phasic ACh release preferentially impacts BLa PNs over BLp PNs.

A) BLa PNs are more sensitive to phasic ACh release than BLp PNs. Weak cholinergic stimulation (a 3ms flash) produced responses in a majority of BLa PNs without producing any responses in BLp PNs. Maximal cholinergic stimulation (a 10ms flash) produced a response in 100 percent of BLa PNs, but only approximately a third of BLp PNs.

B) The amplitude of responses to phasic ACh release in BLa PNs are significantly larger than they are in BLp PNs. This was true of every light flash duration tested (1-4ms, 7ms, and 10ms). These differences likely do

not reflect differences in M1R-coupled GIRK channel expression because the amplitudes of hyperpolarizing responses to bath-applied muscarine were not significantly different between BLa and BLp PNs. Instead, these differences likely reflect a greater cholinergic innervation of BLa compared to BLp, which our lab has shown before (data not included).

3) BLa PNs had significantly larger depolarizing responses to muscarine than BLp PNs, possibly reflecting a greater BLa PNs expression of M1Rs coupled to depolarizing effectors (like KCNQ channels that mediate the M-current). This finding appears to align with our anatomical observation above that M1R expression is higher in the BLa than it is in the BLp.

4) The amount of glutamate evoked from LA terminals innervating BLa PNs is not affected by the AChRs activated by phasic ACh release nor bath-applied α7 and α4β2 nAChR agonists. Importantly, this means that the α7 and α4β2 nAChRs activated by phasic ACh release must be located on glutamate terminals other than those belonging to the LA (presumably cortical because of Jiang et al., 2016).

5) The biphasic response to phasic ACh release bidirectionally and temporally modulates the ability of LA inputs to fire BLa PNs. Phasic ACh release boosts the ability of LA inputs to fire BLa PNs when they arrive during the initial moments after ACh release and substantially hinders their ability to do so when they arrive slightly later. This effect is more muted in the BLp. Here, phasic ACh release does not affect the ability of LA inputs arriving closely after ACh release to fire BLp PNs and reduces the ability of LA inputs arriving later to fire BLp PNs to a

lesser extent than it does in the BLa. The early boosting effect of ACh in the BLa is associative because it is mediated by nAChRs on non-LA (presumably cortical) inputs that, by temporal association, facilitate the ability of LA inputs to fire BLa PNs by providing additional depolarization via the mechanism in #1 above. The later hindering effect of ACh in the BLa and BLp is mediated by postsynaptic mAChRs (presumably M1Rs coupled to GIRK channels per #1 above), and not $GABA_B$ receptors. This biphasic membrane potential response could serve as a mechanism by which ACh – acting through nAChRs and mAChRs on different circuit components at slightly different timepoints – enhances the signal to noise ratio of behaviorally relevant sensory information entering the BL. The differential effects between BLa and BLp could also have implications for how the amygdala processes valence.

Chapter 5:

1) At the 160ms interval from Chapter 4 above, when postsynaptic M1Rs – which can potentiate NMDA receptor currents in other brain areas (Buchanan et al., 2010; Calabresi et al., 1998; Dennis et al., 2016; Giessel and Sabatini 2010; Marino et al., 1998; Sur et al., 2003; Tigaret et al., 2018) – are activated, phasic ACh release decreases the size of AMPA and NMDA receptor currents at LA-BLa synapses. This decrease is caused by postsynaptic GIRK channel-mediated shunting inhibition (presumably activated by M1Rs per Chapter 4, #1). Although GIRK channels have been shown to shunt AMPA receptor currents before (Chalifoux and Carter 2010; Takigawa and Alzheimer 2002, 2003), we are the

first demonstrate GIRK channel-mediated shunting inhibition of NMDA receptor currents.

2) Phasic ACh release at the 160ms interval does not affect the size of NMDA receptor currents evoked by NMDA puffs in BLa or BLp PNs, despite our observation that GIRK channels activated by phasic ACh release shunt LA-BLa NMDA EPSCs. These differences are likely explained by a differential recruitment of synaptic and extrasynaptic NMDA receptors between the two modes of NMDA receptor stimulation and likely suggest that the GIRK channels activated by phasic ACh preferentially shunt synaptic NMDA receptor currents. Further, due to the small spread zone of phasic ACh release (Sarter and Lustig 2020), these results may suggest that cholinergic terminals innervate BLa PNs somewhere between the synaptic NMDA receptors activated by LA terminals and the soma of BLa PNs. See chapter 5 discussion for further explanation. Finally, the lack of an effect in the BLp is consistent with other comparisons we have made regarding the cholinergic modulation of BLa and BLp PNs (all of Chapter 3; Chapter 4, #2-3, #5), which may reflect a weaker cholinergic innervation of the BLp, which our lab has shown before (data not included).

3) In contrast to #1, but agreement with previous reports (Buchanan et al., 2010; Calabresi et al., 1998; Dennis et al., 2016; Giessel and Sabatini 2010; Marino et al., 1998; Sur et al., 2003; Tigaret et al., 2018), bath-applied mAChR agonist muscarine potentiated LA-BLa NMDA receptor currents. This effect is mediated by M1Rs that prevent SK channels from opening in response to calcium entry through NMDA receptors, also consistent with previous reports (Buchanan et al.,

2010; Dennis et al., 2016; Giessel and Sabatini 2010; Tigaret et al., 2018). By preventing these SK channels from opening, M1Rs potentiate NMDA receptor currents by removing the shunting inhibition that SK channels normally provide on them.

6.2. DISCUSSION OF RESULTS AND SIGNIFICANCE

These studies investigated the impact of ACh on the internal circuitry of the BNC via the combined application of anatomy (confocal immunohistochemistry), brain slice electrophysiology (whole-cell and single unit recordings combined with pharmacology and electrical stimulation of LA), and optogenetics. The experiments performed probed the circuit- and molecular-level mechanisms by which ACh signaling could contribute to attention, learning and memory, and valence processing mediated by BNC, as relatively few studies have done so. As an unintended consequence, these studies also revealed interesting details pertaining to the spatiotemporal dynamics of endogenous ACh release from cholinergic terminals, a topic of much interest and debate in the neuroscience community.

6.2.1. Temporal and associative enhancement of signal-to-noise ratio at the LA-BLa pathway: Cholinergic mechanism of facilitating amygdalar cue detection?

A core finding from our studies is that phasic ACh release (simulating the transient activation of cholinergic inputs in response to salient stimuli per Crouse et al., 2020, among others) temporally enhances the signal-to-noise ratio (SNR) of appropriately timed LA inputs (simulating signals representing environmental

stimuli) at BLa PNs. We propose that this mechanism could be a means by which ACh enhances the detection of behaviorally relevant environmental stimuli (represented by LA terminals signaling to BLa PNs when ACh is initially released) and minimizes the detection of behaviorally irrelevant/distracting environmental stimuli (represented by LA terminals signaling to BLa PNs at a later timepoint). This finding adds to a well-developed body of literature suggesting that ACh enhances attentional performance by maximizing the SNR of sensory inputs by improving their impact on target circuitry of the hippocampus and cortex (Colangelo et al., 2019; Hasselmo 2006; Higley and Picciotto 2014; Lustig and Sarter 2016).

This finding also reveals an additional mechanism by which ACh signaling enhances SNR in the BLa. Unal et al., 2015 reported that a train of endogenous ACh release enhances SNR in the BLa by bidirectionally modulating the excitability of BLa PNs depending on their firing rate at the time of ACh impact. Specifically, this train inhibited spiking via the same GIRK-coupled M1R response we reported here when the cells had low spiking frequencies at the time of ACh impact. However, when ACh from the same train impacted the same cells as they were spiking at higher frequencies, this effect was overcome and replaced with a calcium-dependent afterdepolarization supporting prolonged spiking. This bidirectional effect of sustained ACh release on BLa PN excitability has been replicated by other studies, as well (Aitta-aho et al., 2018; Jiang et al., 2016).

Our mechanism on SNR in the BLa is distinct from the one reported by Unal et al., 2015 in important ways. First, ours is in response to a brief release of ACh (10ms flash) while theirs was in response to sustained ACh release (1,500ms train of 5ms pulses at 10 Hz). The concept that our mechanisms are distinct is further supported by their own results, as they did not report an excitatory effect of ACh in response to a single 5ms flash, a stimulus substantially closer to ours. Aitta-aho et al., 2018 also did not report excitatory effects of brief and single flashes of light. Jiang et al., 2016 only used trains.

Second, as mentioned above, we reveal a mechanism whereby endogenous ACh enhances the SNR of LA inputs by enhancing their impact on BLa PNs in a timing-dependent manner. This is distinct from Unal et al., 2015 because they did not examine the modulatory impact of endogenous ACh on glutamatergic inputs nor how inputs interacted with BLa PNs in the presence of ACh, as we did here. Finally, the cholinergic enhancement of LA impact on BLa PNs that we report is mediated by nAChRs on glutamate terminals and Unal et al., did not report this response (nor did Aitta-aho et al., 2018 and Jiang et al., 2016). Therefore, we reveal an additional mechanism by which ACh signaling enhances SNR in the BLa that is unique to phasic modes of ACh signaling, which simulates cholinergic transients evoked by salient stimuli that are intimately associated with cue-detection and cue-guided behaviors mediated by the cortex (Gritton et al., 2016; Howe et al., 2017; Lu et al., 2020; Parikh et al., 2007; Sarter and Lustig 2019). Our results combined with the other studies mentioned above

point to the interesting possibility that the CBF could differentially impact SNR processing depending on the strength of cholinergic signaling in the BLa.

It is intriguing that we are the first to report the early nicotinic depolarization in response to endogenous ACh release (Aitta-aho et al., 2018; Jiang et al., 2016; Unal et al., 2015). Our experiments combined with pharmacological studies in the BLa revealed these were α7 and α4β2 nAChRs on non-LA glutamate terminals, likely belonging to cortex (Jiang et al., 2013; Jiang and Role, 2008). Importantly, the temporal enhancement of SNR at LA-BLa synapses that we report is associative because the nAChRs responsible for this effect depolarize BLa PNs at the same time as LA terminals unaffected by ACh. To our knowledge, no studies have demonstrated this type of role for nAChRs before, although a recent study did report a similar effect with a slightly different mechanism of action (Urban-Ciecko et al., 2018). This raises the interesting question of whether transient recruitment of presynaptic nAChRs on glutamate terminals represents a common synaptic motif by which phasic ACh facilitates attentional performance throughout the brain. In support of this, nAChRs have been implicated in enhancing attention and deficits in nAChR signaling are associated with attentional deficits in schizophrenia and Alzheimer's disease (Freedman, 2014; Guillem et al., 2011; Hahn, 2015; Parikh et al., 2007; Sarter et al., 2005). It will be interesting to see whether future studies continue to reveal this mechanism in other brain areas.

6.2.2. Differential effects of M1Rs activated by phasic ACh and muscarine on LA-BLa NMDA receptor currents: Bidirectional effect on plasticity depending on ACh signaling strength and the timing of glutamate release at LA-BLa synapses?

Another prominent finding from our studies is that M1R activation bidirectionally modulates the size of synaptic NMDA currents at the LA-BLa pathway depending on the method used to stimulate them. Specifically, the M1Rs recruited by phasic ACh reduce LA-BLa NMDA receptor currents via GIRK channel-mediated shunting inhibition. This is a novel effect of GIRK channels, although they can shunt AMPA currents (Chalifoux and Carter 2010; Takigawa and Alzheimer 2002, 2003). In contrast, the M1Rs recruited by bath-applied muscarine potentiate LA-BLa NMDA receptor currents by preventing the shunting inhibition normally provided by SK channels adjacent to NMDA receptors that normally open in response to NMDA receptor calcium. This mechanism is consistent with studies using bath-applied carbachol in the hippocampus, but we are the first to report it in the BNC. The implications of this latter effect are most obvious and have already been demonstrated in hippocampus: to increase the magnitude of LTP induction. In the amygdala, such an effect would presumably strengthen the acquisition of emotional memories.

Another intriguing thought arises when the potentiating effect of muscarine (which is ubiquitous and non-degrading) is considered alongside the opposite effect of phasic ACh release (which is transient and rapidly degraded): the impact of endogenous ACh on the size of LA-BLa NMDA receptor currents, and by

extension, its influence on LTP and learning and memory may depend on the signaling strength of cholinergic terminals in the BLa and the timing of glutamate release at LA-BLa synapses.

Such a possibility would likely be due to the spatiotemporal dynamics of ACh release from cholinergic terminals and the positioning of such terminals with respect to functionally distinct subpopulations of M1Rs: “synaptic” M1Rs near cholinergic terminals coupled to GIRK channels and “extrasynaptic” M1Rs farther from cholinergic terminals coupled to SK channels. Given the limited spread of phasic ACh (Sarter and Lustig 2020), stronger modes of ACh signaling may be required for endogenous ACh to reach the latter type. This concept of synaptic and extrasynaptic M1Rs has been postulated and partially demonstrated in the BLa before (Aitta-aho et al., 2018; Unal et al., 2015), so these findings would seem to agree. Importantly, for extrasynaptic M1Rs coupled to SK channels to potentiate LA-BLa NMDA receptor currents, the timing of LA input arrival with respect to initial ACh release may need to be more delayed to provide sufficient time for ACh reach them.

6.2.3. Differential cholinergic modulation of BLa and BLp pyramidal neurons: Negative emotional bias?

Throughout these studies, we made a point to compare the effects of ACh on PNs of the BLa and BLp due to an emerging body of literature suggesting these two cell types preferentially process negative and positive emotions. Intriguingly, we consistently saw more pronounced effects of ACh in the BLa.

The BLa expressed substantially higher levels of M1R than the other regions of the BNC, consistent with previous anatomical work from our lab showing the BLa receives a denser cholinergic innervation than the BLp (not shown). Analysis of M1R expression of projector populations proposed to preferentially process negative (CeA projectors) and positive (NAc projectors) valence found that higher M1R expression patterns were correlated with their distribution with respect to BLa, not their projection target. BLa PNs are also more sensitive and have larger response to phasic ACh release, as well as larger depolarizing responses to bath-applied muscarine, than BLp PNs. Finally, the effect of phasic ACh on LA-driven PN output were more muted in the BLp, with no nicotinic facilitation and a smaller muscarinic reduction.

Although it is impossible to say with certainty what the behavioral consequences of these differences are, our results do indicate that ACh signaling preferentially impacts BLa PNs. Because these cells are ascribed to negative emotion, it is reasonable to speculate that ACh may preferentially impact negative emotional circuitry. Perhaps defaulting to negative valence and defensive behaviors over positive valence and repetitive behaviors is evolutionarily advantageous and more beneficial for survival. Perhaps in support of this, a recent review postulated that elevated levels of ACh correlate with a negative encoding bias (Mineur and Picciotto 2021). Perhaps this observation stems from the anatomical and electrophysiological differences between the BLa and BLp that we report here. Future studies will need to explore this further.

6.3. FUTURE DIRECTIONS

1) In our studies here, we measured M1R expression of CeA projectors without accounting for which subnucleus of CeA our CTB 647 injections were targeting. Further, we measured and compared the M1R expression of these neurons against NAc projectors assuming the former and latter represented negative and positive cells based on projection-based definitions of valence from the literature. However, as mentioned in Chapter 3, previous studies have shown that CeC projectors represent negative cells and reside in the BLa while CeL and CeM projectors represent positive cells and reside in the BLp. Therefore, it would be interesting to repeat the experiment comparing M1R expression of CeC projectors against CeL and CeM projectors, as well as NAc projectors against CeC, CeL, and CeM projectors, to see what differences emerge. Based on findings #1 and #2 of Chapter 3 above, I would anticipate CeC projectors would have the highest since they should predominantly reside in the BLa where M1R expression is highest, followed by NAc projectors since we reported that roughly half resided in the BLa and BLp, followed by a tie between CeL and CeM projectors since they should primarily reside in the BLp.

2) We reported differences in the effects of phasic ACh and bath-applied muscarine at various points throughout our studies and speculated that these differences likely reflect the spatiotemporal dynamics of phasic and endogenous ACh release compared to the ubiquitous nature of bath-applied muscarine. Although there are surely plentiful ways to test this hypothesis further, a few would be as follows.

A) Bath-applied muscarine in the BLa produced an initial hyperpolarization (likely M1Rs coupled to GIRK, which we also observed with phasic ACh) followed by a much slower and longer lasting depolarization (presumably mediated by “extrasynaptic” M1Rs coupled to depolarizing effectors (like KCNQ channels that mediate the M-current) that was blocked by ATR. It would be interesting to see whether this response could be replicated under a more sustained mode of ACh signaling that accomplishes larger zone of ACh spread from cholinergic terminals in the slice. If it did, this would suggest the expanded reach of ACh activated more distant M1R responsible depolarizing the cell. The highly efficient degradative enzyme AChE also likely plays important roles in confining ACh’s spread upon release. Therefore, it would also be interesting to assess its role by seeing whether phasic ACh release could elicit the depolarizing response in the presence of AChE inhibitor physostigmine.

B) Phasic ACh did not increase the size of pharmacologically isolated LA-BLa NMDA EPSCs, even in the presence of intracellular GIRK-channel blocker QX-314, but bath-applied muscarine increases the size of these responses via M1Rs coupled to SK channels, suggesting cholinergic terminals could be preferentially positioned near “synaptic” M1Rs coupled to GIRK channels and not “extrasynaptic” M1Rs coupled to SK channels. Like 2.A. above, it would be interesting to see whether repeating this experiment with physostigmine generated an increase in the LA-BLa NMDA EPSC like muscarine did. Alternatively, a more sustained mode of

ACh could be used. It is possible in either of these two cases that the timing to reach SK channel activation after ACh release may also be an important factor, so different intervals between ACh release (whether phasic or sustained) and LA stimulation could also be tested.

3) We focused on determining whether postsynaptic M1Rs activated by phasic ACh release located on BLa PNs could potentiate NMDA receptor currents based on findings in the literature showing that cholinergic agonists in hippocampus did the same. However, we know that α7 and α4β2 nAChRs on presynaptic glutamate terminals are also activated by this same mode of release. It would be interesting to see if aligning this nicotinic event with the arrival of LA-BLa EPSPs would result in a larger current and to subsequently determine whether this was due to a facilitation of the removal of Mg^{2+} block. If this were true, it would be the first demonstration of a facilitation of NMDA receptor currents via presynaptic nAChR-mediated glutamate release and could have implications for the mechanisms by which ACh contributes to the acquisition of emotional memories.

4) Piggybacking on #3, it would also be interesting to see whether aligning the nicotinic response to phasic ACh release with a subthreshold spike-timing-dependent plasticity protocol that pairs glutamate responses from LA and BLa PN action potentials is sufficient to induce LTP. This would be the first demonstration of such a phenomenon and would likely involve the mechanism described in #3 above.

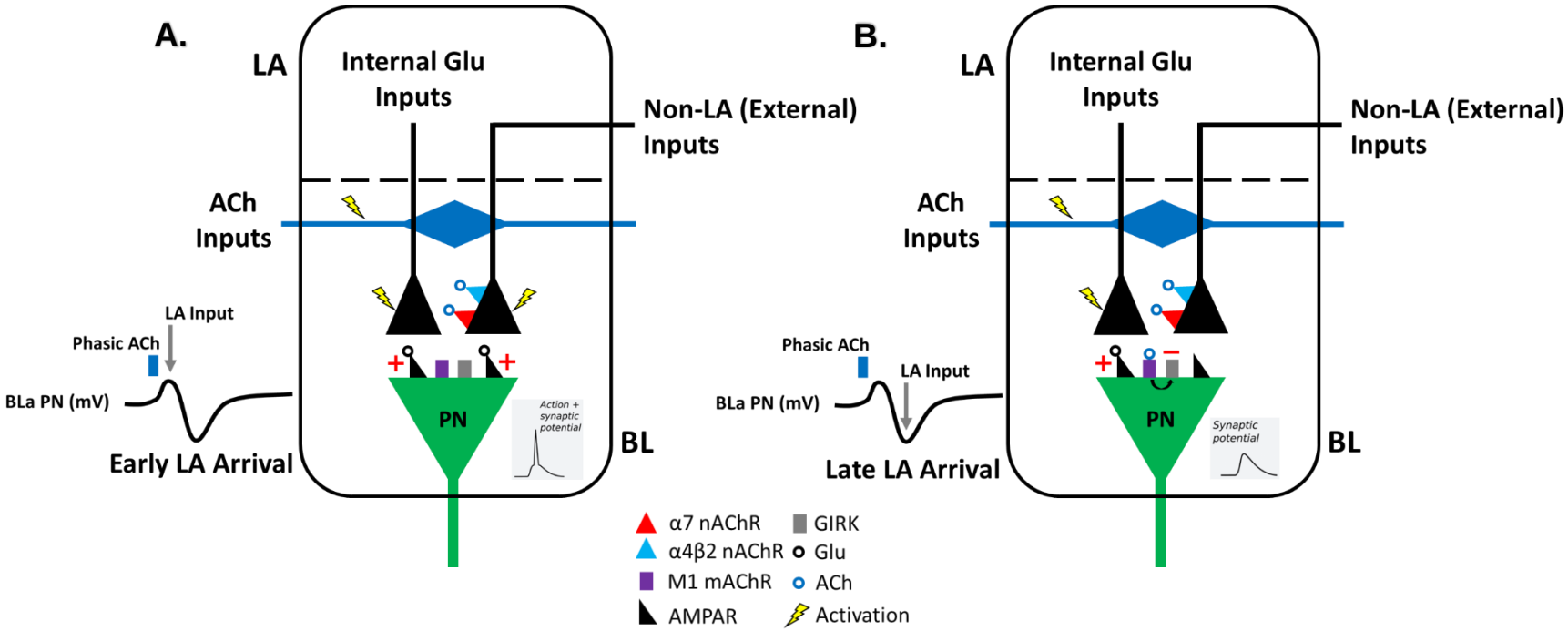

Figure 6.1. Circuit diagram of Chapter 4 findings. A. When LA inputs arrive at BLa PNs during the early cholinergic depolarization, the cells are more likely to fire compared to baseline conditions (the absence of ACh). This effect is associative because two distinct sets of glutamatergic inputs (LA inputs unaffected by ACh and non-LA inputs activated by ACh) associate in time by simultaneously depolarizing the same cell (temporal summation). This effect makes BLa PNs more likely to fire because it brings them closer to action potential threshold. The early cholinergic depolarization is indirect because it is mediated by glutamate release evoked by presynaptic α7 and α4β2 nAChRs on non-LA inputs. **B.** When LA inputs arrive at BLa PNs later, after the cholinergic depolarization has passed and the cholinergic hyperpolarization takes over, the cells are less likely to fire compared to baseline conditions since their membrane potential is farther from action potential threshold. The cholinergic hyperpolarization is direct because it is mediated by postsynaptic M1 mAChRs coupled to GIRK channels.

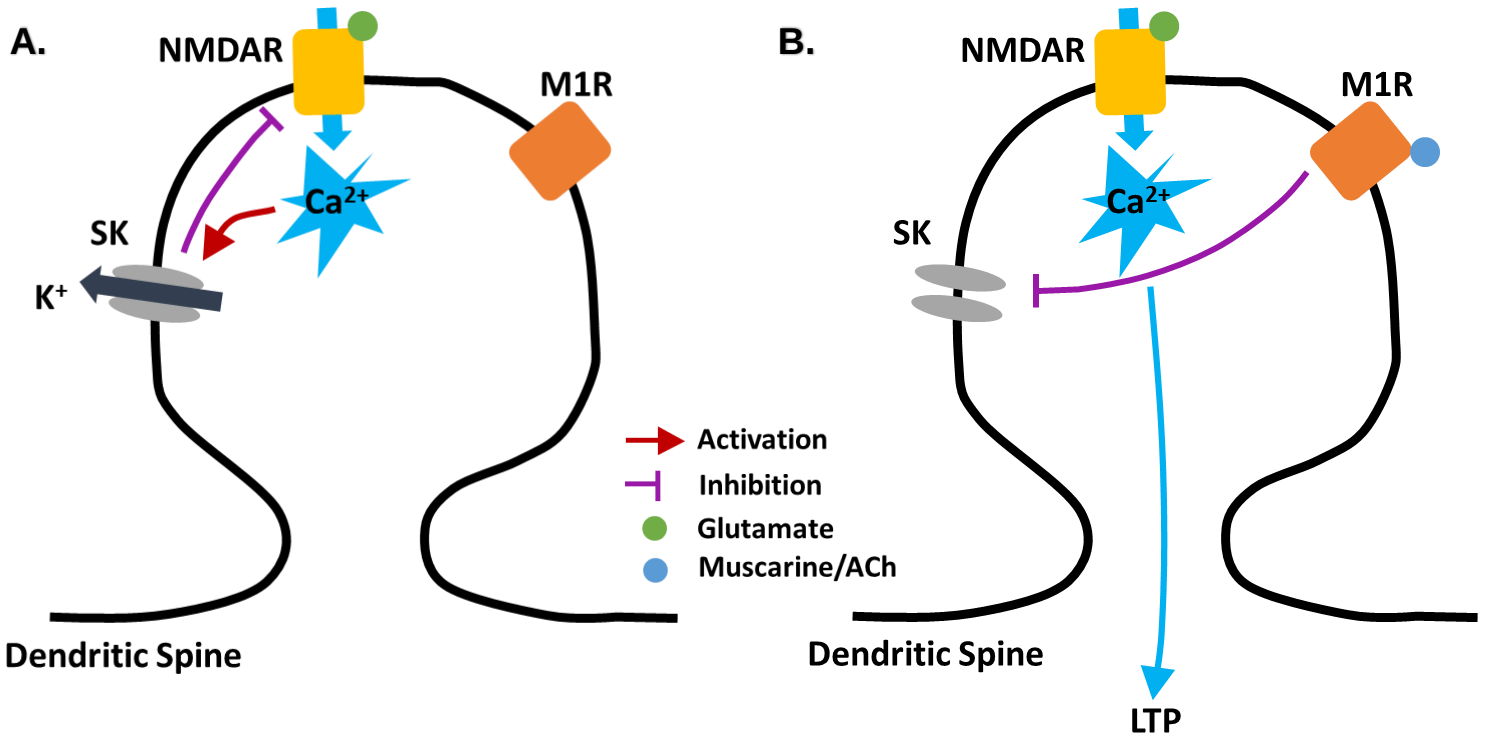

Figure 6.2. Circuit diagram of Chapter 5 findings. A. Under normal conditions, calcium entry through NMDA receptors (NMDARs) at LA-BLa PN synapses activates nearby calcium-sensitive SK channels. Activated SK channels serve as a pore through which NMDAR calcium can exit the cell (shunting inhibition). This effect limits calcium entry into BLa PNs during LA synaptic potentials and minimizes the possibility of LTP induction. **B.** M1 mAChR (M1R) activation leads to inhibition of SK channels. This disinhibits NMDARs and leads to larger calcium currents in the spine, which initiates downstream mechanisms that lead to LTP induction.

REFERENCES

Adinoff, B. (2004). Neurobiologic Processes in Drug Reward and Addiction. Harvard Review of Psychiatry, 12(6), 305–320. https://doi.org/10.1080/10673220490910844

Adolphs, R., Tranel, D., Damasio, H., & Damasio, A. (1994). Impaired recognition of emotion in facial expressions following bilateral damage to the human amygdala. Nature, 372(6507), 669–672. https://doi.org/10.1038/372669a0

Aggleton, J. P., & Passingham, R. E. (1981). Syndrome produced by lesions of the amygdala in monkeys (Macaca mulatta). Journal of Comparative and Physiological Psychology, 95(6), 961–977. https://doi.org/10.1037/h0077848

Aitta-aho, T., Hay, Y. A., Phillips, B. U., Saksida, L. M., Bussey, T. J., Paulsen, O., & Apergis-Schoute, J. (2018). Basal Forebrain and Brainstem Cholinergic Neurons Differentially Impact Amygdala Circuits and Learning-Related Behavior. Current Biology, 28(16), 2557-2569.e4. https://doi.org/10.1016/j.cub.2018.06.064

Ambroggi, F., Ishikawa, A., Fields, H. L., & Nicola, S. M. (2008). Basolateral Amygdala Neurons Facilitate Reward-Seeking Behavior by Exciting Nucleus Accumbens Neurons. Neuron, 59(4), 648–661. https://doi.org/10.1016/j.neuron.2008.07.004

Anderson, A. K., & Phelps, E. A. (2001). Lesions of the human amygdala impair

enhanced perception of emotionally salient events. Nature, 411(6835), 305–309. https://doi.org/10.1038/35077083

Andrade, R. (1991). Blockade of neurotransmitter-activated K+ conductance by QX-314 in the rat hippocampus. European Journal of Pharmacology, 199(2), 259–262. https://doi.org/10.1016/0014-2999(91)90467-5

Arnold, H. M., Burk, J. A., Hodgson, E. M., Sarter, M., & Bruno, J. P. (2002). Differential cortical acetylcholine release in rats performing a sustained attention task versus behavioral control tasks that do not explicitly tax attention. Neuroscience, 114(2), 451–460. https://doi.org/10.1016/S0306-4522(02)00292-0

Babiec, W. E., Jami, S. A., Guglietta, R., Chen, P. B., & O'Dell, T. J. (2017). Differential Regulation of NMDA Receptor-Mediated Transmission by SK Channels Underlies Dorsal-Ventral Differences in Dynamics of Schaffer Collateral Synaptic Function. Journal of Neuroscience, 37(7), 1950–1964. https://doi.org/10.1523/JNEUROSCI.3196-16.2017

Baldwin, A. E., Holahan, M. R., Sadeghian, K., & Kelley, A. E. (2000). N-methyl-D-aspartate receptor-dependent plasticity within a distributed corticostriatal network mediates appetitive instrumental learning. Behavioral Neuroscience, 114(1), 84–98. https://doi.org/10.1037//0735-7044.114.1.84

Baltoumas, F. A., Theodoropoulou, M. C., & Hamodrakas, S. J. (2013). Interactions of the α-subunits of heterotrimeric G-proteins with GPCRs, effectors and RGS proteins: A critical review and analysis of interacting

surfaces, conformational shifts, structural diversity and electrostatic potentials. Journal of Structural Biology, 182(3), 209–218. https://doi.org/10.1016/j.jsb.2013.03.004

Baxter, M. G., Bucci, D. J., Holland, P. C., & Gallagher, M. (1999). Impairments in conditioned stimulus processing and conditioned responding after combined selective removal of hippocampal and neocortical cholinergic input. Behavioral Neuroscience, 113(3), 486–495. https://doi.org/10.1037//0735-7044.113.3.486

Baxter, M. G., & Murray, E. A. (2002). The amygdala and reward. Nature Reviews Neuroscience, 3(7), 563–573. https://doi.org/10.1038/nrn875

Bazelot, M., Bocchio, M., Kasugai, Y., Fischer, D., Dodson, P. D., Ferraguti, F., & Capogna, M. (2015). Hippocampal Theta Input to the Amygdala Shapes Feedforward Inhibition to Gate Heterosynaptic Plasticity. Neuron, 87(6), 1290–1303. https://doi.org/10.1016/j.neuron.2015.08.024

Bazzari, A. H., & Parri, H. R. (2019). Neuromodulators and Long-Term Synaptic Plasticity in Learning and Memory: A Steered-Glutamatergic Perspective. Brain Sciences, 9(11), 300. https://doi.org/10.3390/brainsci9110300

Belova, M. A., Paton, J. J., & Salzman, C. D. (2008). Moment-to-moment tracking of state value in the amygdala. The Journal of Neuroscience: The Official Journal of the Society for Neuroscience, 28(40), 10023–10030. https://doi.org/10.1523/JNEUROSCI.1400-08.2008

Ben-Ari, Y., Zigmond, R. E., Shute, C. C., & Lewis, P. R. (1977). Regional distribution of choline acetyltransferase and acetylcholinesterase within

the amygdaloid complex and stria terminalis system. Brain Research, 120(3), 435–444. https://doi.org/10.1016/0006-8993(77)90397-3

Bermudez, M. A., & Schultz, W. (2010). Reward Magnitude Coding in Primate Amygdala Neurons. Journal of Neurophysiology, 104(6), 3424–3432. https://doi.org/10.1152/jn.00540.2010

Beyeler, A., Chang, C.-J., Silvestre, M., Lévêque, C., Namburi, P., Wildes, C. P., & Tye, K. M. (2018). Organization of Valence-Encoding and Projection-Defined Neurons in the Basolateral Amygdala. Cell Reports, 22(4), 905–918. https://doi.org/10.1016/j.celrep.2017.12.097

Beyeler, A., Namburi, P., Glober, G. F., Simonnet, C., Calhoon, G. G., Conyers, G. F., Luck, R., Wildes, C. P., & Tye, K. M. (2016). Divergent Routing of Positive and Negative Information from the Amygdala during Memory Retrieval. Neuron, 90(2), 348–361. https://doi.org/10.1016/j.neuron.2016.03.004

Blanchard, D. C., & Blanchard, R. J. (1972). Innate and conditioned reactions to threat in rats with amygdaloid lesions. Journal of Comparative and Physiological Psychology, 81(2), 281–290. https://doi.org/10.1037/h0033521

Bloodgood, B. L., & Sabatini, B. L. (2007). Nonlinear Regulation of Unitary Synaptic Signals by CaV2.3 Voltage-Sensitive Calcium Channels Located in Dendritic Spines. Neuron, 53(2), 249–260. https://doi.org/10.1016/j.neuron.2006.12.017

Bocchio, M., Nabavi, S., & Capogna, M. (2017). Synaptic Plasticity, Engrams,

and Network Oscillations in Amygdala Circuits for Storage and Retrieval of Emotional Memories. Neuron, 94(4), 731–743. https://doi.org/10.1016/j.neuron.2017.03.022

Bonda, E., Petrides, M., Ostry, D., & Evans, A. (1996). Specific involvement of human parietal systems and the amygdala in the perception of biological motion. The Journal of Neuroscience: The Official Journal of the Society for Neuroscience, 16(11), 3737–3744.

Bony, G., Szczurkowska, J., Tamagno, I., Shelly, M., Contestabile, A., & Cancedda, L. (2013). Non-hyperpolarizing GABAB receptor activation regulates neuronal migration and neurite growth and specification by cAMP/LKB1. Nature Communications, 4(1), 1800. https://doi.org/10.1038/ncomms2820

Brown, S., & Schafer, E. A. (1888). An Investigation into the Functions of the Occipital and Temporal Lobes of the Monkey's Brain. Philosophical Transactions of the Royal Society of London. B, 179, 303–327.

Brusco, S., Ambrosi, P., Meneghini, S., & Becchetti, A. (2015). Agonist and antagonist effects of tobacco-related nitrosamines on human α4β2 nicotinic acetylcholine receptors. Frontiers in Pharmacology, 6, 201. https://doi.org/10.3389/fphar.2015.00201

Buchanan, K. A., Petrovic, M. M., Chamberlain, S. E. L., Marrion, N. V., & Mellor, J. R. (2010). Facilitation of Long-Term Potentiation by Muscarinic M1 Receptors Is Mediated by Inhibition of SK Channels. Neuron, 68(5), 948–963. https://doi.org/10.1016/j.neuron.2010.11.018

Burns, L. H., Everitt, B. J., & Robbins, T. W. (1994). Intra-amygdala infusion of the N-methyl-D-aspartate receptor antagonist AP5 impairs acquisition but not performance of discriminated approach to an appetitive CS. Behavioral and Neural Biology, 61(3), 242–250. https://doi.org/10.1016/s0163-1047(05)80007-x

Calabresi, P., Centonze, D., Gubellini, P., Pisani, A., & Bernardi, G. (1998). Endogenous ACh enhances striatal NMDA-responses via M1-like muscarinic receptors and PKC activation. The European Journal of Neuroscience, 10(9), 2887–2895. https://doi.org/10.1111/j.1460-9568.1998.00294.x

Campeau, S., Miserendino, M. J., & Davis, M. (1992). Intra-amygdala infusion of the N-methyl-D-aspartate receptor antagonist AP5 blocks acquisition but not expression of fear-potentiated startle to an auditory conditioned stimulus. Behavioral Neuroscience, 106(3), 569–574. https://doi.org/10.1037//0735-7044.106.3.569

Cardinal, R. N., Parkinson, J. A., Hall, J., & Everitt, B. J. (2002). Emotion and motivation: The role of the amygdala, ventral striatum, and prefrontal cortex. Neuroscience & Biobehavioral Reviews, 26(3), 321–352. https://doi.org/10.1016/S0149-7634(02)00007-6

Careaga, M. B. L., Girardi, C. E. N., & Suchecki, D. (2016). Understanding posttraumatic stress disorder through fear conditioning, extinction and reconsolidation. Neuroscience & Biobehavioral Reviews, 71, 48–57. https://doi.org/10.1016/j.neubiorev.2016.08.023

Carlsen, J., & Heimer, L. (1986). A correlated light and electron microscopic immunocytochemical study of cholinergic terminals and neurons in the rat amygdaloid body with special emphasis on the basolateral amygdaloid nucleus. Journal of Comparative Neurology, 244(1), 121–136. https://doi.org/10.1002/cne.902440110

Carrere, M., & Alexandre, F. (2015). A pavlovian model of the amygdala and its influence within the medial temporal lobe. Frontiers in Systems Neuroscience, 9, 41. https://doi.org/10.3389/fnsys.2015.00041

Chalifoux, J. R., & Carter, A. G. (2010). GABAB receptors modulate NMDA receptor calcium signals in dendritic spines. Neuron, 66(1), 101–113. https://doi.org/10.1016/j.neuron.2010.03.012

Chen, S., & Aston-Jones, G. (1995). Evidence that cholera toxin B subunit (CTb) can be avidly taken up and transported by fibers of passage. Brain Research, 674(1), 107–111. https://doi.org/10.1016/0006-8993(95)00020-Q

Chiba, A. A., Bucci, D. J., Holland, P. C., & Gallagher, M. (1995). Basal forebrain cholinergic lesions disrupt increments but not decrements in conditioned stimulus processing. Journal of Neuroscience, 15(11), 7315–7322. https://doi.org/10.1523/JNEUROSCI.15-11-07315.1995

Chubykin, A. A., Roach, E. B., Bear, M. F., & Shuler, M. G. H. (2013). A Cholinergic Mechanism for Reward Timing within Primary Visual Cortex. Neuron, 77(4), 723–735. https://doi.org/10.1016/j.neuron.2012.12.039

Citri, A., & Malenka, R. C. (2008). Synaptic Plasticity: Multiple Forms, Functions,

and Mechanisms. Neuropsychopharmacology, 33(1), 18–41. https://doi.org/10.1038/sj.npp.1301559

Colangelo, C., Shichkova, P., Keller, D., Markram, H., & Ramaswamy, S. (2019). Cellular, Synaptic and Network Effects of Acetylcholine in the Neocortex. Frontiers in Neural Circuits, 13. https://doi.org/10.3389/fncir.2019.00024

Crouse, R. B., Kim, K., Batchelor, H. M., Girardi, E. M., Kamaletdinova, R., Chan, J., Rajebhosale, P., Pittenger, S. T., Role, L. W., Talmage, D. A., Jing, M., Li, Y., Gao, X.-B., Mineur, Y. S., & Picciotto, M. R. (2020). Acetylcholine is released in the basolateral amygdala in response to predictors of reward and enhances the learning of cue-reward contingency. ELife, 9, e57335. https://doi.org/10.7554/eLife.57335

Dalley, J. W., McGaughy, J., O'Connell, M. T., Cardinal, R. N., Levita, L., & Robbins, T. W. (2001). Distinct Changes in Cortical Acetylcholine and Noradrenaline Efflux during Contingent and Noncontingent Performance of a Visual Attentional Task. Journal of Neuroscience, 21(13), 4908–4914. https://doi.org/10.1523/JNEUROSCI.21-13-04908.2001

Dalley, J. W., Theobald, D. E., Bouger, P., Chudasama, Y., Cardinal, R. N., & Robbins, T. W. (2004). Cortical Cholinergic Function and Deficits in Visual Attentional Performance in Rats Following 192 IgG–Saporin-induced Lesions of the Medial Prefrontal Cortex. Cerebral Cortex, 14(8), 922–932. https://doi.org/10.1093/cercor/bhh052

Dasgupta, R., Seibt, F., & Beierlein, M. (2018). Synaptic Release of Acetylcholine Rapidly Suppresses Cortical Activity by Recruiting Muscarinic Receptors

in Layer 4. Journal of Neuroscience, 38(23), 5338–5350. https://doi.org/10.1523/JNEUROSCI.0566-18.2018

de Oliveira, P. G., Ramos, M. L. S., Amaro, A. J., Dias, R. A., & Vieira, S. I. (2019). Gi/o-Protein Coupled Receptors in the Aging Brain. Frontiers in Aging Neuroscience, 11, 89. https://doi.org/10.3389/fnagi.2019.00089

Dennis, S. H., Pasqui, F., Colvin, E. M., Sanger, H., Mogg, A. J., Felder, C. C., Broad, L. M., Fitzjohn, S. M., Isaac, J. T. R., & Mellor, J. R. (2016). Activation of Muscarinic M1 Acetylcholine Receptors Induces Long-Term Potentiation in the Hippocampus. Cerebral Cortex, 26(1), 414–426. https://doi.org/10.1093/cercor/bhv227

Desmarais, P., Weidman, D., Wassef, A., Bruneau, M.-A., Friedland, J., Bajsarowicz, P., Thibodeau, M.-P., Herrmann, N., & Nguyen, Q. D. (2020). The Interplay Between Post-traumatic Stress Disorder and Dementia: A Systematic Review. The American Journal of Geriatric Psychiatry, 28(1), 48–60. https://doi.org/10.1016/j.jagp.2019.08.006

Disney, A. A., & Higley, M. J. (2020). Diverse Spatiotemporal Scales of Cholinergic Signaling in the Neocortex. The Journal of Neuroscience: The Official Journal of the Society for Neuroscience, 40(4), 720–725. https://doi.org/10.1523/JNEUROSCI.1306-19.2019

Domjan, M. (2005). Pavlovian Conditioning: A Functional Perspective. Annual Review of Psychology, 56(1), 179–206. https://doi.org/10.1146/annurev.psych.55.090902.141409

Drever, B. D., Riedel, G., & Platt, B. (2011). The cholinergic system and

hippocampal plasticity. Behavioural Brain Research, 221(2), 505–514. https://doi.org/10.1016/j.bbr.2010.11.037

Drevets, W. C. (2003). Neuroimaging Abnormalities in the Amygdala in Mood Disorders. Annals of the New York Academy of Sciences, 985(1), 420–444. https://doi.org/10.1111/j.1749-6632.2003.tb07098.x

Everitt, B. J., & Robbins, T. W. (1997). Central cholinergic systems and cognition. Annual Review of Psychology, 48, 649–684. https://doi.org/10.1146/annurev.psych.48.1.649

Faber, E. S. L. (2010). Functional interplay between NMDA receptors, SK channels and voltage-gated Ca2+ channels regulates synaptic excitability in the medial prefrontal cortex. The Journal of Physiology, 588(8), 1281–1292. https://doi.org/10.1113/jphysiol.2009.185645

Faber, E. S. L., Delaney, A. J., & Sah, P. (2005). SK channels regulate excitatory synaptic transmission and plasticity in the lateral amygdala. Nature Neuroscience, 8(5), 635–641. https://doi.org/10.1038/nn1450

Fanselow, M. S., & Kim, J. J. (1994). Acquisition of contextual Pavlovian fear conditioning is blocked by application of an NMDA receptor antagonist D,L-2-amino-5-phosphonovaleric acid to the basolateral amygdala. Behavioral Neuroscience, 108(1), 210–212. https://doi.org/10.1037//0735-7044.108.1.210

Feltenstein, M., & See, R. (2007). NMDA receptor blockade in the basolateral amygdala disrupts consolidation of stimulus-reward memory and extinction learning during reinstatement of cocaine-seeking in an animal

model of relapse. Neurobiology of Learning and Memory, 88(4), 435–444. https://doi.org/10.1016/j.nlm.2007.05.006

Fernández de Sevilla, D., & Buño, W. (2010). The muscarinic long-term enhancement of NMDA and AMPA receptor-mediated transmission at Schaffer collateral synapses develop through different intracellular mechanisms. The Journal of Neuroscience: The Official Journal of the Society for Neuroscience, 30(33), 11032–11042. https://doi.org/10.1523/JNEUROSCI.1848-10.2010

Fernando, A., Murray, J., & Milton, A. (2013). The amygdala: Securing pleasure and avoiding pain. Frontiers in Behavioral Neuroscience, 7, 190. https://doi.org/10.3389/fnbeh.2013.00190

Fisher, S. K., & Wonnacott, S. (2012). Chapter 13—Acetylcholine. In S. T. Brady, G. J. Siegel, R. W. Albers, & D. L. Price (Eds.), Basic Neurochemistry (Eighth Edition) (pp. 258–282). Academic Press. https://doi.org/10.1016/B978-0-12-374947-5.00013-4

Freedman, R. (2014). A7-Nicotinic Acetylcholine Receptor Agonists for Cognitive Enhancement in Schizophrenia. Annual Review of Medicine, 65(1), 245–261. https://doi.org/10.1146/annurev-med-092112-142937

Gallagher, M., & Chiba, A. A. (1996). The amygdala and emotion. Current Opinion in Neurobiology, 6(2), 221–227. https://doi.org/10.1016/S0959-4388(96)80076-6

Garduño, J., Galindo-Charles, L., Jiménez-Rodríguez, J., Galarraga, E., Tapia, D., Mihailescu, S., & Hernandez-Lopez, S. (2012). Presynaptic α4β2

nicotinic acetylcholine receptors increase glutamate release and serotonin neuron excitability in the dorsal raphe nucleus. The Journal of Neuroscience: The Official Journal of the Society for Neuroscience, 32(43), 15148–15157. https://doi.org/10.1523/JNEUROSCI.0941-12.2012

Gewirtz, J. C., & Davis, M. (1997). Second-order fear conditioning prevented by blocking NMDA receptors in amygdala. Nature, 388(6641), 471–474. https://doi.org/10.1038/41325

Giessel, A. J., & Sabatini, B. L. (2010). M1 Muscarinic Receptors Boost Synaptic Potentials and Calcium Influx in Dendritic Spines by Inhibiting Postsynaptic SK Channels. Neuron, 68(5), 936–947. https://doi.org/10.1016/j.neuron.2010.09.004

Giocomo, L. M., & Hasselmo, M. E. (2007). Neuromodulation by Glutamate and Acetylcholine can Change Circuit Dynamics by Regulating the Relative Influence of Afferent Input and Excitatory Feedback. Molecular Neurobiology, 36(2), 184–200. https://doi.org/10.1007/s12035-007-0032-z

Goosens, K. A., & Maren, S. (2001). Contextual and Auditory Fear Conditioning are Mediated by the Lateral, Basal, and Central Amygdaloid Nuclei in Rats. Learning & Memory, 8(3), 148–155. https://doi.org/10.1101/lm.37601

Gore, F., Schwartz, E. C., Brangers, B. C., Aladi, S., Stujenske, J. M., Likhtik, E., Russo, M. J., Gordon, J. A., Salzman, C. D., & Axel, R. (2015). Neural Representations of Unconditioned Stimuli in Basolateral Amygdala Mediate Innate and Learned Responses. Cell, 162(1), 134–145.

https://doi.org/10.1016/j.cell.2015.06.027

Gritton, H. J., Howe, W. M., Mallory, C. S., Hetrick, V. L., Berke, J. D., & Sarter, M. (2016). Cortical cholinergic signaling controls the detection of cues. Proceedings of the National Academy of Sciences, 113(8), E1089–E1097. https://doi.org/10.1073/pnas.1516134113

Gu, Z., & Yakel, J. L. (2011). Timing-Dependent Septal Cholinergic Induction of Dynamic Hippocampal Synaptic Plasticity. Neuron, 71(1), 155–165. https://doi.org/10.1016/j.neuron.2011.04.026

Guillem, K., Bloem, B., Poorthuis, R. B., Loos, M., Smit, A. B., Maskos, U., Spijker, S., & Mansvelder, H. D. (2011). Nicotinic Acetylcholine Receptor β2 Subunits in the Medial Prefrontal Cortex Control Attention. Science, 333(6044), 888–891. https://doi.org/10.1126/science.1207079

Guo, W., Robert, B., & Polley, D. B. (2019). The Cholinergic Basal Forebrain Links Auditory Stimuli with Delayed Reinforcement to Support Learning. Neuron, 103(6), 1164-1177.e6. https://doi.org/10.1016/j.neuron.2019.06.024

Haam, J., & Yakel, J. L. (2017). Cholinergic modulation of the hippocampal region and memory function. Journal of Neurochemistry, 142 Suppl 2, 111–121. https://doi.org/10.1111/jnc.14052

Haga, T. (2013). Molecular properties of muscarinic acetylcholine receptors. Proceedings of the Japan Academy, Series B, 89(6), 226–256. https://doi.org/10.2183/pjab.89.226

Hahn, B. (2015). Nicotinic Receptors and Attention. In D. J. K. Balfour & M. R.

Munafò (Eds.), The Neurobiology and Genetics of Nicotine and Tobacco (pp. 103–135). Springer International Publishing. https://doi.org/10.1007/978-3-319-13665-3_5

Hajós, M., Hurst, R. S., Hoffmann, W. E., Krause, M., Wall, T. M., Higdon, N. R., & Groppi, V. E. (2005). The Selective α7 Nicotinic Acetylcholine Receptor Agonist PNU-282987 [N-[(3R)-1-Azabicyclo[2.2.2]oct-3-yl]-4-chlorobenzamide Hydrochloride] Enhances GABAergic Synaptic Activity in Brain Slices and Restores Auditory Gating Deficits in Anesthetized Rats. Journal of Pharmacology and Experimental Therapeutics, 312(3), 1213–1222. https://doi.org/10.1124/jpet.104.076968

Hampel, H., Mesulam, M.-M., Cuello, A. C., Farlow, M. R., Giacobini, E., Grossberg, G. T., Khachaturian, A. S., Vergallo, A., Cavedo, E., Snyder, P. J., & Khachaturian, Z. S. (2018). The cholinergic system in the pathophysiology and treatment of Alzheimer's disease. Brain, 141(7), 1917–1933. https://doi.org/10.1093/brain/awy132

Hangya, B., Ranade, S. P., Lorenc, M., & Kepecs, A. (2015). Central Cholinergic Neurons Are Rapidly Recruited by Reinforcement Feedback. Cell, 162(5), 1155–1168. https://doi.org/10.1016/j.cell.2015.07.057

Hardingham, G. E., & Bading, H. (2010). Synaptic versus extrasynaptic NMDA receptor signalling: Implications for neurodegenerative disorders. Nature Reviews Neuroscience, 11(10), 682–696. https://doi.org/10.1038/nrn2911

Harrison, T. C., Pinto, L., Brock, J. R., & Dan, Y. (2016). Calcium Imaging of Basal Forebrain Activity during Innate and Learned Behaviors. Frontiers in

Neural Circuits, 10, 36. https://doi.org/10.3389/fncir.2016.00036

Hasselmo, M. E. (2006). The role of acetylcholine in learning and memory. Current Opinion in Neurobiology, 16(6), 710–715. https://doi.org/10.1016/j.conb.2006.09.002

Hasselmo, M. E., & Bower, J. M. (1993). Acetylcholine and memory. Trends in Neurosciences, 16(6), 218–222. https://doi.org/10.1016/0166-2236(93)90159-j

Hasselmo, M. E., & Sarter, M. (2011). Modes and models of forebrain cholinergic neuromodulation of cognition. Neuropsychopharmacology: Official Publication of the American College of Neuropsychopharmacology, 36(1), 52–73. https://doi.org/10.1038/npp.2010.104

Hedrick, T., & Waters, J. (2015). Acetylcholine excites neocortical pyramidal neurons via nicotinic receptors. Journal of Neurophysiology, 113(7), 2195–2209. https://doi.org/10.1152/jn.00716.2014

Higley, M. J., & Picciotto, M. R. (2014). Neuromodulation by acetylcholine: Examples from schizophrenia and depression. Current Opinion in Neurobiology, 29, 88–95. https://doi.org/10.1016/j.conb.2014.06.004

Himmelheber, A. M., Sarter, M., & Bruno, J. P. (2000). Increases in cortical acetylcholine release during sustained attention performance in rats. Cognitive Brain Research, 9(3), 313–325. https://doi.org/10.1016/S0926-6410(00)00012-4

Hollmann, M. W., Strumper, D., Herroeder, S., Durieux, M. E., & Warltier, D. C. (2005). Receptors, G Proteins, and Their Interactions. Anesthesiology,

103(5), 1066–1078. https://doi.org/10.1097/00000542-200511000-00022

Howe, W. M., Gritton, H. J., Lusk, N. A., Roberts, E. A., Hetrick, V. L., Berke, J. D., & Sarter, M. (2017). Acetylcholine Release in Prefrontal Cortex Promotes Gamma Oscillations and Theta-Gamma Coupling during Cue Detection. The Journal of Neuroscience: The Official Journal of the Society for Neuroscience, 37(12), 3215–3230. https://doi.org/10.1523/JNEUROSCI.2737-16.2017

Hu, G.-Y., Biró, Z., Hill, R. H., & Grillner, S. (2002). Intracellular QX-314 Causes Depression of Membrane Potential Oscillations in Lamprey Spinal Neurons During Fictive Locomotion. Journal of Neurophysiology, 87(6), 2676–2683. https://doi.org/10.1152/jn.2002.87.6.2676

Janak, P. H., & Tye, K. M. (2015). From circuits to behaviour in the amygdala. Nature, 517(7534), 284–292. https://doi.org/10.1038/nature14188

Jiang, L., Emmetsberger, J., Talmage, D. A., & Role, L. W. (2013). Type III neuregulin 1 is required for multiple forms of excitatory synaptic plasticity of mouse cortico-amygdala circuits. The Journal of Neuroscience: The Official Journal of the Society for Neuroscience, 33(23), 9655–9666. https://doi.org/10.1523/JNEUROSCI.2888-12.2013

Jiang, L., Kundu, S., Lederman, J. D., López-Hernández, G. Y., Ballinger, E. C., Wang, S., Talmage, D. A., & Role, L. W. (2016). Cholinergic Signaling Controls Conditioned Fear Behaviors and Enhances Plasticity of Cortical-Amygdala Circuits. Neuron, 90(5), 1057–1070. https://doi.org/10.1016/j.neuron.2016.04.028

Jiang, L., & Role, L. W. (2008). Facilitation of cortico-amygdala synapses by nicotine: Activity-dependent modulation of glutamatergic transmission. Journal of Neurophysiology, 99(4), 1988–1999. https://doi.org/10.1152/jn.00933.2007

Jimenez, S. A., & Maren, S. (2009). Nuclear disconnection within the amygdala reveals a direct pathway to fear. Learning & Memory, 16(12), 766–768. https://doi.org/10.1101/lm.1607109

Johansen, J. P., Cain, C. K., Ostroff, L. E., & LeDoux, J. E. (2011). Molecular Mechanisms of Fear Learning and Memory. Cell, 147(3), 509–524. https://doi.org/10.1016/j.cell.2011.10.009

Jolkkonen, E., & Pitkänen, A. (1998). Intrinsic connections of the rat amygdaloid complex: Projections originating in the central nucleus. Journal of Comparative Neurology, 395(1), 53–72. https://doi.org/10.1002/(SICI)1096-9861(19980525)395:1<53::AID-CNE5>3.0.CO;2-G

Jones, C. K., Byun, N., & Bubser, M. (2012). Muscarinic and Nicotinic Acetylcholine Receptor Agonists and Allosteric Modulators for the Treatment of Schizophrenia. Neuropsychopharmacology, 37(1), 16–42. https://doi.org/10.1038/npp.2011.199

Joshi, A., Kalappa, B. I., Anderson, C. T., & Tzounopoulos, T. (2016). Cell-Specific Cholinergic Modulation of Excitability of Layer 5B Principal Neurons in Mouse Auditory Cortex. The Journal of Neuroscience: The Official Journal of the Society for Neuroscience, 36(32), 8487–8499.

https://doi.org/10.1523/JNEUROSCI.0780-16.2016

Kantamneni, S. (2015). Cross-talk and regulation between glutamate and GABAB receptors. Frontiers in Cellular Neuroscience, 9, 135. https://doi.org/10.3389/fncel.2015.00135

Karczmar, A. G., Lindstrom, J., & Christopoulos, A. (2007). History of Research on Nicotinic and Muscarinic Cholinergic Receptors. In A. G. Karczmar (Ed.), Exploring the Vertebrate Central Cholinergic Nervous System (pp. 151–162). Springer US. https://doi.org/10.1007/978-0-387-46526-5_4

Killcross, S., Robbins, T. W., & Everitt, B. J. (1997). Different types of fear-conditioned behaviour mediated by separate nuclei within amygdala. Nature, 388(6640), 377–380. https://doi.org/10.1038/41097

Kim, J., Pignatelli, M., Xu, S., Itohara, S., & Tonegawa, S. (2016). Antagonistic negative and positive neurons of the basolateral amygdala. Nature Neuroscience, 19(12), 1636–1646. https://doi.org/10.1038/nn.4414

Kim, J., Zhang, X., Muralidhar, S., LeBlanc, S. A., & Tonegawa, S. (2017). Basolateral to Central Amygdala Neural Circuits for Appetitive Behaviors. Neuron, 93(6), 1464-1479.e5. https://doi.org/10.1016/j.neuron.2017.02.034

Klein, R. C., & Yakel, J. L. (2006). Functional somato-dendritic alpha7-containing nicotinic acetylcholine receptors in the rat basolateral amygdala complex. The Journal of Physiology, 576(Pt 3), 865–872. https://doi.org/10.1113/jphysiol.2006.118232

Klüver, H., & Bucy, P. C. (1937). “Psychic blindness” and other symptoms

following bilateral temporal lobectomy in Rhesus monkeys. American Journal of Physiology, 119, 352–353.

Kozak, R., Bruno, J. P., & Sarter, M. (2006). Augmented Prefrontal Acetylcholine Release during Challenged Attentional Performance. Cerebral Cortex, 16(1), 9–17. https://doi.org/10.1093/cercor/bhi079

Kozak, R., Martinez, V., Young, D., Brown, H., Bruno, J. P., & Sarter, M. (2007). Toward a neuro-cognitive animal model of the cognitive symptoms of schizophrenia: Disruption of cortical cholinergic neurotransmission following repeated amphetamine exposure in attentional task-performing, but not non-performing, rats. Neuropsychopharmacology: Official Publication of the American College of Neuropsychopharmacology, 32(10), 2074–2086. https://doi.org/10.1038/sj.npp.1301352

Kuchibhotla, K. V., Gill, J. V., Lindsay, G. W., Papadoyannis, E. S., Field, R. E., Sten, T. A. H., Miller, K. D., & Froemke, R. C. (2017). Parallel processing by cortical inhibition enables context-dependent behavior. Nature Neuroscience, 20(1), 62–71. https://doi.org/10.1038/nn.4436

Laszlovszky, T., Schlingloff, D., Hegedüs, P., Freund, T. F., Gulyás, A., Kepecs, A., & Hangya, B. (2020). Distinct synchronization, cortical coupling and behavioral function of two basal forebrain cholinergic neuron types. Nature Neuroscience, 23(8), 992–1003. https://doi.org/10.1038/s41593-020-0648-0

LeDoux, J. (2007). The amygdala. Current Biology, 17(20), R868–R874. https://doi.org/10.1016/j.cub.2007.08.005

LeDoux, J. E. (2000). Emotion circuits in the brain. Annual Review of Neuroscience, 23, 155–184. https://doi.org/10.1146/annurev.neuro.23.1.155

LeDoux, J. E., Cicchetti, P., Xagoraris, A., & Romanski, L. M. (1990). The lateral amygdaloid nucleus: Sensory interface of the amygdala in fear conditioning. Journal of Neuroscience, 10(4), 1062–1069. https://doi.org/10.1523/JNEUROSCI.10-04-01062.1990

Lee, H. J., Choi, J.-S., Brown, T. H., & Kim, J. J. (2001). Amygdalar NMDA Receptors Are Critical for the Expression of Multiple Conditioned Fear Responses. Journal of Neuroscience, 21(11), 4116–4124. https://doi.org/10.1523/JNEUROSCI.21-11-04116.2001

Lee, S., Kim, S.-J., Kwon, O.-B., Lee, J. H., & Kim, J.-H. (2013). Inhibitory networks of the amygdala for emotional memory. Frontiers in Neural Circuits, 7, 129. https://doi.org/10.3389/fncir.2013.00129

Lee, S.-H., Govindaiah, G., & Cox, C. L. (2010). Selective Excitatory Actions of DNQX and CNQX in Rat Thalamic Neurons. Journal of Neurophysiology, 103(4), 1728–1734. https://doi.org/10.1152/jn.00540.2009

Letzkus, J. J., Wolff, S. B. E., Meyer, E. M. M., Tovote, P., Courtin, J., Herry, C., & Lüthi, A. (2011). A disinhibitory microcircuit for associative fear learning in the auditory cortex. Nature, 480(7377), 331–335. https://doi.org/10.1038/nature10674

Levin, E. D. (2002). Nicotinic receptor subtypes and cognitive function. Journal of Neurobiology, 53(4), 633–640. https://doi.org/10.1002/neu.10151

Li, S., Nai, Q., Lipina, T. V., Roder, J. C., & Liu, F. (2013). A7nAchR/NMDAR coupling affects NMDAR function and object recognition. Molecular Brain, 6(1), 1–10. https://doi.org/10.1186/1756-6606-6-58

Lin, S.-C., & Nicolelis, M. A. L. (2008). Neuronal Ensemble Bursting in the Basal Forebrain Encodes Salience Irrespective of Valence. Neuron, 59(1), 138–149. https://doi.org/10.1016/j.neuron.2008.04.031

Liu, C.-H., Coleman, J. E., Davoudi, H., Zhang, K., & Hussain Shuler, M. G. (2015). Selective Activation of a Putative Reinforcement Signal Conditions Cued Interval Timing in Primary Visual Cortex. Current Biology, 25(12), 1551–1561. https://doi.org/10.1016/j.cub.2015.04.028

Losonczy, A., Makara, J. K., & Magee, J. C. (2008). Compartmentalized dendritic plasticity and input feature storage in neurons. Nature, 452(7186), 436–441. https://doi.org/10.1038/nature06725

Lu, Y., Sarter, M., Zochowski, M., & Booth, V. (2020). Phasic cholinergic signaling promotes emergence of local gamma rhythms in excitatory–inhibitory networks. European Journal of Neuroscience, 52(6), 3545–3560. https://doi.org/10.1111/ejn.14744

Luján, R., Maylie, J., & Adelman, J. P. (2009). New sites of action for GIRK and SK channels. Nature Reviews Neuroscience, 10(7), 475–480. https://doi.org/10.1038/nrn2668

Luscher, C., & Malenka, R. C. (2012). NMDA Receptor-Dependent Long-Term Potentiation and Long-Term Depression (LTP/LTD). Cold Spring Harbor Perspectives in Biology, 4(6), a005710–a005710.

https://doi.org/10.1101/cshperspect.a005710

Lustig, C., & Sarter, M. (2016). Attention and the Cholinergic System: Relevance to Schizophrenia. Current Topics in Behavioral Neurosciences, 28, 327–362. https://doi.org/10.1007/7854_2015_5009

Lyketsos, C. G., Carrillo, M. C., Ryan, J. M., Khachaturian, A. S., Trzepacz, P., Amatniek, J., Cedarbaum, J., Brashear, R., & Miller, D. S. (2011). Neuropsychiatric symptoms in Alzheimer's disease. Alzheimer's & Dementia : The Journal of the Alzheimer's Association, 7(5), 532–539. https://doi.org/10.1016/j.jalz.2011.05.2410

Lynch, M. A. (2004). Long-Term Potentiation and Memory. Physiol Rev, 84, 50.

MacDonald, J. F., Jackson, M. F., & Beazely, M. A. (2007). G protein-coupled receptors control NMDARs and metaplasticity in the hippocampus. Biochimica et Biophysica Acta (BBA) - Biomembranes, 1768(4), 941–951. https://doi.org/10.1016/j.bbamem.2006.12.006

Maquet, P., Péters, J.-M., Aerts, J., Delfiore, G., Degueldre, C., Luxen, A., & Franck, G. (1996). Functional neuroanatomy of human rapid-eye-movement sleep and dreaming. Nature, 383(6596), 163–166. https://doi.org/10.1038/383163a0

Maren, S. (1999). Long-term potentiation in the amygdala: A mechanism for emotional learning and memory. Trends in Neurosciences, 22(12), 561–567. https://doi.org/10.1016/S0166-2236(99)01465-4

Maren, S. (2001). Neurobiology of Pavlovian fear conditioning. Annual Review of Neuroscience, 24, 897–931.

https://doi.org/10.1146/annurev.neuro.24.1.897

Maren, S., Aharonov, G., Stote, D. L., & Fanselow, M. S. (1996). N-methyl-D-aspartate receptors in the basolateral amygdala are required for both acquisition and expression of conditional fear in rats. Behavioral Neuroscience, 110(6), 1365–1374. https://doi.org/10.1037/0735-7044.110.6.1365

Marino, M. J., Rouse, S. T., Levey, A. I., Potter, L. T., & Conn, P. J. (1998). Activation of the genetically defined m1 muscarinic receptor potentiates N-methyl-D-aspartate (NMDA) receptor currents in hippocampal pyramidal cells. Proceedings of the National Academy of Sciences, 95(19), 11465–11470. https://doi.org/10.1073/pnas.95.19.11465

Martinez, J. L., & Derrick, B. E. (1996). Long-term potentiation and learning. Annual Review of Psychology, 47, 173–203. https://doi.org/10.1146/annurev.psych.47.1.173

McCullough, K. M., Daskalakis, N. P., Gafford, G., Morrison, F. G., & Ressler, K. J. (2018). Cell-type-specific interrogation of CeA Drd2 neurons to identify targets for pharmacological modulation of fear extinction. Translational Psychiatry, 8(1), 164. https://doi.org/10.1038/s41398-018-0190-y

McDonald, A. J. (1982). Cytoarchitecture of the central amygdaloid nucleus of the rat. The Journal of Comparative Neurology, 208(4), 401–418. https://doi.org/10.1002/cne.902080409

McDonald, A. J. (1991a). Topographical organization of amygdaloid projections to the caudatoputamen, nucleus accumbens, and related striatal-like

areas of the rat brain. Neuroscience, 44(1), 15–33. https://doi.org/10.1016/0306-4522(91)90248-m

Mcdonald, A. J. (1991b). Organization of amygdaloid projections to the prefrontal cortex and associated striatum in the rat. Neuroscience, 44(1), 1–14. https://doi.org/10.1016/0306-4522(91)90247-L

McDonald, A. J. (2020). Chapter 1 - Functional neuroanatomy of the basolateral amygdala: Neurons, neurotransmitters, and circuits. In J. H. Urban & J. A. Rosenkranz (Eds.), Handbook of Behavioral Neuroscience (Vol. 26, pp. 1–38). Elsevier. https://doi.org/10.1016/B978-0-12-815134-1.00001-5

McDonald, A. J., & Mascagni, F. (2010). Neuronal localization of m1 muscarinic receptor immunoreactivity in the rat basolateral amygdala. Brain Structure and Function, 215(1), 37–48. https://doi.org/10.1007/s00429-010-0272-y

McDonald, A. J., & Mott, D. D. (2021). Neuronal localization of m1 muscarinic receptor immunoreactivity in the monkey basolateral amygdala. Journal of Comparative Neurology, 529(10), 2450–2463. https://doi.org/10.1002/cne.25104

McGaughy, J., Everitt, B. J., Robbins, T. W., & Sarter, M. (2000). The role of cortical cholinergic afferent projections in cognition: Impact of new selective immunotoxins. Behavioural Brain Research, 115(2), 251–263. https://doi.org/10.1016/S0166-4328(00)00262-X

McGaughy, J., Kaiser, T., & Sarter, M. (1996). Behavioral vigilance following infusions of 192 IgG-saporin into the basal forebrain: Selectivity of the behavioral impairment and relation to cortical AChE-positive fiber density.

Behavioral Neuroscience, 110(2), 247–265. https://doi.org/10.1037//0735-7044.110.2.247

McGaughy, J., & Sarter, M. (1998). Sustained attention performance in rats with intracortical infusions of 192 IgG-saporin-induced cortical cholinergic deafferentation: Effects of physostigmine and FG 7142. Behavioral Neuroscience, 112(6), 1519–1525. https://doi.org/10.1037//0735-7044.112.6.1519

Meng, W., Wang, S., Yao, L., Zhang, N., & Li, D. (2017). Muscarinic Receptors Are Responsible for the Cholinergic Modulation of Projection Neurons in the Song Production Brain Nucleus RA of Zebra Finches. Frontiers in Cellular Neuroscience, 11, 51. https://doi.org/10.3389/fncel.2017.00051

Mineur, Y. S., & Picciotto, M. R. (2021). The role of acetylcholine in negative encoding bias: Too much of a good thing? The European Journal of Neuroscience, 53(1), 114–125. https://doi.org/10.1111/ejn.14641

Miserendino, M. J., Sananes, C. B., Melia, K. R., & Davis, M. (1990). Blocking of acquisition but not expression of conditioned fear-potentiated startle by NMDA antagonists in the amygdala. Nature, 345(6277), 716–718. https://doi.org/10.1038/345716a0

Mori, E., Ikeda, M., Hirono, N., Kitagaki, H., Imamura, T., & Shimomura, T. (1999). Amygdalar Volume and Emotional Memory in Alzheimer's Disease. American Journal of Psychiatry, 156(2), 216–222. https://doi.org/10.1176/ajp.156.2.216

Morrisett, R. A., Mott, D. D., Lewis, D. V., Swartzwelder, H. S., & Wilson, W. A.

(1991). GABAB-receptor-mediated inhibition of the N-methyl-D-aspartate component of synaptic transmission in the rat hippocampus. The Journal of Neuroscience: The Official Journal of the Society for Neuroscience, 11(1), 203–209.

Mott, D. D., Li, Q., Okazaki, M. M., Turner, D. A., & Lewis, D. V. (1999). GABA B -Receptor–Mediated Currents in Interneurons of the Dentate-Hilus Border. Journal of Neurophysiology, 82(3), 1438–1450. https://doi.org/10.1152/jn.1999.82.3.1438

Muller, J. F., Mascagni, F., & McDonald, A. J. (2006). Pyramidal cells of the rat basolateral amygdala: Synaptology and innervation by parvalbumin-immunoreactive interneurons. Journal of Comparative Neurology, 494(4), 635–650. https://doi.org/10.1002/cne.20832

Muller, J. F., Mascagni, F., & McDonald, A. J. (2011). Cholinergic innervation of pyramidal cells and parvalbumin-immunoreactive interneurons in the rat basolateral amygdala. The Journal of Comparative Neurology, 519(4), 790–805. https://doi.org/10.1002/cne.22550

Muller, J. F., Mascagni, F., Zaric, V., & McDonald, A. J. (2013). Muscarinic cholinergic receptor M1 in the rat basolateral amygdala: Ultrastructural localization and synaptic relationships to cholinergic axons: M1R in the Basolateral Amygdala. Journal of Comparative Neurology, 521(8), 1743–1759. https://doi.org/10.1002/cne.23254

Muñoz, W., & Rudy, B. (2014). Spatiotemporal specificity in cholinergic control of neocortical function. Current Opinion in Neurobiology, 26, 149–160.

https://doi.org/10.1016/j.conb.2014.02.015

Namburi, P., Beyeler, A., Yorozu, S., Calhoon, G. G., Halbert, S. A., Wichmann, R., Holden, S. S., Mertens, K. L., Anahtar, M., Felix-Ortiz, A. C., Wickersham, I. R., Gray, J. M., & Tye, K. M. (2015). A circuit mechanism for differentiating positive and negative associations. Nature, 520(7549), 675–678. https://doi.org/10.1038/nature14366

Nelson, A., & Mooney, R. (2016). The Basal Forebrain and Motor Cortex Provide Convergent yet Distinct Movement-Related Inputs to the Auditory Cortex. Neuron, 90(3), 635–648. https://doi.org/10.1016/j.neuron.2016.03.031

Nestler, E. J., Barrot, M., DiLeone, R. J., Eisch, A. J., Gold, S. J., & Monteggia, L. M. (2002). Neurobiology of Depression. Neuron, 34(1), 13–25. https://doi.org/10.1016/S0896-6273(02)00653-0

Neugebauer, V. (2015). Amygdala pain mechanisms. Handbook of Experimental Pharmacology, 227, 261–284. https://doi.org/10.1007/978-3-662-46450-2_13

Newman, L. A., & McGaughy, J. (2008). Cholinergic Deafferentation of Prefrontal Cortex Increases Sensitivity to Cross-Modal Distractors during a Sustained Attention Task. Journal of Neuroscience, 28(10), 2642–2650. https://doi.org/10.1523/JNEUROSCI.5112-07.2008

Ngo-Anh, T. J., Bloodgood, B. L., Lin, M., Sabatini, B. L., Maylie, J., & Adelman, J. P. (2005). SK channels and NMDA receptors form a Ca2+-mediated feedback loop in dendritic spines. Nature Neuroscience, 8(5), 642–649. https://doi.org/10.1038/nn1449

Oda, Y. (1999). Choline acetyltransferase: The structure, distribution and pathologic changes in the central nervous system. Pathology International, 49(11), 921–937. https://doi.org/10.1046/j.1440-1827.1999.00977.x

Offermanns, S. (2003). G-proteins as transducers in transmembrane signalling. Progress in Biophysics and Molecular Biology, 83(2), 101–130. https://doi.org/10.1016/S0079-6107(03)00052-X

Otmakhova, N. A., & Lisman, J. E. (2004). Contribution of Ih and GABAB to synaptically induced afterhyperpolarizations in CA1: A brake on the NMDA response. Journal of Neurophysiology, 92(4), 2027–2039. https://doi.org/10.1152/jn.00427.2004

Otto, M. W., Moshier, S. J., Kinner, D. G., Simon, N. M., Pollack, M. H., & Orr, S. P. (2014). De Novo Fear Conditioning Across Diagnostic Groups in the Affective Disorders: Evidence for Learning Impairments. Behavior Therapy, 45(5), 619–629. https://doi.org/10.1016/j.beth.2013.12.012

Palacios-Filardo, J., & Mellor, J. R. (2019). Neuromodulation of hippocampal long-term synaptic plasticity. Current Opinion in Neurobiology, 54, 37–43. https://doi.org/10.1016/j.conb.2018.08.009

Pallas-Bazarra, N., Draffin, J., Cuadros, R., Antonio Esteban, J., & Avila, J. (2019). Tau is required for the function of extrasynaptic NMDA receptors. Scientific Reports, 9(1), 9116. https://doi.org/10.1038/s41598-019-45547-8

Paolone, G., Angelakos, C. C., Meyer, P. J., Robinson, T. E., & Sarter, M. (2013). Cholinergic Control over Attention in Rats Prone to Attribute Incentive Salience to Reward Cues. The Journal of Neuroscience, 33(19),

8321–8335. https://doi.org/10.1523/JNEUROSCI.0709-13.2013

Pape, H.-C., & Pare, D. (2010). Plastic Synaptic Networks of the Amygdala for the Acquisition, Expression, and Extinction of Conditioned Fear. Physiological Reviews, 90(2), 419–463. https://doi.org/10.1152/physrev.00037.2009

Papouin, T., Dunphy, J. M., Tolman, M., Dineley, K. T., & Haydon, P. G. (2017). Septal Cholinergic Neuromodulation Tunes the Astrocyte-Dependent Gating of Hippocampal NMDA Receptors to Wakefulness. Neuron, 94(4), 840-854.e7. https://doi.org/10.1016/j.neuron.2017.04.021

Parikh, V., Kozak, R., Martinez, V., & Sarter, M. (2007). Prefrontal Acetylcholine Release Controls Cue Detection on Multiple Timescales. Neuron, 56(1), 141–154. https://doi.org/10.1016/j.neuron.2007.08.025

Park, E.-J., Nam, R.-H., Choi, S., & Lee, C.-J. (2004). Carbachol induces a form of long-term potentiation in lateral amygdala. NeuroReport, 15(8), 1339–1343.

Passetti, F., Dalley, J. W., O'connell, M. T., Everitt, B. J., & Robbins, T. W. (2000). Increased acetylcholine release in the rat medial prefrontal cortex during performance of a visual attentional task. European Journal of Neuroscience, 12(8), 3051–3058. https://doi.org/10.1046/j.1460-9568.2000.00183.x

Paton, J. J., Belova, M. A., Morrison, S. E., & Salzman, C. D. (2006). The primate amygdala represents the positive and negative value of visual stimuli during learning. Nature, 439(7078), 865–870.

https://doi.org/10.1038/nature04490

Peck, C. J., & Salzman, C. D. (2014). Amygdala neural activity reflects spatial attention towards stimuli promising reward or threatening punishment. ELife, 3, e04478. https://doi.org/10.7554/eLife.04478

Penzo, M. A., Robert, V., Tucciarone, J., De Bundel, D., Wang, M., Van Aelst, L., Darvas, M., Parada, L. F., Palmiter, R. D., He, M., Huang, Z. J., & Li, B. (2015). The paraventricular thalamus controls a central amygdala fear circuit. Nature, 519(7544), 455–459. https://doi.org/10.1038/nature13978

Pessoa, L. (2010). Emotion and cognition and the amygdala: From “what is it?” to “what’s to be done?” Neuropsychologia, 48(12), 3416–3429. https://doi.org/10.1016/j.neuropsychologia.2010.06.038

Petrovic, M. M., Nowacki, J., Olivo, V., Tsaneva-Atanasova, K., Randall, A. D., & Mellor, J. R. (2012). Inhibition of post-synaptic Kv7/KCNQ/M channels facilitates long-term potentiation in the hippocampus. PloS One, 7(2), e30402. https://doi.org/10.1371/journal.pone.0030402

Pi, G., Gao, D., Wu, D., Wang, Y., Lei, H., Zeng, W., Gao, Y., Yu, H., Xiong, R., Jiang, T., Li, S., Wang, X., Guo, J., Zhang, S., Yin, T., He, T., Ke, D., Li, R., Li, H., … Wang, J. (2020). Posterior basolateral amygdala to ventral hippocampal CA1 drives approach behaviour to exert an anxiolytic effect. Nature Communications, 11(1), 183. https://doi.org/10.1038/s41467-019-13919-3

Picciotto, M. R., Higley, M. J., & Mineur, Y. S. (2012). Acetylcholine as a neuromodulator: Cholinergic signaling shapes nervous system function

and behavior. Neuron, 76(1), 116–129. https://doi.org/10.1016/j.neuron.2012.08.036

Pidoplichko, V. I., Prager, E. M., Aroniadou-Anderjaska, V., & Braga, M. F. M. (2013). A7-Containing nicotinic acetylcholine receptors on interneurons of the basolateral amygdala and their role in the regulation of the network excitability. Journal of Neurophysiology, 110(10), 2358–2369. https://doi.org/10.1152/jn.01030.2012

Pignatelli, M., & Beyeler, A. (2019). Valence coding in amygdala circuits. Current Opinion in Behavioral Sciences, 26, 97–106. https://doi.org/10.1016/j.cobeha.2018.10.010

Pitkänen, A., Savander, V., & LeDoux, J. E. (1997). Organization of intra-amygdaloid circuitries in the rat: An emerging framework for understanding functions of the amygdala. Trends in Neurosciences, 20(11), 517–523. https://doi.org/10.1016/S0166-2236(97)01125-9

Power, A. E., McIntyre, C. K., Litmanovich, A., & McGaugh, J. L. (2003a). Cholinergic modulation of memory in the basolateral amygdala involves activation of both m1 and m2 receptors. Behavioural Pharmacology, 14(3), 207–213.

Power, A. E., Vazdarjanova, A., & McGaugh, J. L. (2003b). Muscarinic cholinergic influences in memory consolidation. Neurobiology of Learning and Memory, 80(3), 178–193. https://doi.org/10.1016/s1074-7427(03)00086-8

Power, J. M., & Sah, P. (2008). Competition between calcium-activated K+

channels determines cholinergic action on firing properties of basolateral amygdala projection neurons. The Journal of Neuroscience: The Official Journal of the Society for Neuroscience, 28(12), 3209–3220. https://doi.org/10.1523/JNEUROSCI.4310-07.2008

Pu, Z., Krugers, H. J., & Joëls, M. (2009). Beta-adrenergic facilitation of synaptic plasticity in the rat basolateral amygdala in vitro is gradually reversed by corticosterone. Learning & Memory (Cold Spring Harbor, N.Y.), 16(2), 155–160. https://doi.org/10.1101/lm.1272409

PubMed entry. (n.d.). Retrieved September 4, 2021, from http://www.ncbi.nlm.nih.gov/pubmed/27418070

Radnikow, G., & Feldmeyer, D. (2018). Layer- and Cell Type-Specific Modulation of Excitatory Neuronal Activity in the Neocortex. Frontiers in Neuroanatomy, 12. https://doi.org/10.3389/fnana.2018.00001

Rammes, G., Steckler, T., Kresse, A., Schütz, G., Zieglgänsberger, W., & Lutz, B. (2000). Synaptic plasticity in the basolateral amygdala in transgenic mice expressing dominant-negative cAMP response element-binding protein (CREB) in forebrain. European Journal of Neuroscience, 12(7), 2534–2546. https://doi.org/10.1046/j.1460-9568.2000.00108.x

Rodrigues, S. M., Schafe, G. E., & LeDoux, J. E. (2001). Intra-Amygdala Blockade of the NR2B Subunit of the NMDA Receptor Disrupts the Acquisition But Not the Expression of Fear Conditioning. Journal of Neuroscience, 21(17), 6889–6896. https://doi.org/10.1523/JNEUROSCI.21-17-06889.2001

Rogan, M. T., Stäubli, U. V., & LeDoux, J. E. (1997). Fear conditioning induces associative long-term potentiation in the amygdala. Nature, 390(6660), 604–607. https://doi.org/10.1038/37601

Sah, P., Faber, E. S. L., Lopez De Armentia, M., & Power, J. (2003). The Amygdaloid Complex: Anatomy and Physiology. Physiological Reviews, 83(3), 803–834. https://doi.org/10.1152/physrev.00002.2003

Sam, C., & Bordoni, B. (2021). Physiology, Acetylcholine. In StatPearls. StatPearls Publishing. http://www.ncbi.nlm.nih.gov/books/NBK557825/

Santiago, L. J., & Abrol, R. (2019). Understanding G Protein Selectivity of Muscarinic Acetylcholine Receptors Using Computational Methods. International Journal of Molecular Sciences, 20(21), 5290. https://doi.org/10.3390/ijms20215290

Sarter, M., Gehring, W. J., & Kozak, R. (2006). More attention must be paid: The neurobiology of attentional effort. Brain Research Reviews, 51(2), 145–160. https://doi.org/10.1016/j.brainresrev.2005.11.002

Sarter, M., Hasselmo, M. E., Bruno, J. P., & Givens, B. (2005). Unraveling the attentional functions of cortical cholinergic inputs: Interactions between signal-driven and cognitive modulation of signal detection. Brain Research Reviews, 48(1), 98–111. https://doi.org/10.1016/j.brainresrev.2004.08.006

Sarter, M., & Lustig, C. (2019). Cholinergic double duty: Cue detection and attentional control. Current Opinion in Psychology, 29, 102–107. https://doi.org/10.1016/j.copsyc.2018.12.026

Sarter, M., & Lustig, C. (2020). Forebrain Cholinergic Signaling: Wired and

Phasic, Not Tonic, and Causing Behavior. The Journal of Neuroscience: The Official Journal of the Society for Neuroscience, 40(4), 712–719. https://doi.org/10.1523/JNEUROSCI.1305-19.2019

Sarter, M., Lustig, C., Berry, A. S., Gritton, H., Howe, W. M., & Parikh, V. (2016). What do phasic cholinergic signals do? Neurobiology of Learning and Memory, 130, 135–141. https://doi.org/10.1016/j.nlm.2016.02.008

Sarter, M., Lustig, C., Howe, W. M., Gritton, H., & Berry, A. S. (2014). Deterministic functions of cortical acetylcholine. European Journal of Neuroscience, 39(11), 1912–1920. https://doi.org/10.1111/ejn.12515

Sarter, M., Parikh, V., & Howe, W. M. (2009). Phasic acetylcholine release and the volume transmission hypothesis: Time to move on. Nature Reviews. Neuroscience, 10(5), 383–390. https://doi.org/10.1038/nm2635

Scarpelli, S., Bartolacci, C., D'Atri, A., Gorgoni, M., & De Gennaro, L. (2019). The Functional Role of Dreaming in Emotional Processes. Frontiers in Psychology, 10, 459. https://doi.org/10.3389/fpsyg.2019.00459

Schaaf, C. P. (2014). Nicotinic acetylcholine receptors in human genetic disease. Genetics in Medicine, 16(9), 649–656. https://doi.org/10.1038/gim.2014.9

Schumann, C. M., Bauman, M. D., & Amaral, D. G. (2011). Abnormal structure or function of the amygdala is a common component of neurodevelopmental disorders. Neuropsychologia, 49(4), 745–759. https://doi.org/10.1016/j.neuropsychologia.2010.09.028

Shayegan, D. K., & Stahl, S. M. (2005). Emotion processing, the amygdala, and outcome in schizophrenia. Progress in Neuro-Psychopharmacology and

Biological Psychiatry, 29(5), 840–845. https://doi.org/10.1016/j.pnpbp.2005.03.002

Shen, W.-X., & Horn, J. P. (1998). Mecamylamine selectively blocks nicotinic receptors on vasomotor sympathetic C neurons. Brain Research, 788(1–2), 118–124. https://doi.org/10.1016/S0006-8993(97)01520-5

Sigurdsson, T., Doyère, V., Cain, C. K., & LeDoux, J. E. (2007). Long-term potentiation in the amygdala: A cellular mechanism of fear learning and memory. Neuropharmacology, 52(1), 215–227. https://doi.org/10.1016/j.neuropharm.2006.06.022

Sison, M., & Gerlai, R. (2011). Behavioral performance altering effects of MK-801 in zebrafish (Danio rerio). Behavioural Brain Research, 220(2), 331–337. https://doi.org/10.1016/j.bbr.2011.02.019

Skov, J., Andreasen, M., Hablitz, J. J., & Nedergaard, S. (2011). Baclofen and Adenosine Inhibition of Synaptic Transmission at CA3-CA1 Synapses Display Differential Sensitivity to K+ Channel Blockade. Cellular and Molecular Neurobiology, 31(4), 587–596. https://doi.org/10.1007/s10571-011-9652-y

Smirnov, S., Paalasmaa, P., Uusisaari, M., Voipio, J., & Kaila, K. (1999). Pharmacological Isolation of the Synaptic and Nonsynaptic Components of the GABA-Mediated Biphasic Response in Rat CA1 Hippocampal Pyramidal Cells. The Journal of Neuroscience, 19(21), 9252–9260. https://doi.org/10.1523/JNEUROSCI.19-21-09252.1999

Spruston, N., Stuart, G., & Häusser, M. (2016). Principles of dendritic integration.

In G. Stuart, N. Spruston, & M. Häusser (Eds.), Dendrites (pp. 351–398). Oxford University Press. https://doi.org/10.1093/acprof:oso/9780198745273.003.0012

Stuber, G. D., Sparta, D. R., Stamatakis, A. M., van Leeuwen, W. A., Hardjoprajitno, J. E., Cho, S., Tye, K. M., Kempadoo, K. A., Zhang, F., Deisseroth, K., & Bonci, A. (2011). Excitatory transmission from the amygdala to nucleus accumbens facilitates reward seeking. Nature, 475(7356), 377–380. https://doi.org/10.1038/nature10194

Sturgill, J. F., Hegedus, P., Li, S. J., Chevy, Q., Siebels, A., Jing, M., Li, Y., Hangya, B., & Kepecs, A. (2020). Basal forebrain-derived acetylcholine encodes valence-free reinforcement prediction error. BioRxiv, 2020.02.17.953141. https://doi.org/10.1101/2020.02.17.953141

Sun, Y., Gooch, H., & Sah, P. (2020). Fear conditioning and the basolateral amygdala (9:53). F1000Research. https://doi.org/10.12688/f1000research.21201.1

Sur, C., Mallorga, P. J., Wittmann, M., Jacobson, M. A., Pascarella, D., Williams, J. B., Brandish, P. E., Pettibone, D. J., Scolnick, E. M., & Conn, P. J. (2003). N-desmethylclozapine, an allosteric agonist at muscarinic 1 receptor, potentiates N-methyl-D-aspartate receptor activity. Proceedings of the National Academy of Sciences of the United States of America, 100(23), 13674–13679. https://doi.org/10.1073/pnas.1835612100

Takigawa, T., & Alzheimer, C. (2002). Phasic and tonic attenuation of EPSPs by inward rectifier K+ channels in rat hippocampal pyramidal cells. The

Journal of Physiology, 539(Pt 1), 67–75. https://doi.org/10.1113/jphysiol.2001.012883

Takigawa, T., & Alzheimer, C. (2003). Interplay between activation of GIRK current and deactivation of Ih modifies temporal integration of excitatory input in CA1 pyramidal cells. Journal of Neurophysiology, 89(4), 2238–2244. https://doi.org/10.1152/jn.00957.2002

Taylor, P., & Brown, J. H. (1999). Synthesis, Storage and Release of Acetylcholine. Basic Neurochemistry: Molecular, Cellular and Medical Aspects. 6th Edition. https://www.ncbi.nlm.nih.gov/books/NBK28051/

Teles-Grilo Ruivo, L. M., Baker, K. L., Conway, M. W., Kinsley, P. J., Gilmour, G., Phillips, K. G., Isaac, J. T. R., Lowry, J. P., & Mellor, J. R. (2017). Coordinated Acetylcholine Release in Prefrontal Cortex and Hippocampus Is Associated with Arousal and Reward on Distinct Timescales. Cell Reports, 18(4), 905–917. https://doi.org/10.1016/j.celrep.2016.12.085

Tigaret, C. M., Chamberlain, S. E. L., Sadowski, J. H. L. P., Hall, J., Ashby, M. C., & Mellor, J. R. (2018). Convergent Metabotropic Signaling Pathways Inhibit SK Channels to Promote Synaptic Plasticity in the Hippocampus. The Journal of Neuroscience, 38(43), 9252–9262. https://doi.org/10.1523/JNEUROSCI.1160-18.2018

Trang, A., & Khandhar, P. B. (2021). Physiology, Acetylcholinesterase. In StatPearls. StatPearls Publishing. http://www.ncbi.nlm.nih.gov/books/NBK539735/

Turchi, J., & Sarter, M. (1997a). Cortical acetylcholine and processing capacity:

Effects of cortical cholinergic deafferentation on crossmodal divided attention in rats. Cognitive Brain Research, 6(2), 147–158. https://doi.org/10.1016/S0926-6410(97)00027-X

Turchi, J., & Sarter, M. (1997b). Cortical acetylcholine and processing capacity: Effects of cortical cholinergic deafferentation on crossmodal divided attention in rats. Cognitive Brain Research, 6(2), 147–158. https://doi.org/10.1016/S0926-6410(97)00027-X

Tye, K. M. (2018). Neural Circuit Motifs in Valence Processing. Neuron, 100(2), 436–452. https://doi.org/10.1016/j.neuron.2018.10.001

Tye, K. M., Stuber, G. D., de Ridder, B., Bonci, A., & Janak, P. H. (2008). Rapid strengthening of thalamo-amygdala synapses mediates cue–reward learning. Nature, 453(7199), 1253–1257. https://doi.org/10.1038/nature06963

Unal, C. T., Pare, D., & Zaborszky, L. (2015). Impact of Basal Forebrain Cholinergic Inputs on Basolateral Amygdala Neurons. The Journal of Neuroscience, 35(2), 853–863. https://doi.org/10.1523/JNEUROSCI.2706-14.2015

Urban-Ciecko, J., Jouhanneau, J.-S., Myal, S. E., Poulet, J. F. A., & Barth, A. L. (2018). Precisely Timed Nicotinic Activation Drives SST Inhibition in Neocortical Circuits. Neuron, 97(3), 611-625.e5. https://doi.org/10.1016/j.neuron.2018.01.037

van Goethem, N. P., Paes, D., Puzzo, D., Fedele, E., Rebosio, C., Gulisano, W., Palmeri, A., Wennogle, L. P., Peng, Y., Bertrand, D., & Prickaerts, J.

(2019). Antagonizing α7 nicotinic receptors with methyllycaconitine (MLA) potentiates receptor activity and memory acquisition. Cellular Signalling, 62, 109338. https://doi.org/10.1016/j.cellsig.2019.06.003

Wang, C., Kang-Park, M.-H., Wilson, W. A., & Moore, S. D. (2002). Properties of the Pathways From the Lateral Amygdal Nucleus to Basolateral Nucleus and Amygdalostriatal Transition Area. Journal of Neurophysiology, 87(5), 2593–2601. https://doi.org/10.1152/jn.2002.87.5.2593

Washburn, M. S., & Moises, H. C. (1992). Muscarinic responses of rat basolateral amygdaloid neurons recorded in vitro. The Journal of Physiology, 449, 121–154. https://doi.org/10.1113/jphysiol.1992.sp019078

Watanabe, Y., Ikegaya, Y., Saito, H., & Abe, K. (1995). Roles of GABAA, NMDA and muscarinic receptors in induction of long-term potentiation in the medial and lateral amygdala in vitro. Neuroscience Research, 21(4), 317–322. https://doi.org/10.1016/0168-0102(94)00867-F

Weiskrantz, L. (1956). Behavioral changes associated with ablation of the amygdaloid complex in monkeys. Journal of Comparative and Physiological Psychology, 49(4), 381–391. https://doi.org/10.1037/h0088009

Wess, J., Eglen, R. M., & Gautam, D. (2007). Muscarinic acetylcholine receptors: Mutant mice provide new insights for drug development. Nature Reviews Drug Discovery, 6(9), 721–733. https://doi.org/10.1038/nrd2379

Wilson, M. A., & Fadel, J. R. (2017). Cholinergic regulation of fear learning and extinction: Cholinergic Regulation of Fear Learning and Extinction. Journal

of Neuroscience Research, 95(3), 836–852. https://doi.org/10.1002/jnr.23840

Yajeya, J., De La Fuente, A., Criado, J. M., Bajo, V., Sánchez-Riolobos, A., & Heredia, M. (2000). Muscarinic agonist carbachol depresses excitatory synaptic transmission in the rat basolateral amygdala in vitro. Synapse (New York, N.Y.), 38(2), 151–160. https://doi.org/10.1002/1098-2396(200011)38:2<151::AID-SYN6>3.0.CO;2-K

Yang, C., McKenna, J. T., Zant, J. C., Winston, S., Basheer, R., & Brown, R. E. (2014). Cholinergic Neurons Excite Cortically Projecting Basal Forebrain GABAergic Neurons. Journal of Neuroscience, 34(8), 2832–2844. https://doi.org/10.1523/JNEUROSCI.3235-13.2014

Yang, Y., & Calakos, N. (2013). Presynaptic long-term plasticity. Frontiers in Synaptic Neuroscience, 5, 8. https://doi.org/10.3389/fnsyn.2013.00008

Yang, Y., Wang, Z.-H., Jin, S., Gao, D., Liu, N., Chen, S.-P., Zhang, S., Liu, Q., Liu, E., Wang, X., Liang, X., Wei, P., Li, X., Li, Y., Yue, C., Li, H., Wang, Y.-L., Wang, Q., Ke, D., … Wang, J.-Z. (2016). Opposite monosynaptic scaling of BLP–vCA1 inputs governs hopefulness- and helplessness-modulated spatial learning and memory. Nature Communications, 7(1), 11935. https://doi.org/10.1038/ncomms11935

Zhang, W.-H., Zhang, J.-Y., Holmes, A., & Pan, B.-X. (2021). Amygdala Circuit Substrates for Stress Adaptation and Adversity. Biological Psychiatry, 89(9), 847–856. https://doi.org/10.1016/j.biopsych.2020.12.026

Zhang, X., Kim, J., & Tonegawa, S. (2020). Amygdala Reward Neurons Form

and Store Fear Extinction Memory. Neuron, 105(6), 1077-1093.e7. https://doi.org/10.1016/j.neuron.2019.12.025

Zhu, P. J., Stewart, R. R., McIntosh, J. M., & Weight, F. F. (2005). Activation of nicotinic acetylcholine receptors increases the frequency of spontaneous GABAergic IPSCs in rat basolateral amygdala neurons. Journal of Neurophysiology, 94(5), 3081–3091. https://doi.org/10.1152/jn.00974.2004